NORWEGIAN UNIVERSITY OF SCIENCE AND TECHNOLOGY

Department of

Marine Technology

Hydrodynamics

Interaction between bodies in a viscous flow

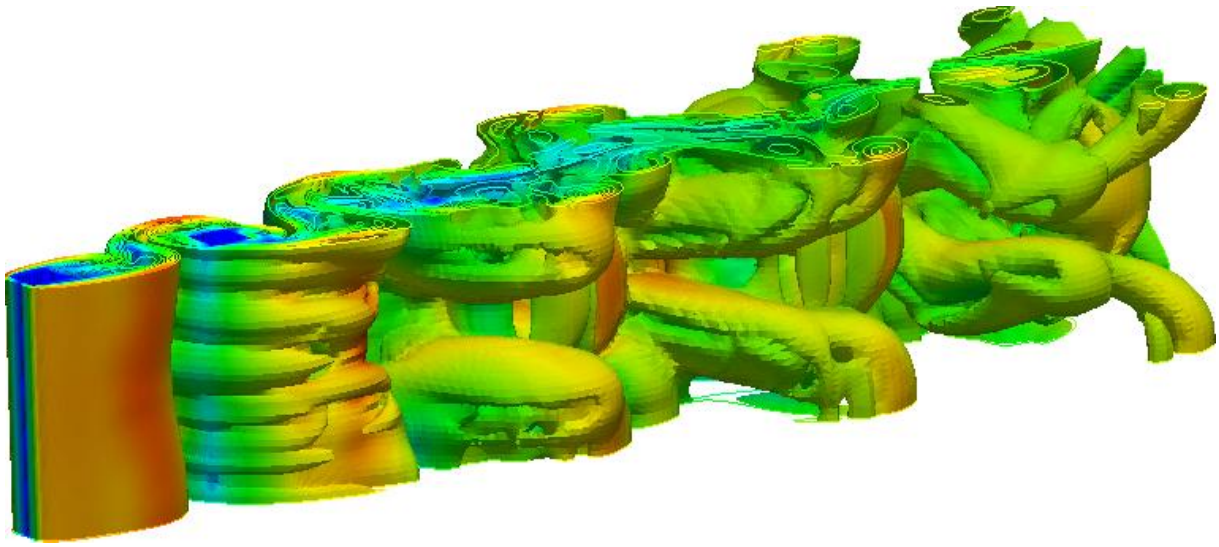

Jan Marius Hovrud

for the degree

Master of Science

Supervisors: Prof. Bjørnar Pettersen (NTNU)

Ph.D. candidate Tufan Arslan (NTNU)

Start: January 2011

End: June 2011

Preface

The Master Thesis serves as the conclusion to the author's education at the Norwegian University of Science and Technology, Department of Marine Technology. This report will be the sole foundation for grading the Master Thesis.

I would like to express my greatest gratitude to Professor Bjørnar Pettersen and Ph.D. candidate Tufan Arslan for their excellent feedback and assistance during my Master Thesis work. I would also like to thank my student colleagues for assistance and enlightenment throughout the work. Lastly, thanks to NTNU's IT department for assistance with my startup problems on the computing facility Njord.

I hereby certify that this work is done without the collaboration of anyone. The work described is entirely original.

Jan Marius Hovrud

Trondheim, June 14, 2011

Abstract

Using the open-source CFD-solver OpenFOAM with a numerical scheme which is first order in time and second order in space, calculations of unsteady 3D flow around two cylinders in tandem arrangement at low Reynolds number (Re = 200) have been performed. Calculations have been done both with and without the assumption of symmetry with respect to y = 0; the latter being a crude model of a free surface. For the case of no symmetry aspect ratio, number of elements in spanwise direction and boundary condition on the front and back faces is discussed. The investigation has been done with special emphasis on the effect of separation distance and the flow in the gap between the cylinders. For the cases where symmetry about y = 0 is assumed, the influence of the boundary condition on this plane has also been investigated.

For the case of no symmetry it is found that the 3D effects inherent in a flow in infinite fluid at Re = 200 are inhibited for separation distances less than four diameters when an aspect ratio of six diameters is used. For $S \leq 0.5$ and $S \geq 3$ distinct low-frequency force pulsations are observed. Pulsations are suppressed for S = 1, 2. The differences and actual changeover between single and double vortex shedding flow schemes is discussed.

For the case of symmetry the flow is always 2D and the final solution is time-independent. Different boundary conditions on y = 0 are investigated. The influence of varying S/D is generally smaller than for the case without symmetry. Detached and reattached flow is studied and differences between cases with and without mirror condition are discussed. Recirculations zones below, behind and between the cylinders are studied.

The results are presented as integral quantities such as average and rms drag and lift coefficients, Strouhal number and pulsation periods, as well as more detailed quantities such as pressure, vorticity, velocity, velocity vectors and streamlines.

Contents

List of symbols

D	Diameter of cylinders
L	Length from upstream face of cylinder1 to downstream face of cylinder2
L_u	Upstream extent of domain for the case of no symmetry
L_{uFS}	Upstream extent of domain for the case of symmetry about y = 0
L_d	Downstream extent of domain
H	Distance between top and bottom planes for infinite fluid
H_{FS}	Distance between surface and bottom plane for mirror conditions
h	Height of cylinders for mirror conditions
A	Aspect ratio of the cylinders
N_x	Number of cells in the x-direction (streamwise)
N_y	Number of cells in the y-direction (cross stream)
N_z	Number of cells in the z-direction (spanwise)
Δt	Time step
Co_{mean}	Mean Courant number in the whole domain
Co_{max}	Maximum Courant number
f_v	Vortex shedding frequency
T_v	Vortex shedding period
f_p	Force pulsation frequency
T_p	Force pulsation period
A_f	Frontal area of one cylinder
Re_{c1}	Critical Reynolds number for primary instability (vortex shedding)
Re_{c2}	Critical Reynolds number for secondary instability (mode A wavelengths)
S_c	Critical separation distance for double vortex shedding
L_s	Separation point motion
L_r	Length of recirculation zone
x_r	x-position for end point of recirculation zone

List of figures

List of tables

NTNU
Norges teknisk-naturvitenskapelige universitet
Institutt for marin teknikk

HOVEDOPPGAVE I MARIN HYDRODYNAMIKK

VÅR 2011

FOR

Stud.techn. Jan Marius Hovrud

INTERAKSJON MELLOM LEGEMER I EN VISKØS STRØM
(Interaction between bodies in a viscous flow)

Oppgaven er motivert ut fra problematikken knyttet til interaksjon mellom to skip som ligger veldig nær hverandre i en tverrstrøm. Kandidaten skal se på to enkle 3D geometrier med kvadratisk tverrsnitt plassert på forskjellig måte i forhold til hverandre i en strøm på tvers. I første omgang analyseres/simuleres strømningen omkring to identiske tverrsnitt med forskjellig avstand (gap) og for forskjellige Reynolds tall. Krefter (Cd, CL) og Strouhalstall dokumenters sammen med detaljerte størrelser fra strømningen (trykk, hastigheter,...). Spesielt undersøkes detaljer i gapet mellom legemene.
Forskjellige konfigurasjoner, størrelse og strømningsretninger analyseres. I den grad tiden tillater det brukes animasjoner for å illustrere dynamikken.
Effekten av fri overflate skal også undersøkes spesielt. Innføres symmetriplan, kan forskjellige fri-overflate betingelser undersøkes. Problemet som da modelleres er likt to rektangulære skipsseksjoner ved siden av hverandre (side-by-side).
I den grad tiden tillater det kan seksjonenes form tilnærmes aktuelle skipsseksjoner.

Kandidaten skal i besvarelsen legge frem sitt personlige bidrag til løsning av de problemer som oppgaven stiller. Påstander og konklusjoner som legges frem, skal underbygges med matematiske utledninger og logiske resonnementer der de forskjellige trinn tydelig fremgår. I besvarelsen skal det klart fremgå hva som er kandidatens eget arbeid, og hva som er tatt fra andre kilder.
Kandidaten skal utnytte de muligheter som finnes til å skaffe seg relevant litteratur for det problemområdet kandidaten skal bearbeide.
Besvarelsen skal være oversiktlig og gi en klar fremstilling av resultater og vurderinger. Det er viktig at teksten er velskrevet og klart redigert med tabeller og figurer. Besvarelsen skal gjøres så kortfattet som mulig, men skrives i klart språk.
Besvarelsen skal inneholde oppgaveteksten, forord, innholdsfortegnelse, sammendrag, hoveddel, konklusjon med anbefalinger for videre arbeid, symbolliste, referanser og eventuelle vedlegg. Alle figurer, tabeller og ligninger skal nummereres.
Det forutsettes at Institutt for marin teknikk, NTNU, fritt kan benytte seg av resultatene i sitt forskningsarbeid, da med referanse til studentens besvarelse.

Besvarelsen leveres i to eksemplar innen 14. juni 2011.

Bjørnar Pettersen
Professor

Faglig veileder: Stipendiat Tufan Arslan

1 Introduction

The motivation for this report is the challenges concerning ship-ship interaction; specifically the flow around two midship sections placed side-by-side in a cross flow.

From time to time ships need to moor alongside each other e.g. for cargo transfer or replenishing operations. A relevant issue here in Norway is a lightering operation where oil is transferred from a large tanker from Russia to a smaller shuttle tanker which can travel along the Norwegian coast. Preferably one would want to execute such an operation in sheltered areas, but this is rearely possible. If this operation were to be carried out in a current, the close proximity between the hulls would of course introduce hydrodynamic interaction.

In such a situation it is important to know the forces and moments acting on the hulls, and how the hulls respond to the cross flow. The force and moments are brought about by pressure fields, and depending on separation distance, size ratio (though not investigated in this study) and current velocity, we can get attractive or repulsive forces between the hulls. In such a situation, the ship masters are not interested in the small details of the flow, but rather the forces and moments on their ship as a whole. Of interest for engineers and scientists, however, are not only the integral parameters, but also the local dynamic loading and flow structures.

The study of bluff body flows is of fundamental interest for scientists, and is important in many engineering problems. In many cases engineering structures have a rectangular or near-rectangular cross section, i.e. bridge sections, skyscrapers, towers, masts and of course, the topic for this report, a ship's midship section.

In this study all simulations have been done with incompressible laminar flow. With laminar flow one avoids the complications of turbulence and simply has more control, but all the physics are still present. Understanding the the laminar flow around the bodies should be the first step before introducing turbulence. This study has been more turned towards understanding flow phenomena in laminar flow in infinite fluid and with a crude free surface model.

This Master Thesis has been a part of an ongoing research project on ship-ship interaction at the Norwegian University of Science and Technology with Ph.D. candidate Tufan Arslan and Prof. Bjørnar Pettersen from the Department of Marine Technology, and Prof. Helge I. Andersson, Department of Energy and Process Engineering in the lead roles. The project will continue for another two years after this Master Thesis work is submitted.

Most of the literature studied during the work with this Master Thesis concerns 2D and 3D numerical calculations of the flow around square and rectangular bodies in single configurations, at low to moderate Reynolds number (up to Re = 1000). Some of the literature also deals with experimental results of flows around the same type of bodies. Ahmad Sohankar, Christoffer Norberg and Lars Davidson (hereinarfter known as Sohankar et al.) at

Chalmers University of Technology in Gothenburg, Sweden, deserve a special mention as I have used as many as six of their excellent articles to guide me in the troubled waters of flow around bluff bodies.

1.1 Flow configurations

The first approximation of two midship sections in a cross flow is two equally sized square cylinders in a tandem configuration in infinite fluid. The influence of the separation, S/D, between the two bodies will be studied. It is varied from S/D = 4 to S/D = 0.1. In addition, simulations with a rectangular cylinder with length 2.1D have been done, to investigate the effect of the gap at the smallest separation distance of S/D = 0.1.

The geometry and flow is defined in figures 1.1 and 1.2.

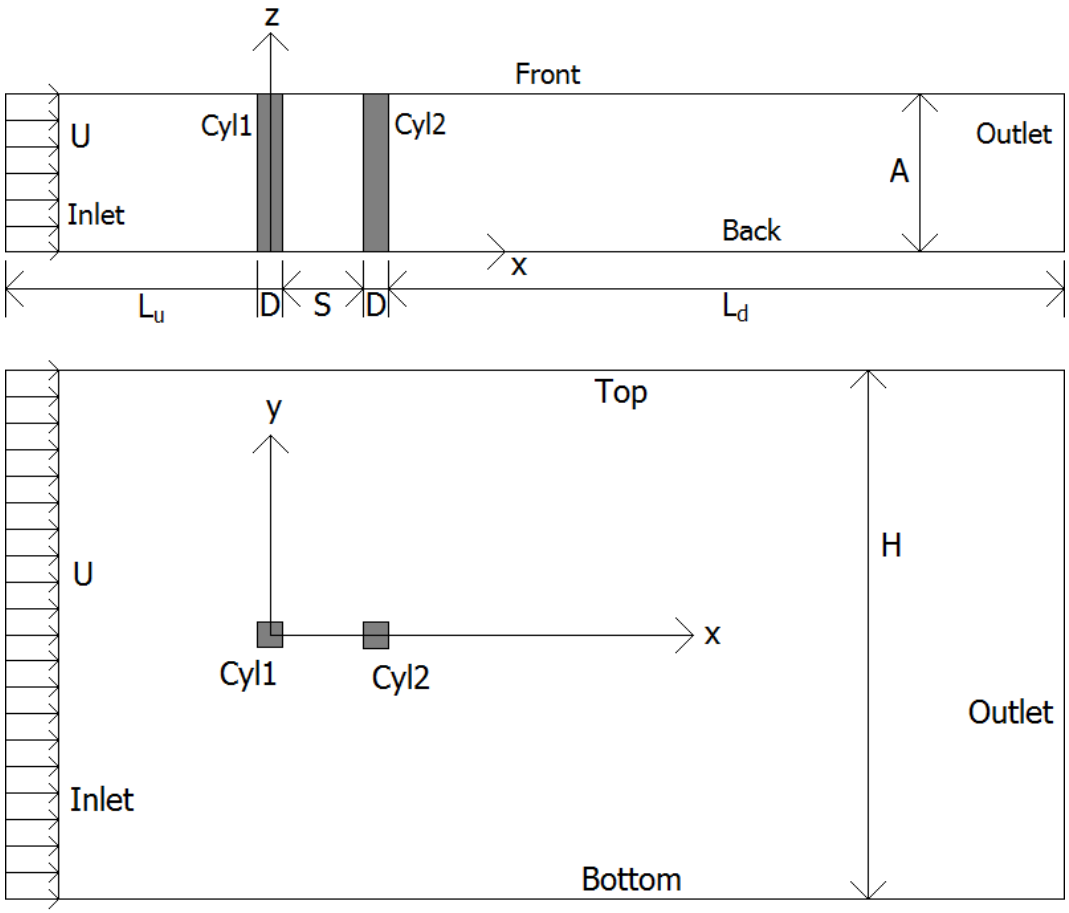

Figure 1.1: Flow configuration in xy- and xz-planes with boundary names

In my OpenFOAM files the top and bottom faces go as one as *topAndBottom* and the front and back faces as *frontAndBack*. This naming style is typical for OpenFOAM.

Figure 1.2 shows the inlet, back face and cylinders for the case with S/D = 4.

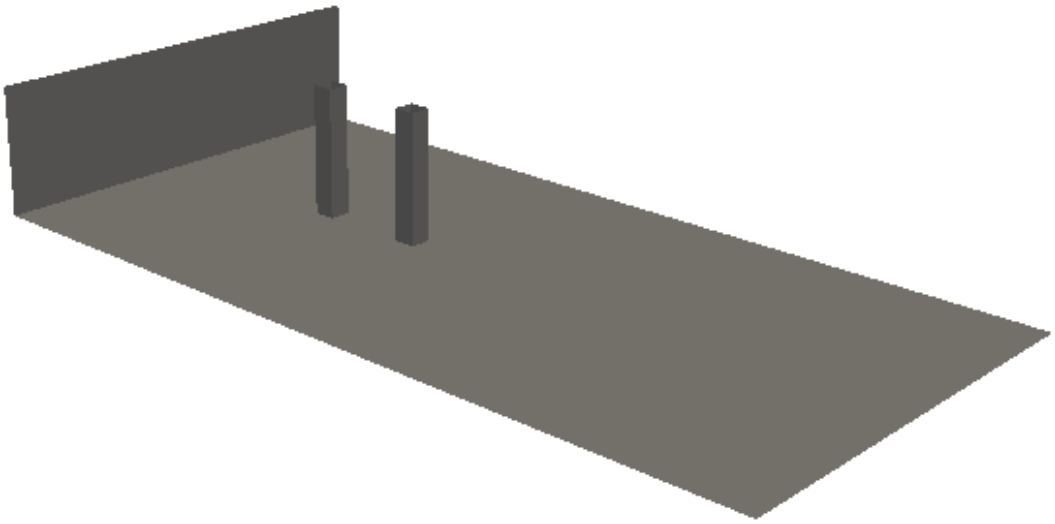

Figure 1.2: Inlet, back face and cylinders for S/D = 4

The free surface is difficult to tackle and is beyond the scope of this study. But by introducing a splitter plate in the gap between the cylinders and in the wake, we will get our first approximation to the problem. This can be seen in figure 1.3 which shows the inlet, cylinders, back plane and splitter plate.

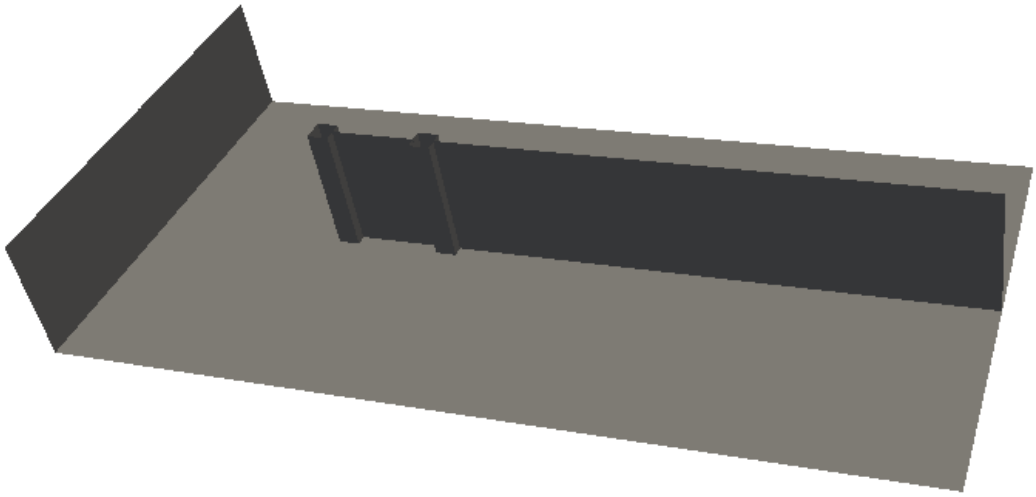

Figure 1.3: Domain with splitter plate

The configurations shown in figures 1.2 will be investigated in chapter 4 and the configuration in figure 1.3 will be discussed in chapter 5.

The most natural thing to do after introducing a splitter plate, would be to divide the domain in half by assuming symmetry with respect to y = 0. This way a rigid surface can be modeled. This will have a stricter boundary condition than a free surface, an interface between water and air which is free to move.

The rigid surface can be modeled by the OpenFOAM boundary conditions *wall* or *symmetryPlane*. Using wall we get a rigid surface where neither velocity component is allowed (no-slip condition), whereas symmetryPlane boundary condition allows tangential velocity, but no normal velocity (slip condition). A free surface allows both, governed by certain free surface conditions.

Wall is clearly the stricter boundary condition, but the ideology is to start with a strict boundary condition and then loosen it up. The next step would be a surface which is free to move, but as mentioned this is beyond the scope of this report.

The runs have been named *TCE_SD* for the case of no symmetry about y = 0 and *TCE_FS_SD* for the case of symmetry. (TCE = Two Cylinders, Equal; FS = Free Surface; SD = separation). The former configuration will be investigated in chapter 4 and the latter in chapter 5.

2 Mathematical formulation and software tools

The open source CFD solver OpenFOAM has been used to solve the incompressible continuity and Navier-Stokes equations for laminar flow (here in tensor form):

$$\frac{\partial u_i}{\partial x_i} = 0 \tag{2.1}$$

$$\frac{\partial u_i}{\partial t} + u_j \frac{\partial u_i}{\partial x_j} = -\frac{1}{\rho}\frac{\partial p}{\partial x_i} + \frac{\partial}{\partial x_j}\left[\nu \frac{\partial u_i}{\partial x_j}\right] \tag{2.2}$$

The Reynolds and Strouhal numbers are based on the cross stream dimension of the cylinder, D, and the uniform inlet velocity, U:

$$\mathrm{Re} = \frac{UD}{\nu} \tag{2.3}$$

$$St = \frac{f_v D}{U} \tag{2.4}$$

ν is the kinematic viscosity of the fluid and f_v is the peak frequency in the calculated spectral density.

Length is non-dimensionalized by D, velocity by U and time by D/U. Fluid forces are non-dimensionalized by the frontal area, A_f, and the dynamic pressure of the upstream flow, $0.5\rho U^2$.

$$C_D = \frac{F_D}{0.5\rho U^2 A_f} \tag{2.5}$$

$$C_L = \frac{F_L}{0.5\rho U^2 A_f} \tag{2.6}$$

We work with kinematic pressure, i.e. dynamic pressure divided by the density, which is constant in this incompressible flow.

2.1 OpenFOAM

OpenFOAM (Open Field Operation and Manipulation) is a C++ toolbox for customization and extension of numerical solvers for continuum mechanics, such as CFD or FEA (Finite element analysis). It operates under Linux/Unix. OpenFOAM comes with a growing collection of pre-written solvers applicable to a wide range of problems, including multiphase flows, combustion and molecular dynamics, to mention a few. OpenFOAM is an open source code. The access to the source code means anything can be customized by the user, in many cases knows as a ”foamer”.

For this study the rather simple solver icoFoam has been used. icoFoam solves laminar and incompressible flows. That is, we have constant fluid properties. The numerical scheme used in this study is first order in time and second order in space. Files defining the numerical treatment of various mathematical quantities for can be found on the enclosed CD (fvSchemes and fvSolution).

2.2 Other software tools

For mesh generation I have used the in-house software Mega developed at the Department of Marine Technology, NTNU. This program creates a structured mesh.

For 3D calculations the supercomputer Njord located at Gløshaugen, NTNU, Trondheim has been used. It has a total of 2976 cores (at the time of writing). My 3D calculations have been run on 128 cores and calculation time for 30,000 time steps on a mesh with 4-5 million cells has been around 150,000 – 170,000 seconds (around 1.5 – 2 days), although actual physical time has usually been a couple of days more due to the LoadLeveler queue system on Njord. Njord is used purely for calculations; it has no pre- or post-processing capabilities. This implies a lot of data transfer between Njord and a computer which has these capabilities.

For 2D simulations I have used Calculator, the Linux based computing facilities at the Marine Technology Center in Trondheim, because unlike Njord it has built-in post-processing capabilities. However Calculator is too slow for 3D simulations. Calculator has also been used for mesh generation in Mega, both for 2D and 3D simulations.

The software used for visualization of the flow field is paraView/paraFoam, a part of the OpenFOAM software package. This has been used to create velocity and pressure color plots, streamline and vector plots, contour plots and more.

The integral values $C_{D_{ave}}$, $C_{L_{rms}}$, St etc. have been calculated, and graphs generated, in Microsoft Excel 2007. For calculation of Strouhal number the Fourier analysis add-on tool for Excel 2007 has been used to find the dominating frequency from the lift force signals. The drag force signals have also been analyzed. Alternatively one could use the signal from a pressure or velocity probe placed in a cylinder’s wake to find the Strouhal number. All spreadsheets can be found on the enclosed CD. To calculate $C_{L_{rms}}$ I have used the formula STDEV(range) which calculates standard deviation. This will be equal to the rms value.

3 Domain, boundary conditions, initial condition

Before breaking new ground with a two-cylinder setup both with and without the assumption of symmetry, it was necessary to make sure the domain and boundary conditions are sensible.

Part of the challenge in pre-processing is the fact that the physical domain is unbounded whereas a numerical domain must be made bounded without disrupting the solution. Also, the physical domain is a continuous system which we need to divide into a finite number of components in space (and time). The grid cells must be small enough not to affect the solution significantly, but unnecessarily small cells will give unnecessarily long computation time. In areas with large gradients (e.g. close to the cylinder surface, and especially around the cylinders' sharp corners) small cells are necessary, while for areas with small gradients (e.g. close to the top and bottom faces) one can get away with larger cells without a problem. Boundary conditions must also be chosen to replicate nature as accurately as possible.

Several preparation tests have been done to make sure the solution is reliable. Part of this work has been done in my project work *Project report TMR 4520: Interaction between bluff bodies* [3] and the knowledge attained there is brought into the current study. The same mesh will be used, but extended to three dimensions.

In my project work [3] for one cylinder at Re = 100 in a 2D flow, the values for upstream extent L_u, downstream extent L_d and height H were found to be $L_u = 9.5$, $L_d = 29.5$ and H = 20 (non-dimensionalized by D), respectively. These values have been used as a basis in the current study at Re = 200. A blockage $\beta = 1/H = 5$ % was found to be sufficiently low in [3]. This is supported by the findings of Sohankar et al. (1995) [9].

While the tests in [3] were done at Re = 100, the present tests are done at Re = 200. At Re = 100 the flow will separate from the cylinder's trailing edge, whereas it will separate from its leading edge at Re = 200. This is discussed in detail in e.g. Okajima [4], Franke et al. [8], Sohankar et al. (1995) [9] and Sohankar et al. (1997) [10] and will also be discussed later in the report. It is assumed that the conclusions made for Re = 100 will be valid for Re = 200 as well.

To be discussed in the following are boundary conditions (BCs) and initial conditions (ICs), aspect ratio and number of spanwise elements. All of these tests have been done with one cylinder, assuming the introduction of a second cylinder in the wake won't change the conclusion. The most important difference is the fact that the wake will be shorter, but as we shall see later, it is sufficient even for the most demanding case.

The mesh used for the preparation tests is shown in figure 3.1. Number of cells in each xy plane is 21,600. The mesh has been called *Trapezemesh*.

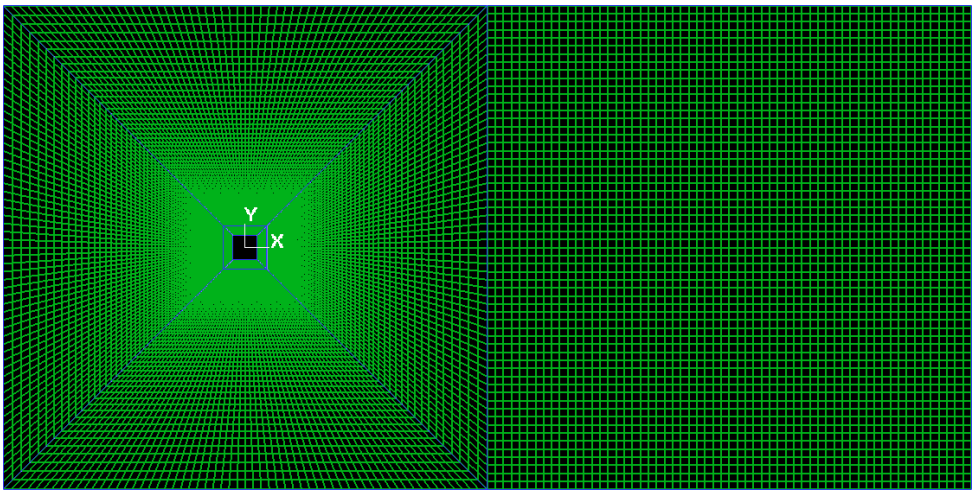

Figure 3.1: Trapeze mesh

The domain's dimensions are defined the same way as described in figures 1.1 and 1.2.

The time step Δt was adjusted prior to and kept constant during each run. The value of Δt was around 0.003, which gave a maximum Courant number Co_{max} in the range 0.7 to 0.9 in all runs. During the start-up, Co_{max} rose from an initial value around 0.5 to a value around 1.5 during the first few time steps before stabilizing around 0.7 to 0.9 as the solution progressed. The rise during the first few time steps was the critical phase where, if the time step was chosen too high, the Courant number would increase unbounded and the calculation would crash.

3.1 Boundary and initial conditions

Most of the boundary and initial conditions from my project work [3] have been used in this study, but some reconsideration had to be done since the calculations now are extended to three dimensions. Most notably, the boundary condition on the frontAndBack planes (xy-planes) had to be revised. All boundary and initial conditions are summarized in table 3.1, and the files used to define them in OpenFOAM can be found on the enclosed CD.

In the following, changes from [3] will be discussed.

Boundary condition on the frontAndBack planes: As OpenFOAM uses the finite volume method to solve the Navier-Stokes equations, the domain always needs to be three-dimensional. But by having only one cell in the z-direction you effectively create a 2D solution. This was done in [3]. For 2D calculations the frontAndBack planes require no solution and therefore the boundary condition is *empty*. When extending the calculation to

three dimensions (i.e. introducing more than one cell in the z-direction, allowing the flow to vary along this axis), the question becomes: what is the 3D version of *empty*?

As it turns out, there is not one correct answer to this. There are mainly three options: *wall*, *symmetryPlane* and *cyclic*. Wall allows no velocity components (though it allows gradients) and is obviously unphysical in this context as the flow should go past the planes unhindered.

symmetryPlane allows tangential velocity, but no normal velocity (here: w = 0). It also requires zero normal gradients of all variables. It is well knows that normal velocity gradients are what creates friction. The shear stress on a xy-surface is given by [22]:

$$\tau_w = \mu \frac{\partial u}{\partial z} \text{ in the x-direction} \tag{3.1}$$

$$\tau_w = \mu \frac{\partial v}{\partial z} \text{ in the y-direction} \tag{3.2}$$

With zero normal gradients the friction on the plane will be zero. Since we want the flow to go past unhindered, this is a good result. The fluid feels no resistance from the surface. The only problem is that we do not allow normal velocity. And since we want to replicate an infinitely long cylinder in a bounded domain, i.e. we don't consider end effects, we should in principle allow all three velocity components in any xy-plane in the domain, even the frontAndBack planes. If the flow is two-dimensional everywhere (w is zero or close to zero compared to u and v), a symmetry plane will not impose any unphysical limitation on the flow and it will work fine.

But this is not always the case. In cases where w cannot be considered small compared to u and v, i.e. the flow is three-dimensional, we need a boundary condition which allows all three velocity components on the boundaries. The answer is a cyclic boundary condition. In OpenFOAM this is done by running a script which writes several large files that describe the linkage between the two borders. With the two borders linked together, all velocities (and also pressure and other properties) on one border will be transferred to the other, allowing all three velocity components in any xy-plane in the domain. And when the planes are far enough away from each other they will not interfere.

This will be the closest approximation to the flow around a cylinder with infinite aspect ratio. The replication of velocities from one plane to the other will also ensure continuity in the flow.

The boundary condition for velocity and pressure on the actual outlet face will be discussed in a bit more detail. Together with the long downstream extent of the domain it must 1) allow the fluid to exit the domain with a smooth discharge of vortices, 2) have a minimal effect on flow near the outlet, and 3) have a negligible effect on the near-body flow [11]. The outlet boundary condition used on velocity throughout this study is of the Neumann type, just like in [3]. This boundary condition specifies the value of the normal derivative on a boundary. In this case this derivate is set to zero, i.e. we require that the velocity has zero gradient at the outlet: $\partial u_i / \partial x = 0$. This is specified in OpenFOAM by setting *zeroGradient* for the velocity. The boundary condition for pressure is p = 0 on the whole face, i.e. no kinematic/dynamic pressure on the outlet face. In OpenFOAM: *uniform 0*.

Initial conditions on the internal field: In [3] *uniform (0 0 0)* was used for the velocity in the internal field, the enclosed fluid volume. The parenthesis defines the three velocity components as (u v w) and *uniform* indicates that these (u v w) will be the same in all points in the field. This initial condition means the fluid in the whole domain is still before the simulation starts. The initial and boundary condition on the inlet is *uniform (1 0 0)*. From the initial condition to the first time step the fluid will be abruptly accelerated to a velocity of 1.

In the current study I changed the initial condition in the internal field to *uniform (1 0 0)* to avoid this abrupt acceleration of the fluid as this condition means it is already accelerated when the simulation starts. I found out I could use a somewhat higher Δt since Co_{max} would not rise quite as high in the most critical phase of the startup described in chapter 3.

For pressure *uniform 1e-12* was used as initial condition. This means there is no static pressure, only kinematic pressure (dynamic pressure divided by the constant density). The reason for having 1e-12 and not exactly 0 is that Njord couldn't handle the zero in this particular case. No matter what time step I used, the Courant number exploded and the solution gave a pressure singularity. This problem with 0 only occurred here. With uniform 1e-12 all problems were eliminated.

All boundary and initial conditions are summarized in table 3.1 below. Notice the three different cases for the frontAndBack plane dependent on the flow and domain.

Name	Plane	IC on U	IC on p	BC on U	BC on p
frontAndBack 3D flow, 3D domain	xy	cyclic	cyclic	cyclic	cyclic
frontAndBack 2D flow, 3D domain	xy	symmetryPlane	symmetryPlane	symmetryPlane	symmetryPlane
frontAndBack 2D flow, 2D domain	xy	empty	empty	empty	empty
inlet	yz	uniform (1 0 0)	zeroGradient	uniform (1 0 0)	zeroGradient
outlet	yz	zeroGradient	uniform 0	zeroGradient	uniform 0
cylinder	xz and yz	uniform (0 0 0)	zeroGradient	uniform (0 0 0)	zeroGradient
topAndBottom	xz	symmetryPlane	symmetryPlane	symmetryPlane	symmetryPlane
internalField	-	uniform (1 0 0)	uniform 1-e12	-	-

Table 3.1: Boundary and initial conditions

3.2 Aspect ratio

When expanding from the 2D world of my project work to 3D calculations in the current study, in addition to introducing new boundary conditions I also had to consider the aspect ratio of the cylinder(s). Although not strictly correct, a 2D simulation can be considered as having an aspect ratio A = 0.

Since we in this study wanted to model the flow around two square cylinders with infinite aspect ratio (no end effects), we had to use an aspect ratio high enough to capture the flow phenomena inherent in such a flow. The flow around a *sufficiently long* square cylinder at Re = 200 is inherently three-dimensional [13]. The decisive factor is the aspect ratio, as the three-dimensionality is brought about by unstable mode A wavelengths. These are waves which wish to appear along the span of the cylinder. As discussed in Sohankar et al. (feb 1999) [12], similar to the flow around circular cylinders (CC flow), there exists a band of unstable mode A wavelengths in the flow around a square cylinder (SC flow) as well. When the aspect ratio is larger than or comparable to the largest unstable wavelength, 3D effects will appear. When a too low aspect ratio is used the 3D effects are suppressed, and the solution will be inaccurate.

When a flow calculation is started from zero, it will take some time before the primary instability occurs: the von Kármán vortex shedding. This always starts out as two-dimensional [11], and will occur if the Reynolds number is above a certain value, the critical onset Reynolds number for vortex shedding, Re_{c1}. For a square cylinder with the same blockage as used in this study, $\beta = 5$ %, Sohankar et al. (1998) [11] report this value to be $Re_{c1} = 51.2 \pm 1$ when scaled with the diameter.

When the Reynolds number increases further and exceeds a certain value, Re_{c2}, we will get a transition from 2D to 3D in the wake due to a second wake instability caused by the unstable mode A wavelengths. We get a three-dimensional distortion of the primary two-dimensional

von Kármán vortices. This transition in SC flow has been investigated in detail by Sohankar et al. (feb 1999) [12], Luo et al. 2006 [17] and Saha et al. (2002) [18]. Sohankar et al. [12] have found Re_{c2} to be between 150 and 200 for $\beta = 5.6$ %, which means a flow at Re = 200 is inherently three-dimensional and it is therefore important to use a high enough aspect ratio. According to Barkley & Henderson (1996) [19], the critical aspect ratio for mode A instabilities in transitional CC flow is about four diameters (3.96 ± 0.02 to be exact). One would assume that the critical aspect ratio in SC flow is similar.

The aspect ratios tested in the present study were A = 3, 6, 9, 12 and 15. All simulations used the cyclic boundary condition on the frontAndBack planes. The number of spanwise elements was chosen to be 10 per 6 diameters. This is investigated in the next section, and while the conclusion there is that the necessary resolution is 40 elements per 6 diameters, the waves will also trigger for $N_z = 10$. This number was chosen from a purely practical standpoint, as it should demand only a quarter of the calculation time compared to $N_z = 40$. I did lots of calculations in that period of time and I could not afford to have long computing time.

Like in [12] and [13], 3D effects were observed for $A \geq 6$. However, at A = 3, the flow stayed two-dimensional, which means A = 3 is too low to trigger the inherent 3D effects. Intermediate values between A = 3 and A = 6 were not investigated.

A	N_z	C_D ave 2D	C_L rms 2D	C_D ave 3D	C_L rms 3D
3	5	1.565	0.449	-	-
6	10	1.564	0.448	1.492	0.298
9	15	1.564	0.447	1.481	0.271
12	20	1.564	0.447	1.494	0.290
15	25	1.563	0.447	1.483	0.254

Table 3.2: Averaged C_D and C_L values for different A

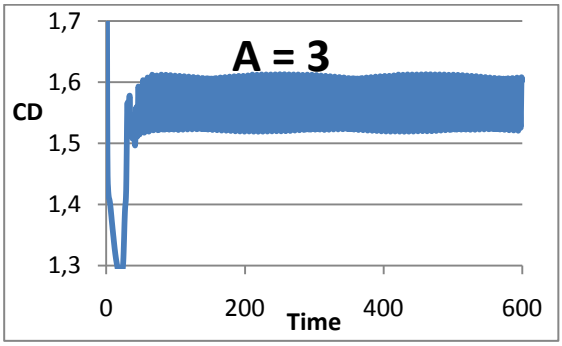

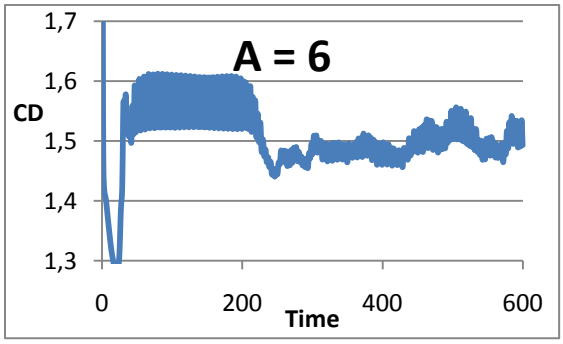

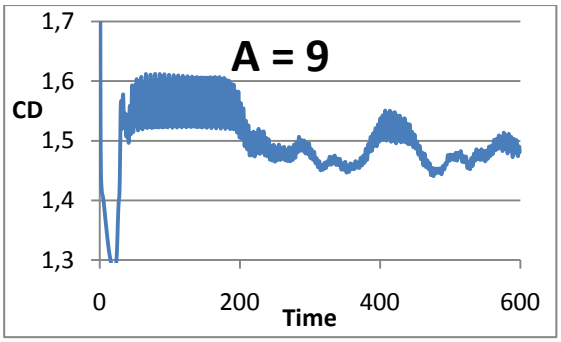

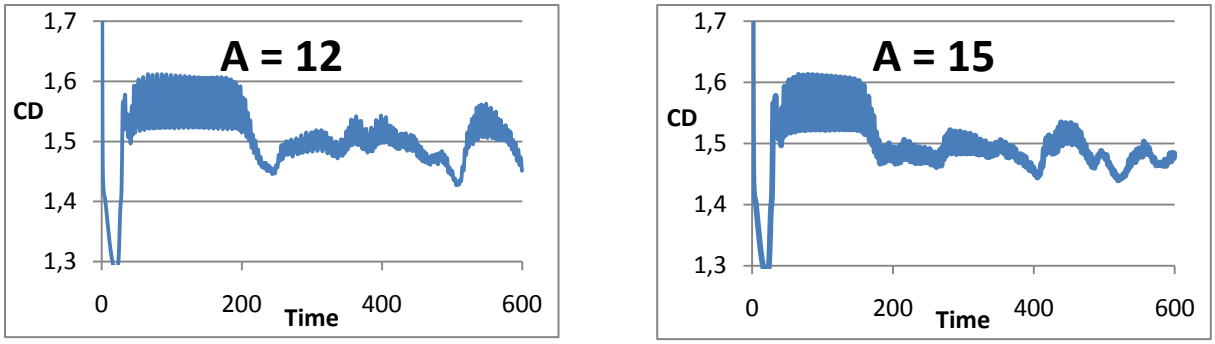

Figure 3.2: C_D signal for the different aspect ratios

For $A \geq 6$ there were very small differences between the averaged integrals quantities C_D and C_L, both for the 2D and the 3D flow, and also their graphs look similar. The reason for the larger variations in averaged 3D values is probably the short averaging period. It is however important to notice that integral parameters such as C_D and C_L for the cylinders as a whole can even out small variations in the flow. Therefore an inspection of the flow fields was done as well. This inspection revealed no significant differences between the flows. As mentioned, there is a requirement for a certain spanwise resolution, so an increase in A would have to be followed by a proportional increase in number of spanwise elements. This will be discussed in the next section. Since a higher-than-6 aspect ratio would not improve the solution, only require more grid cells and give longer computational time, larger files and more memory usage, the value A = 6 was used. This value was also used by Sohankar et al. (feb 1999) [12] and Sohankar et al. (jul 1999) [13].

In addition to the long wavelength mode A, short wavelength mode B instabilities might also be present in transitional flow. These appear with a wavelength of about 1 diameter [12]. According to Williamson [14] these will show up for Re = 230 upwards in CC flow. Robichaux et al. [20] have found the corresponding number for SC flow to be Re = 190. The Mode A and B instabilities and transition from 2D to 3D flow will be discussed more in chapter 4 in connection with force pulsations.

Lastly it is worth mentioning that with $150 < Re_{c2} < 200$ no erroneous simplifications were made by using a 2D domain in my project work [3] at Re = 100. This conclusion is also valid for a two-cylinder setup as the second cylinder will not trigger three-dimensionality any earlier. In fact, it will in some cases inhibit three-dimensionality altogether. This will be investigated in detail in chapter 4.

3.3 Number of elements in spanwise direction

The number of elements in spanwise direction (z-direction), N_z, must be high enough to give smooth transitions between the elements and adequately resolve the details of the flow. Values of N_z = 10, 20, 30 and 40 were studied. The cyclic boundary condition on the frontAndBack planes was used for all four runs. All calculations exhibited 3D effects, but as can be seen from figure 3.3, the pulsations became more regular as N_z increased. The turnover point is between N_z = 20 and N_z = 30. Thus, N_z = 10 and N_z = 20 were not viable options. Also, we can see that 3D effects are triggered earlier for higher N_z up to N_z = 30 (notice the longer total calculation time for N_z = 40).

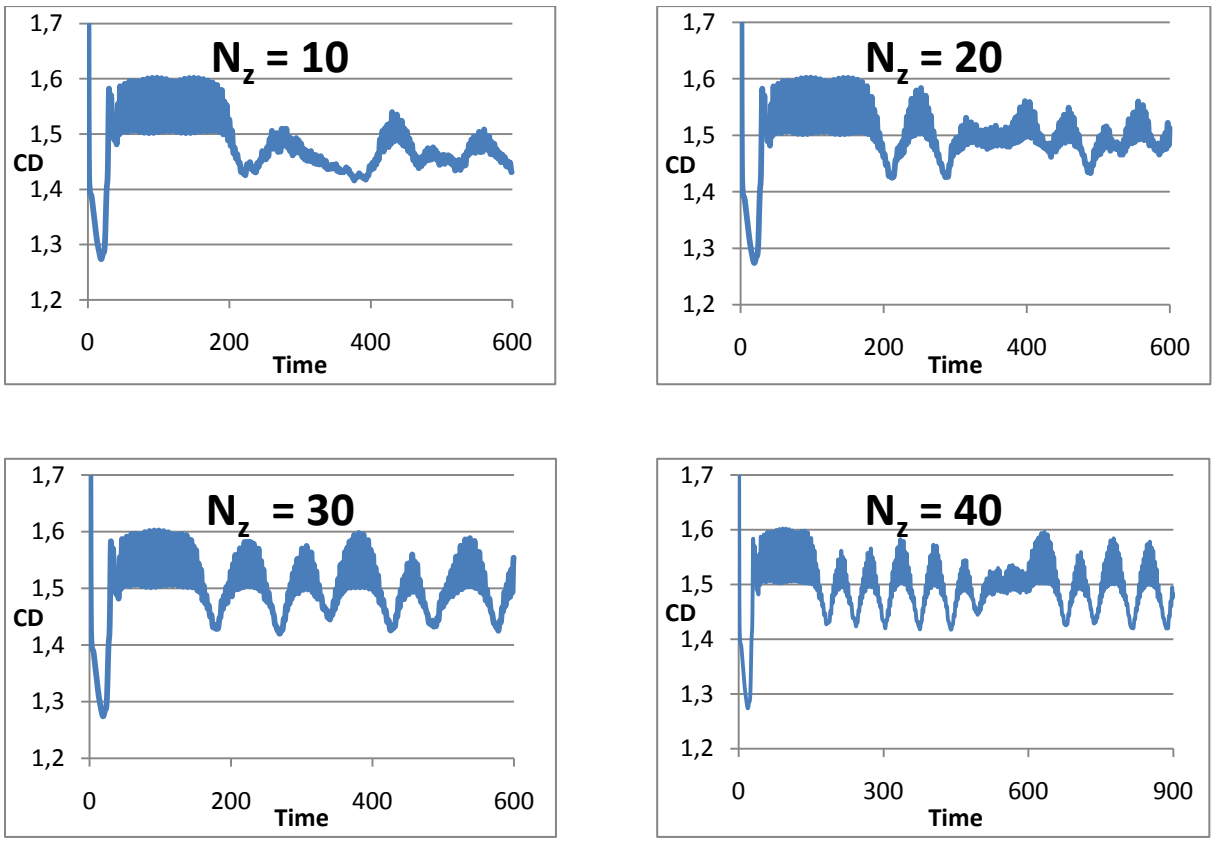

Figure 3.3: C_D signal for different N_z values

The integral quatities C_D and C_L varied very little for different N_z values, but inspection of the flow field, specifically the velocity and pressure in a plane two diameters downstream, releveal too low resolution for N_z < 40. As mentioned in the previous section, integral quatities tend to even out variations.

I could have chosen N_z even higher, but one always has to consider the trade-off in terms of calculation time. As the pulsations proved to be regular at N_z = 40 and the spanwise resolution was allright, this value is assumed adequate.

It is interesting to note that Sohankar et al. (feb 1999) [12] used $N_z = 25$ for A = 6 and $N_z = 41$ for A = 10, and they described the pulsations as "seemingly random in time," but it seems the pulsations desire to to regular when the resolution is good enough. In [12] $N_z = 25$ for A = 6 was too low to reveal the regularity of the pulsations, which in my runs showed up for $N_z \geq 30$.

These force pulsations will be discussed in detail in chapter 4.

4 Results and discussion for two-cylinder flow in infinite fluid (TCE)

With domain size, boundary conditions, aspect ratio and number of elements along the span sorted, I was ready to break new ground with studies of the flow around two cylinders in tandem.

For the two-cylinder setup used in this study I used the same total domain length (40 diameters) for all calculations. This was done mostly for practical reasons as it reduced the amount of work on the mesh when changing the separation, S/D. This implies that the distance from the second cylinder to the outlet varies depending on the separation distance. For the case of highest separation, S/D = 4, the downstream extent, L_u = 24.5 diameters. Even though this is lower than the 30 diameters found in [3], it is argued that introducing a second cylinder will not nearly make the flow doubly disrupted. The velocity and pressure fields felt far downstream will not be very different between a case with one cylinder and a case with two cylinders. Sohankar et al. [10] have found the necessary downstream extent around 26 diameters for Re = 200 and one cylinder. The value L_d = 24.5 for this study's worst case is regarded to be sufficient.

However, a very demanding decision was made before starting calculations on TCE, namely a change of mesh type. This was done due to a number of reasons and will be explained in detail in the next section.

4.1 Mesh change

After preparation tests I understood that Trapezemesh had some flaws. I constructed a new type of mesh with the same dimensions as Trapezemesh, but with only rectangular cells (i.e. no skewed cells). The new mesh type was named Crossmesh and can be seen in figure 4.1 below.

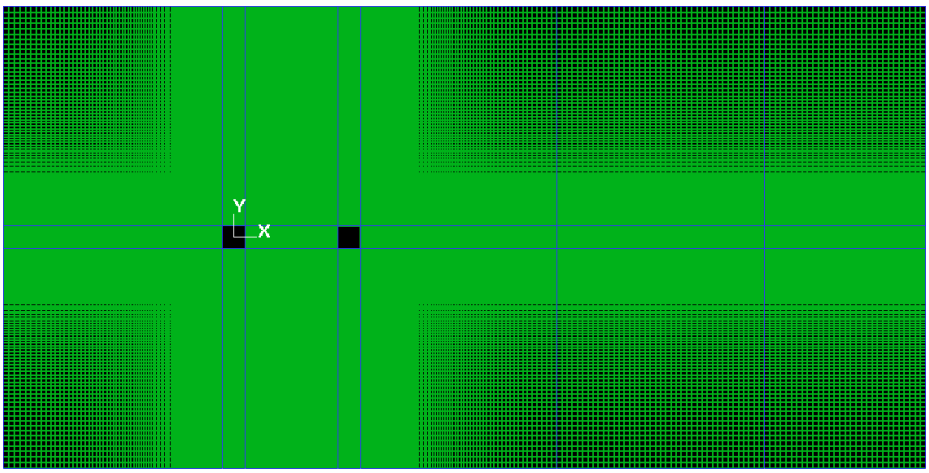

Figure 4.1: Crossmesh for a two-cylinder configuration with S/D = 4

The main problem with Trapezemesh, as can be seen from figure 3.1 (for one cylinder), is that the height of the cells outside the cylinders will be inversely proportional to the number of cells along the cylinder surface. This means one needs very many cells along the cylinder surface and still the cells some distance away from the cylinder will be large. To avoid too high cell aspect ratio (height/width) one would need to increase the width of the cells as well. This would of course be the case for both single and tandem setup; see [3]. The areas of the mesh close to and further away from the cylinder will be refered to as near-field and far-field, respectively. The problem of far-field resolution being dependent of near-field resolution will be larger for larger H/D ratio, and for this case H/D = 20, which implies a 20-fold increase in cell height (and about the same for width) from the cylinder wall to the outer boundary.

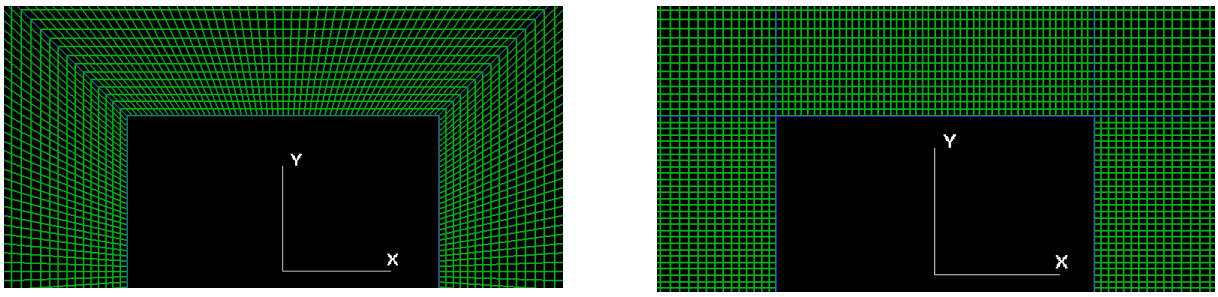

Figure 4.2: Comparsion between near-field resolution for Trapezemesh and Crossmesh

Trapezemesh has 60 cells along both the horizontal and vertical side of the cylinder, and this is more than enough for near-field resolution, but still gives unreasonably large cells in the far-field. This is mainly a problem for the cross stream and downstream directions, as too large cells will give significant numerical damping and details in the vortices and wake will be lost. In the upstream direction it is less of a problem as the flow is close to uniform.

As can be seen from a comparison of Crossmesh and Trapezemesh, the former has a much better far-field resolution with a minimal and insignificant decrease in near-field resolution. Visual inspection of figure 4.2 confirms this. Also, the ratio between the largest and smallest cell in the mesh is smaller for Crossmesh, which means Co_{mean} is not as small when Co_{max} is close to one, where we want it to be.

It did not make sense to use a reworked (or “maxed-out”) Trapezemesh with 100 cells along a cylinder surface (the maximum number of cells along one line in Mega) when it was evident that the mesh was flawed. The far-field dependence of near-field resolution is a sign that Trapezemesh is not suitable for this type of flow. It could make more sense for a flow with larger blockage, i.e. a flow where H/D was considerably closer to unity than is the case for my flow.

Crossmesh has 50 cells along one side of the cylinder, compared to 60 for Trapezemesh, and the number of elements outwards from the cylinder wall, both vertical and horizontal was 100. The distribution of nodes was adjusted to make the cells close to the cylinder surfaces

approximately square, and to give a smooth variation of cell size outwards from the cylinder surface [25]. In my project work [3] I learned the importance of the cells in the area around the cylinders' corners being square or close to square. The flow makes a tight turn around the corner, going from predominantly vertical to predominantly horizontal. It is quite logical that the cells in this area should be square. This is also brough up in *Meshing applied to CFD* by K. Sørli [25]: "Element aspect ratio (width/height) should be near 1 where flow is muli-dimensional".

In Mega this clustering is adjusted according to a geometric series with some increment. The sum of the length of the elements, that is, the total length from the cylinder surface to the outer boundary is given as the sum of the geometric series [27]:

$$S = \sum_{k=0}^{n-1} ar^k = a\frac{1-r^n}{1-r} \tag{4.1}$$

where a is the dimension of the first cell from the wall, n is the number of elements and r is the increment. The increment was adjusted to give approximately square cells by visual inspection. The value r = 1.025 was chosen. The value for a then becomes

$$a = S \cdot \frac{1-r}{1-r^n} = 9.5 \cdot \frac{1-1.025}{1-1.025^{100}} = 0.022 \approx 0.02 \tag{4.2}$$

So we see that the cells along the cylinder surface are indeed approximately square.

The number of cells in the gap between the cylinders was adjusted according to the length of the gap, and their size ratios were adjusted according to a similar geometric series, but clustered to both ends, i.e. towards the cylinders, to give square cells in those areas. The number of grid cells is $N_y = 250$ in the y-direction and $350 \leq N_x \leq 470$ in the x-direction, dependent of the separation distance S/D; i.e. between 90,000 and 120,000 cells for each xy-plane. With $N_z = 40$ this gave a total number of cells roughly between 4 and 5 millions.

A somewhat surprising discovery was made in terms of the time step Δt. For Trapezemesh the necessary time step was around 0.003 (cf. chapter 3) whereas with Crossmesh I could increase it to 0.01 to 0.0125 and still maintain a similar Co_{max}. This more than three-fold increase in time step cannot only be attributed to the small reduction in number of elements along the cylinder surface (50 down from 60). I suspect the skewed cells create some difficulties and require a very low time step Δt. Such a low Δt necessitates very many time steps in total for a calculation. Even if the total number of cells is not very large, the calculation will take a long time.

The increase in Δt for Crossmesh leads to a much lower total number of time steps for a calculation, but this can then counteracted by considerably increasing the number of cells for Crossmesh. With similar calculation time, Crossmesh will be favorable, as it has much better far-field resolution. I quickly noticed a drawback with the Crossmesh though, and that was the fact that the increase in number of elements increased the amounts of data and required much more memory from my computer when it came to visualization in paraView.

In the appendix a spreadsheet with comparison between a maxed-out Trapezemesh and Crossmesh can be found. The calculation on Trapezemesh with about 180,000 cells took about 180,000 seconds (50 hours) whereas the calculation on Crossmesh with about 240,000 took about 30,000 seconds (about 8 hours) thanks to the high increase in Δt. It is quite clear that Crossmesh also has a big advantage in terms of calculation time.

It is by no means ideal to change mesh in the middle of the study, but I did not have time to do all the tests from chapter 3 again on the new grid. Nor did it make sense to do the rest of the thesis work on a grid I felt was less suitable. It is assumed that the conclusions on domain size, aspect ratio, number of spanwise cells and outlet boundary condition is independent of the type of mesh.

Just like in chapter 3, Δt is adjusted prior to each run and kept constant during the TCE runs. The smallest cells in the domain are found in the gap. Since the separation distance, number of cells in the gap and also the clustering increment was adjusted for each run there was a little variation in the size of the smallest cell. Therefore I could increase Δt to 0.0125 for some of the runs. Co_{max} hovered around 0.8 ± 0.1 in all runs.

I have run a one-cylinder case, named OneCyl, with $A = 6$, $N_z = 40$ and cyclic boundary condition on the frontAndBack planes to confirm that Crossmesh agrees with the literature; see chapter 4.2. This case is also used for comparison with TCE_4D.

Finally, a note on symmetryPlane and cyclic in relation to the TCE runs: All TCE runs and the OneCyl run were prepared with cyclic boundary condition on the frontAndBack planes and run on Njord a week or so before Easter. On Njord any file which has not been changed (or "touched") for 21 days will be deleted. I was aware of this, but I forgot it. During the holidays all TCE simulations and the OneCyl simulation were deleted. I had collected all the force coefficients data from all simulations, but the data for the flow fields themselves, which I of course needed for visualization, was lost forever. Thankfully I had a copy of the foundation for all runs (mesh, initial conditions, boundary conditions etc.) on my computer, so I was able to transfer these files to Njord and redo all the calculations. In this process some changes were made, as the force coefficients data showed that the runs for $S/D \leq 3$ exhibited no significant 3D effects. The cyclic boundary condition was deemed unnecessary and the cases for $S/D \leq 3$ were rerun with symmetryPlane as BC on the frontAndBack planes as it implied less files to transfer to Njord. OneCyl and TCE_4D were rerun with the cyclic boundary condition.

Comparing the old and the new force coefficient data for the cases with $S/D \leq 3$ no discernable difference between cyclic and symmetryPlane was found.

4.2 OneCyl, force pulsations and 3D effects

As a verification of the validity of crossmesh I did a run with one cylinder with all settings found in chapter 3, i.e. A = 6, N_z = 40, L_u = 9.5, L_d = 29.5 and cyclic boundary condition on the frontAndBack planes. The time step was $\Delta t = 0.01$, and the number of cells 85,360 in one xy-plane. This is considerably higher than Trapezemesh's 21,600, and displays Crossmesh's much better far-field resolution as the near-field resolution is approximately the same.

Authors	C_D ave	C_L rms	St
Present study[1]	1.493	0.429	0.148
Hovrud 2010 [3][2]	1.582	-	0.162
Sohankar et al. (1999) [12][3]	1.460	0.320	0.170
Sohankar et al. (1998) [11]	1.439	0.227	0.167
Sohankar et al. (1995) [9]	1.424	0.240	0.165
Franke et al. (1990) [8]	1.600	0.620*	0.157

Table 4.1: Comparison of OneCyl with literature

*) 0.620 is the amplitude, A_{CL}. If the signal is assumed sinusoidal, C_L rms is given as [24]: $A_{CL} / \sqrt{2} = 0.640 / \sqrt{2} = 0.453$

From table 4.1 we see that we have very good agreement on C_D average. C_L rms is predicted a little high and St a little low, but the agreement is still satisfactory.

From the C_D and C_L signals (figure 4.3) we can see the point in time where transition to 3D flow begins as the point where the force coefficients drop (around t = 120). For this configuration with laminar flow, 3D effects will only appear after a period of 2D transient shedding flow.

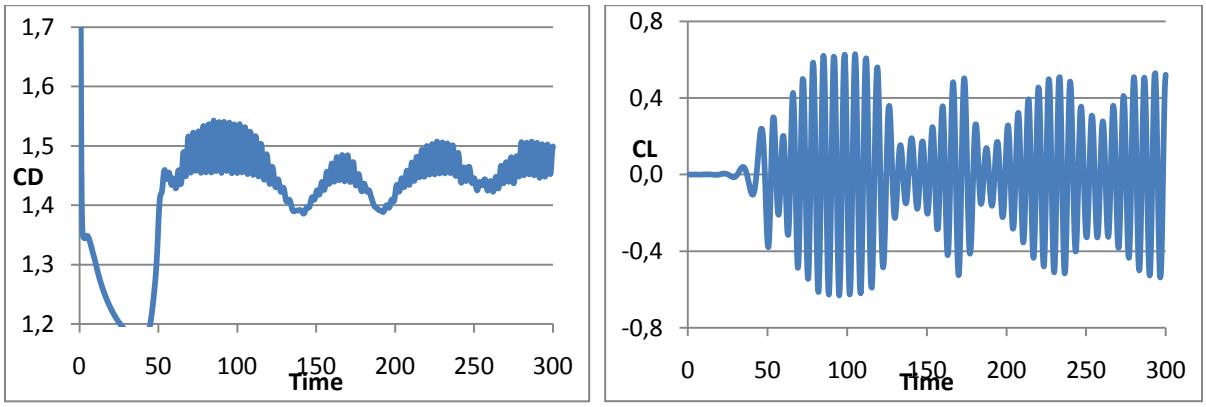

Figure 4.3: C_D and C_L signals for OneCyl

In figure 4.3 we see the same pulsations as in figure 3.3. The characteristic time periods with high and low force levels are known as HF and LF regions, respectively [12]. Sohankar et al.

[1] Crossmesh, 2D part of the C_D and C_L graphs
[2] Trapezemesh, one-off run with Re = 200
[3] 2D part of the C_D and C_L graphs

(feb 1999) [12] suggest that the spanwise coupling of forces is lower in LF regions than HF regions. They show this by dividing then span into sections and calculating the spanwise sectional drag coefficient. In LF regions there is a difference of 10 % between the highest and lowest sectional drag coefficient value, compared to only about 1 % in an HF region. The reason for the lower spanwise coupling in LF regions is that the degree of three-dimensionaliy in the flow is higher in LF regions and lower in HF regions. With higher three-dimensionality comes a higher degree of spreading of forces. Basically, the forces along the span do not work in the same direction at the same time, lowering the total force on the cylinder.

The characteristic force pulsations are part of the transition from 2D to 3D flow [12], which they found to begin at a Reynolds number between 150 and 200. Saha et al. (2002) [18] later found the critical Reynolds number to be between 150 and 175. In [12] it is suggested that the pulsations are related to some coupling mechanisms between the primary 2D instability (von Kármán vortex shedding) and secondary mode A instabilities. In their simulations pulsations were observed in the region Re = 200–300. For Re > 300 they suggest that the high degree of three-dimensionality in the near wake will mask the increased spanwise coupling of forces in the HF regions and thus the pulsations will be indiscernible.

The pulsations will be present both in the 2D and 3D part of the flow development. In the present case we see one 2D pulsation before the transition the 3D (the "arc" in the C_D graph from time $t \approx 60$ to $t \approx 120$ in figure 4.3). The Strouhal number St = 0.148, corresponding to a shedding period of about 6.8 time units. The pulsation period was found to be 64 time units (approximately 9.5 shedding periods). Sohankar et al. [12] found the pulsation period to be around 60-100 time units in a flow where the pulsations were not as regular as in this case due to a lower N_z (cf. chapter 3.3).

The shedding frequency is primarily governed by the two-dimensional instability without any new time scale introduced from the secondary three-dimensional structures [15], which means the vortex shedding frequency should be close to the same for both the 2D and 3D part of flow. An inspection of the C_D and C_L signals showed that this is true for the HF region. For the 2D and HF regions a vortex shedding period of 6.7 time units was found through inspection of the plots in Excel. However, for the LF region the vortex shedding period was found to be 7.2 time units. The reason for the difference will be discussed later in this chapter in connection to figure 4.7.

The Strouhal numbers in this study will be based on the peak in the spectral density; in this case St = 0.148 corresponding to a shedding period $T_v = 6.8$ time units.

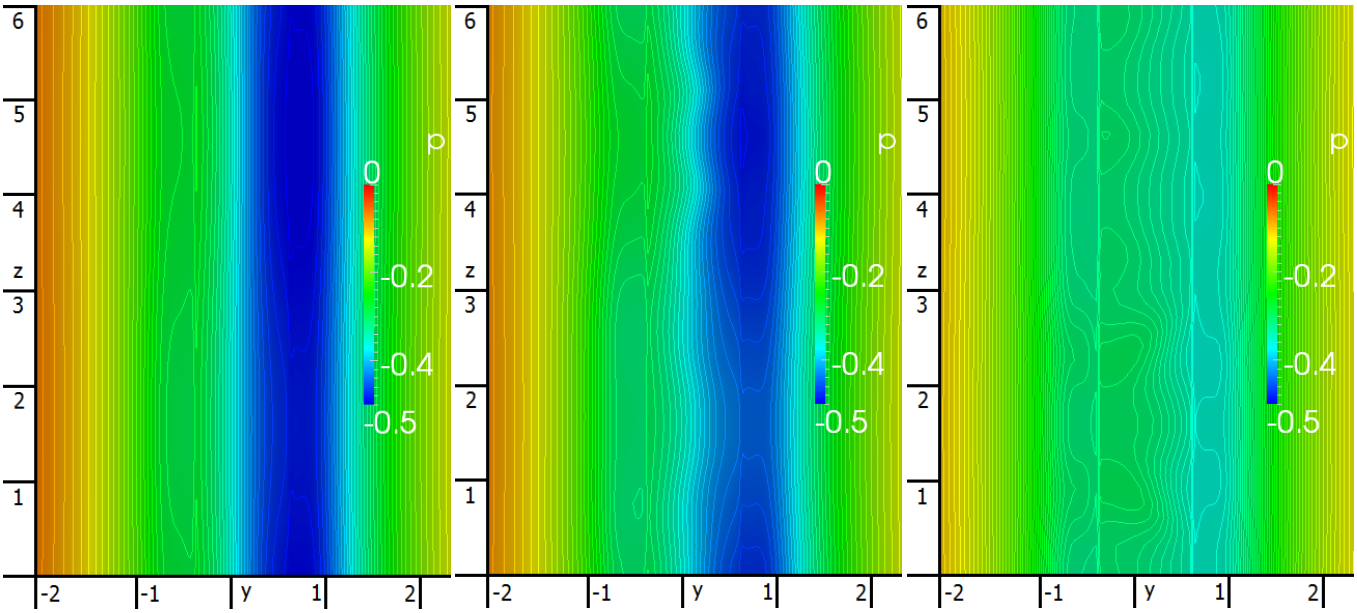

Figure 4.4: Pressure contours on downstream face of cylinder

Figure 4.4 shows the pressure on the downstream face of the cylinder for three time steps which all correspond to instants of maximum drag and lift (i.e. maximum unsymmetry), but different states of flow development. Left: t = 98 (2D region), C_D = 1.536, Δp = 0.01; middle: t = 233 (HF region), C_D = 1.504, Δp = 0.01; right: t = 187 (LF region), C_D = 1.398, Δp = 0.005. At this low Reynolds number the viscous part of the drag is insignificant [8], [12]. The main part of the drag comes from the pressure differential between the upstream and downstream faces of the cylinder. Since the pressure on the upstream face is approximately the same for all three time steps, the pressure on the downstream face is what dictates the difference in force between the three.

Although not entirely obvious from the figure, there is a larger spanwise variation of pressure in the LF region, shown by the pressure contours. But, more importantly it seems, the mean value of the pressure in the LF region is notably higher (lower absolute value), shown by the color grading. In fact, the difference between HF and LF is much bigger than the difference between HF and the 2D region.

We can also see that what we call a ‘2D region’ is not entirely two-dimensional, but figure 4.6 shows that the three-dimensionality is insignificant compared to the HF and LF regions. Although $|y| > 2$ is chopped off in figure 4.4, we can also see that the kinematic pressure will approach zero as we move away from the centerline.

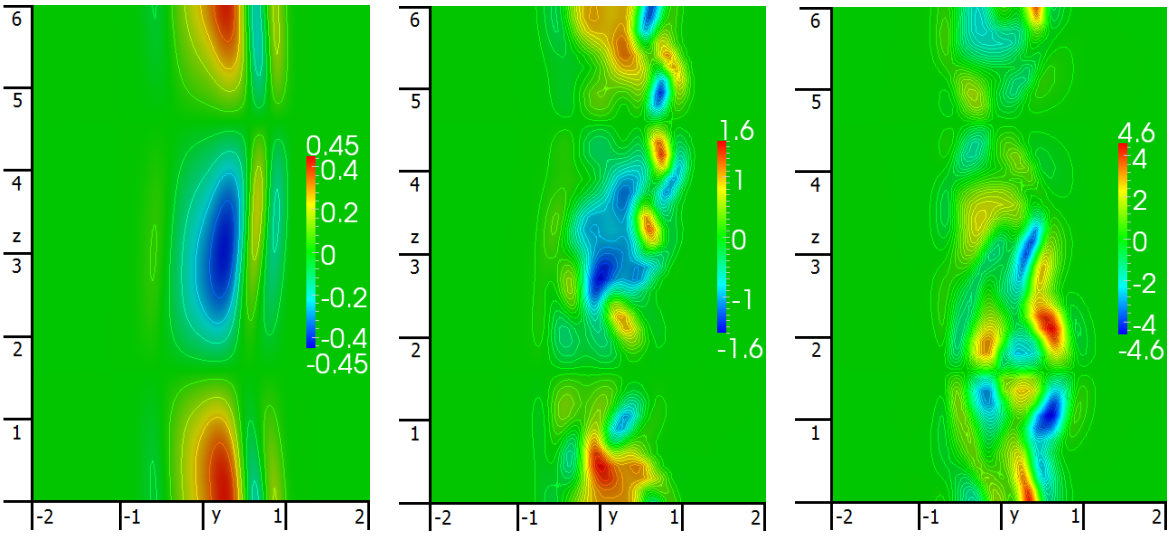

Figure 4.5: Streamwise vorticity (ω_x) in x = 2.5 (2D downstream)

Figure 4.5 shows streamwise vorticity two diameters downstream of cylinder1. Left: t = 98 (2D region), $\Delta\omega_x$ = 0.1; middle: t = 233 (HF region) $\Delta\omega_x$ = 0.1; right: t = 187 (LF region), $\Delta\omega_x$ = 0.2. Here we have siginificant 3D effects. Even the 2D region seems to have quite a bit of three-dimensionality, but it is important to notice the different scales on the figure. ω_x in the 2D region is three to four times smaller than in the HF region, which again is about three times smaller than in the LF region. The vortices in the LF region are much more intense. This could suggest that for an LF region the point of transition to 3D flow is further upstream than in an HF region.

In the 2D region we see an obvious mode A wave with wavelength six diameters. This mode A instability is what triggers the three-dimensionality we see in the middle and right part of figure 4.5. The calculations by Sohankar et al. (feb 1999) [12] also exhibited a mode A wave with wavelength six diameters for A = 6. In their calculation with A = 10 the corresponding mode A wavelength was five diameters. This suggests that the wavelength is directly related to the aspect ratio.

In the HF region we can still make out a mode A wave, but in addition we can notice short wavelength mode B instabilities with wavelength around one diameter. This implies that the onset Reynolds number for mode B instabilities is less than 200 in the present study. This is contrary to Luo et al. [17] who through experiments found the critical Reynolds number for onset of mode B instabilities to be 204 and Saha et al. [18] whose calculations exhibited mode B instabilities from Re = 250 upwards. The fact that the study by Luo et al. is experimental and the present study is numerical is enough to account for that discrepancy.

Both 3D regions look fairly chaotic compared to the 2D region, but the vorticity is three times stronger in the LF region. Also, the mode A wave is less apparent in the LF region than the HF region, the LF region being dominated by mode B stuctures.

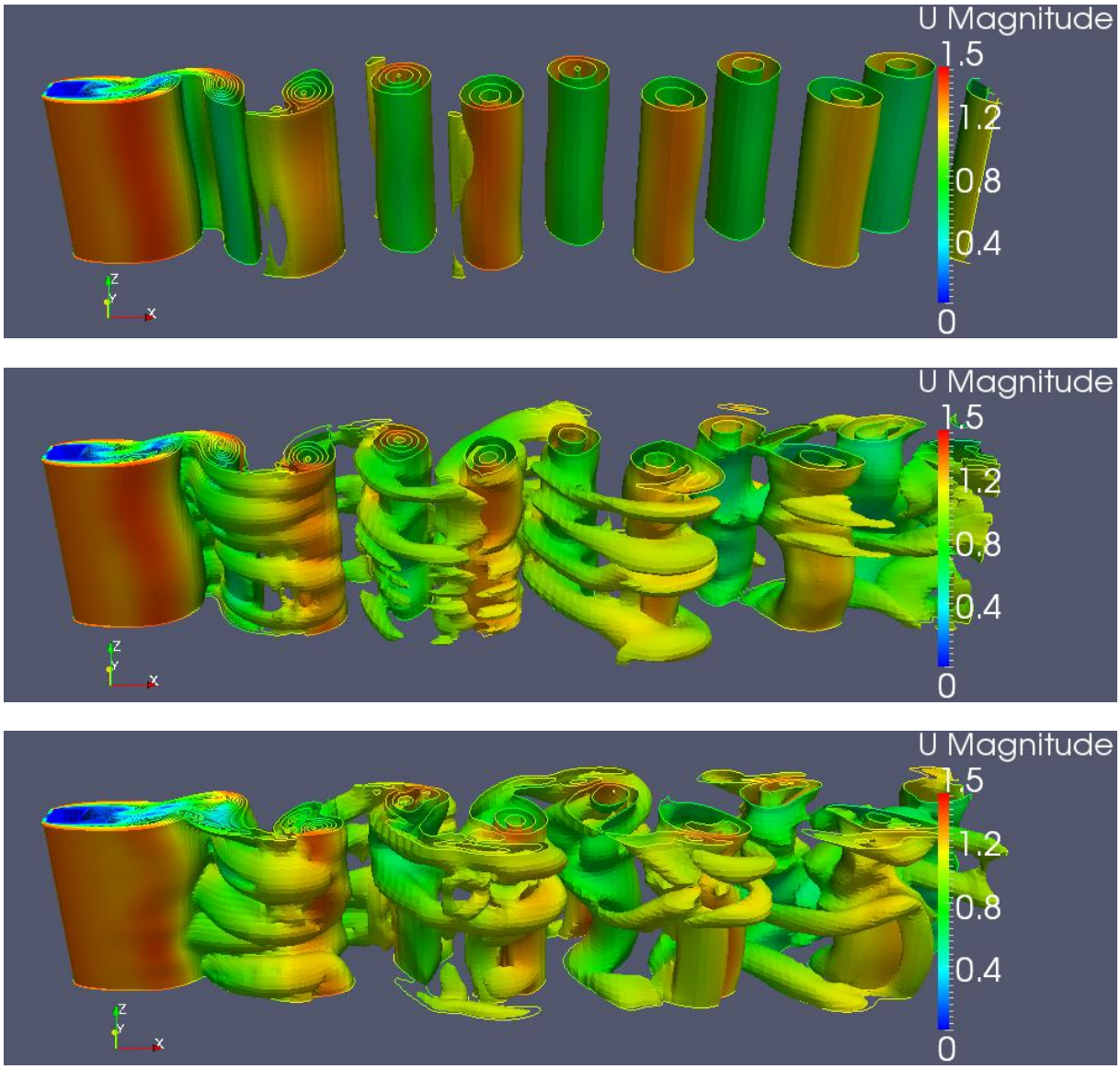

Figure 4.6: Contours of vorticity magnitude with color by the velocity magnitude

Figure 4.6 shows contours of vorticity magnitude. Notice that the contours are colored by velocity magnitude. Top: t = 98 (2D region); middle: t = 233 (HF region); bottom: t = 187 (LF region). $\Delta\omega_{mag} = 0.35$. In the 2D region we can see tiny indications of 3D-effects in the wake, but the wake is essentially, though not 100 %, two-dimensional. In the shear layer on the cylinder's left (seen from the wake) small signs of a mode A wave can be seen. This is the mode A wave seen in figure 4.5 left.

In this figure it seems the biggest difference is between the 2D region and HF/LF, while previous discussions in this chapter have pointed towards a bigger difference between LF and HF/2D. That is because we so far have compared the near wake and the pressure on the cylinder itself, while we in figure 4.6 mainly notice the far wake, which is highly three-dimensional both for HF and LF. Still, the HF seems a little bit more ordered. In the shear layer on the cylinder's left we notice the same mode A wave as in the 2D region, but it is a bit

more apparent. In the LF region there are signs of both mode A and mode B waves in this shear layer.

The suggestion that the point of transition to 3D is closer to the cylinder in the LF region is not very apparent in figure 4.6. And this would not explain the 2D pulsations, only the 3D pulsation. But comparing the near wake parts we can see that in the LF region the shear layers seem stretched compared to the 2D and HF regions. Could the explanation be that the shear layers are subsequently stretched and compressed during a pulsation period? To investigate this we look at spanwise vorticity (ω_z) in a cut at the midspan (z = 3) for the three time steps.

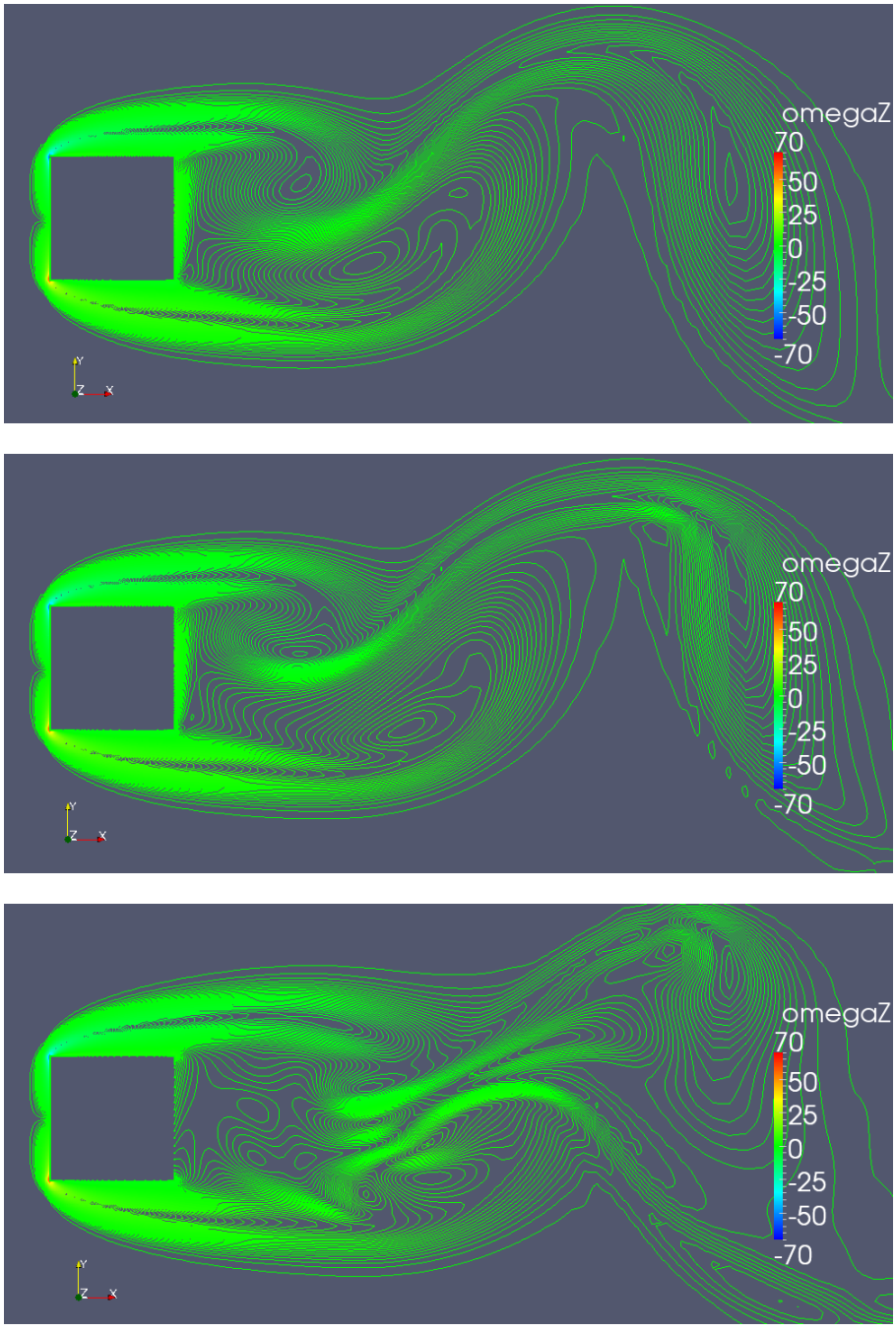

Figure 4.7: Spanwise vorticity (ω_z) at z = 3 (midspan)

Figure 4.7 shows spanwise vorticity, ω_z, at the midspan. All three time steps correspond to instants of maximum lift. Top: t = 98 (2D region), C_L = 0.601; middle: t = 233 (HF region), C_L = 0.502; bottom: t = 187 (LF region), C_L = 0.127. $\Delta\omega_z$ = 0.14. Comparing the top and middle figures we see once again that the difference between the 2D region and the HF region seems smaller than between HF and LF. The shear layer from the upper side of the cylinder rolls up closer to the centerline in HF region than in the 2D region. This pushes the core of the lower side vortex further away from the centerline and also further downstream (see table 4.2). Also, the first detached vortex looks a bit more deformed in the HF plot than the 2D plot. Otherwise the plots look pretty similar. A comparison between the middle and bottom figures shows that the flow in the LF region is noticeably more chaotic. The most interesting result is that the shear layers do not develop in exactly the same way in the HF and LF regions. For LF we can clearly see that the shear layers extend further downstream before rolling up to von Kármán vortices. This is especially apparent for the shear layer from the upper side cylinder. The distance from the cylinder to the vortex cores is higher for LF than HF. The implication is that the energy of the vortices is spread further downstream in the LF-region, giving smaller forces (both means and fluctuations). In the 2D and HF regions the energy is concentrated closer to the cylinder. The position of the vortex cores in the three regions is shown in table 4.2.

Region	x-position of upper vortex core	x-position of lower vortex core	y-position of upper vortex core	y-position of lower vortex core
2D	1.5	2	0.3	-0.35
HF	1.5	2.4	0.1	-0.5
LF	2.1	2.5	0.25	-0.45

Table 4.2: Position of vortex cores for 2D, HF and LF regions

Another implication of the fact that the first vortex (upper) rolls up closer to the cylinder in the HF region than in the LF region, is that the frequency of vortex shedding will be lower in the LF region than in the HF and 2D regions. This is what was observed when inspecting the drag and lift signals. This was also observed by Sohankar et al. (jul 1999) [13].

So, we see that the reason for the pulsation is the motion of the position where the shear layers roll up. This happens both for 2D and 3D flow (see chapter 4.4 and 4.7 for discussions on 2D pulsations), but it appears in slightly different fashions in the two cases.

Going back to figure 4.3 we see that for drag the fluctuations are notably larger in HF regions than in LF regions. For lift we see that the envelope curve decreases faster than it increases. The lift signal has a beginning sawtooth shape. Since sawtooth waves are created by a sine wave and its harmonics, one could think that the pulsation is the base wave and the vortex shedding is the harmonic. In this case we have $f_v = 9.5 \cdot f_p$, so not strictly a harmonic, but a combination of two such waves will give a slight sawtooth shape.

One would of course expect larger fluctuations at points of time where the mean force is high, i.e. in HF regions, and the opposite in LF regions, but the ratios of fluctuations and means are

much larger than can be accounted for only by the variation in mean force. Inspecting the drag signal these values were found:

C_D average HF region	1.504
C_D average LF region	1.398
Ratio of averages	**1.076**
C_D amplitude HF region	0.052
C_D amplitude LF region	0.0023
Ratio of amplitudes	**22.6**

Table 4.3: C_D in HF and LF regions

A low ratio of averages would be expected as the main part of the drag on the cylinder does not come from the vortex shedding anyway. For lift the difference between HF and LF regions is much higher. The mean is of course zero, so we can only compare rms values. With C_L rms HF = 0.502 and C_L rms LF = 0.127 we get a ratio of about 4. It seems the stretching and compression of the shear layer has a fundamental effect on the fluctuating drag. Two possible reasons are that the drag might be more sensitive to variation on three-dimensionality in the flow, and it might be affected more because it points in the main flow direction (x-direction).

From figures 4.6 and 4.7 one could conclude that there are two contributors to the lower force levels and fluctuations in the LF regions: a) the vortices are stretched; their energy is spread over a larger area and further downstream, and b) the higher three-dimensionality reduces the spanwise coupling of forces.

4.3 TCE_4D

For the highest separation distance investigated in this study, S/D = 4, we observe both the 3D effects and pulsations seen for OneCyl. Interestingly, and perhaps worryingly, this case needed a slightly unsymmetric inflow (u = 1, v = 0.01) to trigger 2D vortex shedding. With a completely symmetric inflow the strange results was that only 3D vortex shedding was triggered. This was the only case which needed such treatment.

One would be inclined to wonder how big a difference there is between TCE_4D and OneCyl. How much does the second cylinder in the wake affect the upstream cylinder? Must the separation S/D be much higher before the cylinders get completely independent? Table 4.4 shows a comparison of C_D ave, C_D rms, C_L rms, St and T_p (pulsation period) for OneCyl and TCE_4D. For TCE_4D only the forces on cylinder1 are considered of course. Note that the average and rms value for the 3D region might be affected by a finite averaging period.

Case	C_D ave 2D	C_D ave 3D	C_D rms 2D	C_D rms 3D	C_L rms 2D	C_L rms 3D	St	T_p
OneCyl	1.494	1.445	0.030	0.031	0.429	0.272	0.148	64
TCE_4D	1.479	1.435	0.066	0.036	0.668	0.528	0.133	64

Table 4.4: Force coefficients, St and T_p for OneCyl and TCE_4D

Values for C_D average are very similar both in the 2D and 3D part of the flows (around 1 % difference). However, the rms values for both drag and lift are in general very different, with the exception of C_D rms 3D. The C_D and C_L signals for both cases are shown in figure 4.8.

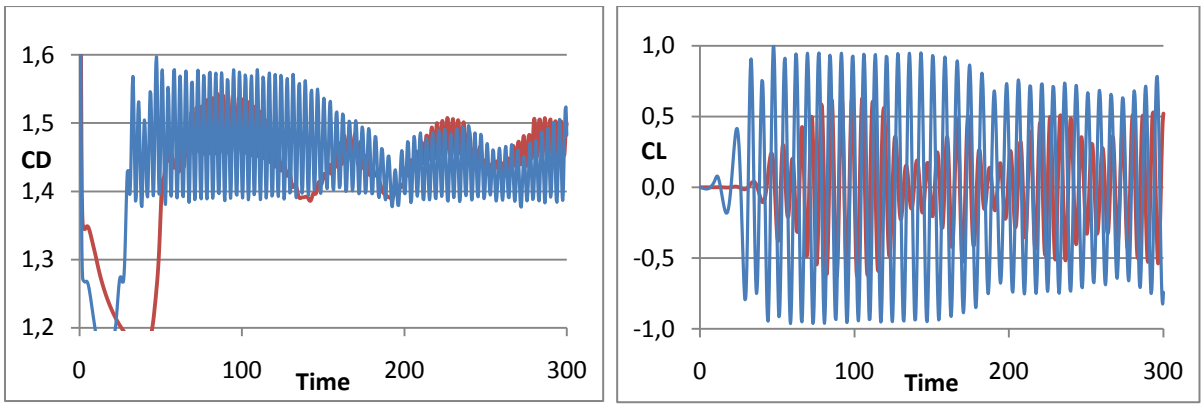

Figure 4.8: C_D and C_L signals for OneCyl (red) and cylinder1 in TCE_4D (blue)

From figure 4.8 we can clearly see that the rms lift and drag values are much higher for TCE_4D, while the average drag values are more similar. It is evident that cylinder2 has a large effect on the flow; at least the fluctuations. The average drag values being so similar suggests that the average pressure field on the downstream face of cylinder1 in TCE_4D is pretty similar to that on the downstream face of OneCyl. For such a low Reynolds number as used in this study, the frictional contribution to the total drag is negligible [8], [9], [10], and

the pressure on the upstream face will the constant stagnation pressure. Thus the main contribution to drag comes from the lower pressure, i.e. suction, on the downstream face.

The pulsation periods for TCE_4D and OneCyl are equal whereas there is a little difference in Strouhal number. The former could indicate that the pulsation period is controlled only by cylinder1. That is, it is the stretching and compression of the wake of cylinder1 which creates the pulsation. As for the Strouhal number it seems cylinder2 has an effect, lowering St by about 10 % compared to OneCyl.

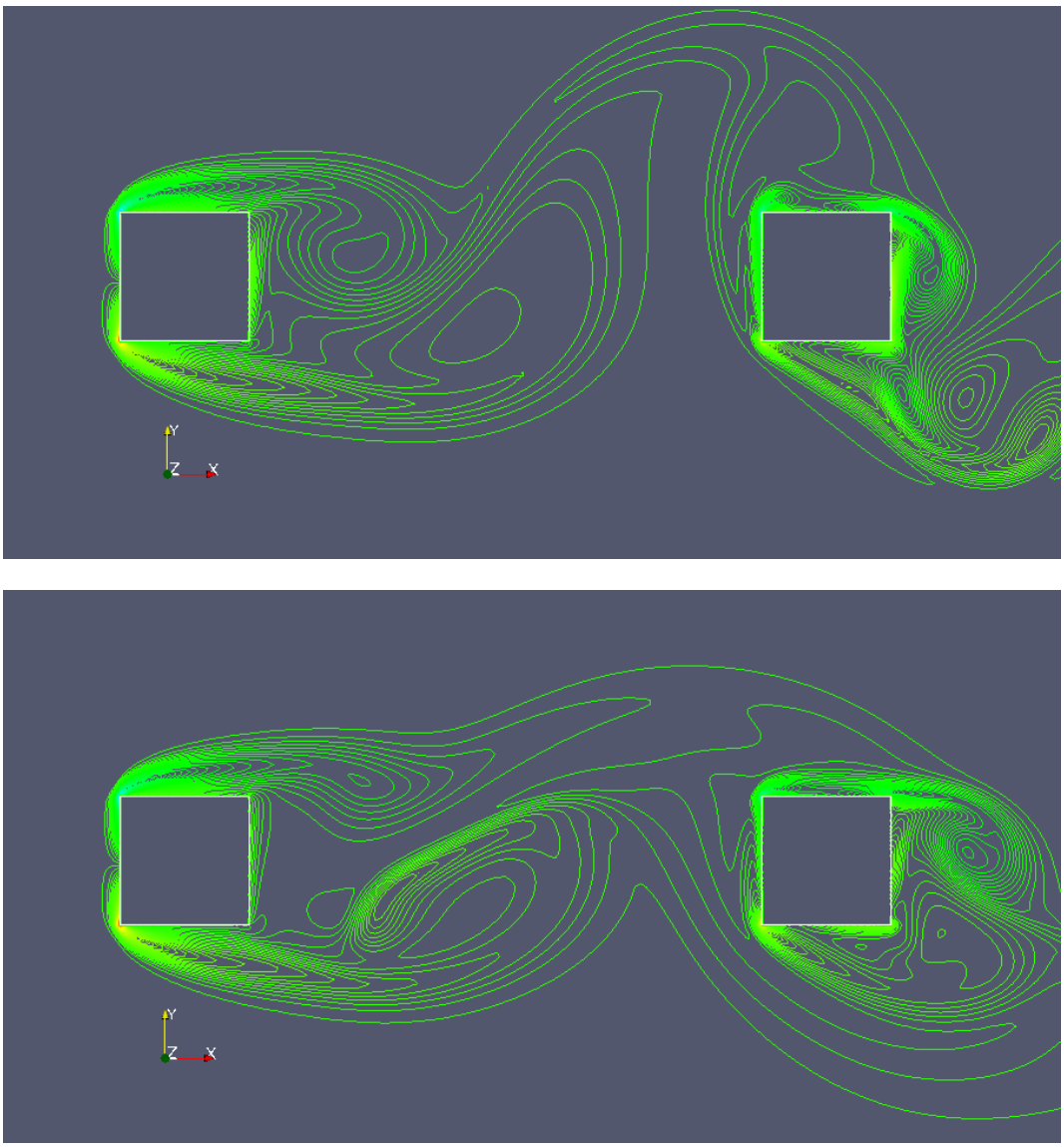

Figure 4.9: Spanwise vorticity (ω_z) at z = 3 (midspan)

Figure 4.9 shows contours of spanwise vorticity (ω_z) in HF and LF regions, respectively. The time steps correspond to instants of maximum lift. Top: t = 303 (HF region), C_L cyl1 = 0.812; Bottom: t = 198 (LF region), C_L cyl1 = 0.684. Whereas for OneCyl it was pretty straight

forward to see that the near-wake of cylinder1 goes through a series of stretching and compression during a pulsation period, this is not easy to see here. In fact, the biggest difference is that for HF the wake seems to be wider. This is in contrast to OneCyl where the wake was at its widest in the LF region. It is clear that cylinder2 has a great effect on the flow. At S/D = 4 the cylinders are far from being independent.

Looking at the numbers, we see that the difference in forces between the HF and LF region is notably smaller than for OneCyl. The lift coefficient is 16 % lower in the LF region for TCE_4D and 75 % lower for OneCyl. The corresponding values for drag are 5 % for TCE_4D and 7 % for OneCyl. For TCE_4D the average and rms values of forces are larger, but the difference between HF and LF regions is smaller. It should be noted, however, that the finite time span for calculation of averages and rms values could affect the results. Simply, the LF region chosen for OneCyl may be a more extreme LF region than the LF region chosen for TCE_4D, and similarly for the HF region.

The TCE_4D case is characterized by high levels of forces and large force fluctuations. Table 4.5 shows average drag and rms drag and lift for the two cylinders in both 2D and 3D regions. Notice that these are averages over the whole 2D and 3D periods whereas the HF and LF regions are extreme cases in within the 3D region.

	2D region	**3D region**
C_D ave cyl1	1.479	1.435
C_D rms cyl1	0.066	0.036
C_L rms cyl1	0.668	0.528
C_D ave cyl2	2.226	1.568
C_D rms cyl2	0.427	0.286
C_L rms cyl2	1.927	1.729

Table 4.5: Average force coefficients for TCE_4D

From table 4.5 we can see that the transition from 2D to 3D has a much larger effect on cylinder2. The spreading of forces and lower spanwise coupling of forces in a three-dimensional flow will have a great effect on cylinder2. The high degree of three-dimensionality in the 3D region (both HF and LF) can be seen in figure 4.10 below.

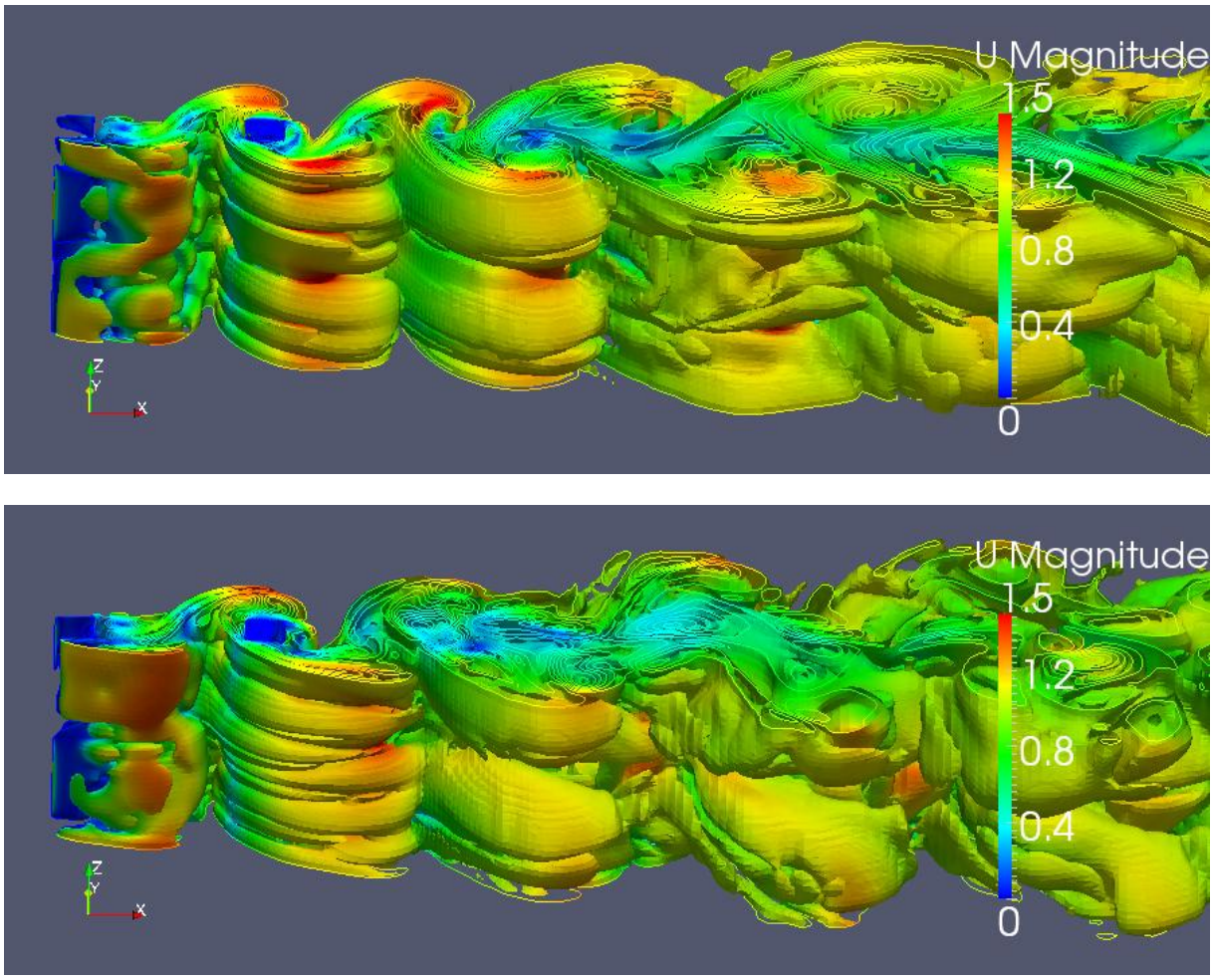

Figure 4.10: Contours of vorticity magnitude colored by velocity magnitude

Figure 4.10 shows contours of vorticity magnitude colored by velocity magnitude for HF (top figure) and LF region (bottom figure). We clearly see the high degree of three-dimensionality in the flow. There seems to be a higher number of mode B instabilities for TCE_4D than for OneCyl; see figure 4.6. In the shear layer on the left side of cylinder2 (seen from the wake) we see a mode A instability with wavelength of about six diameters (like in figures 4.5 and 4.6) and mode B instabilities with wavelength about one diameter. The mode B waves seem to develop in the shear layer on the left side of cylinder2 and they seem to be dominant within a region close this cylinder. Further downstream there is a mix of mode A and mode B structures. This is the same as demonstrated in Henderson (1997) [15].

When we see how three-dimensional and chaotic the flow seems around cylinder2, one would wonder whether a higher spanwise resolution is required. I did a run with $N_z = 80$ and found no appreciable difference. $N_z = 40$ was considered sufficient. As mentioned before there is also a trade-off in terms of calculation time which needs to be considered.

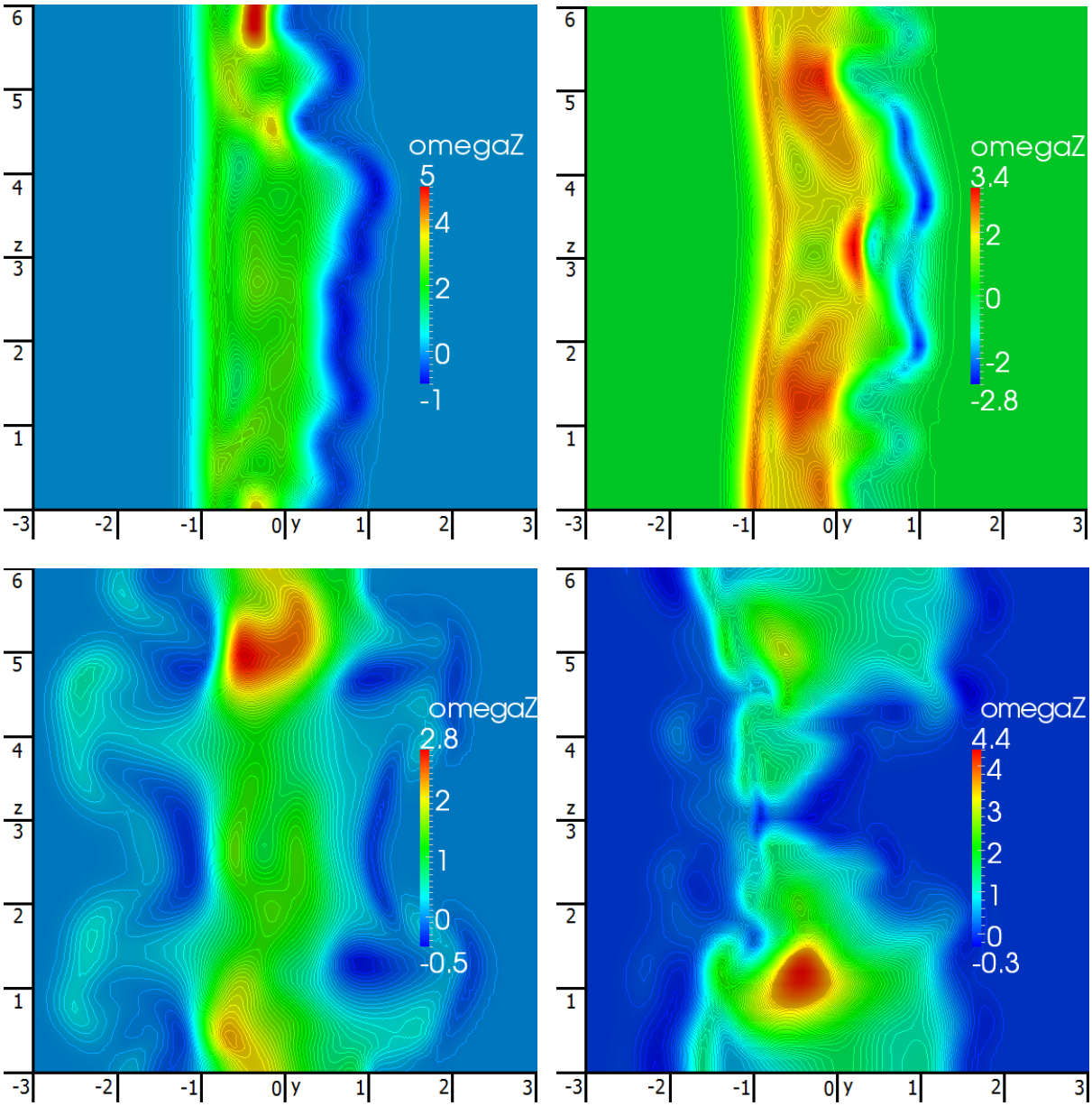

Figure 4.11: Streamwise vorticity (ω_x) 2D downstream of each cylinder for HF and LF

Figure 4.11 shows streamwise vorticity (ω_x) at positions 2D downstream of each cylinder in HF and LF regions. Top left: x = 2.5 in HF region; top right: x = 2.5 in LF region; bottom left: x = 7.5 in HF region; bottom right: x = 7.5 in LF region. Notice the difference in color in the plots because only the color scale for the top right figure has zero in the middle. It is difficult to extract a deep meaning out of figure 4.11, but comparing the total range in the four cases we get 6 and 6.2 in x = 2.5 in HF and LF, respectively. In x = 7.5 the corresponding values are 3.3 and 4.7. The intensity of the vorticity seems to be lower 2D downstream of the second cylinder than 2D downstream of the first one, and the difference between HF and LF regions seems to be higher at x = 7.5. Also we can see that the vorticity spreads out further from the centerline (y = 0) in x = 7.5.

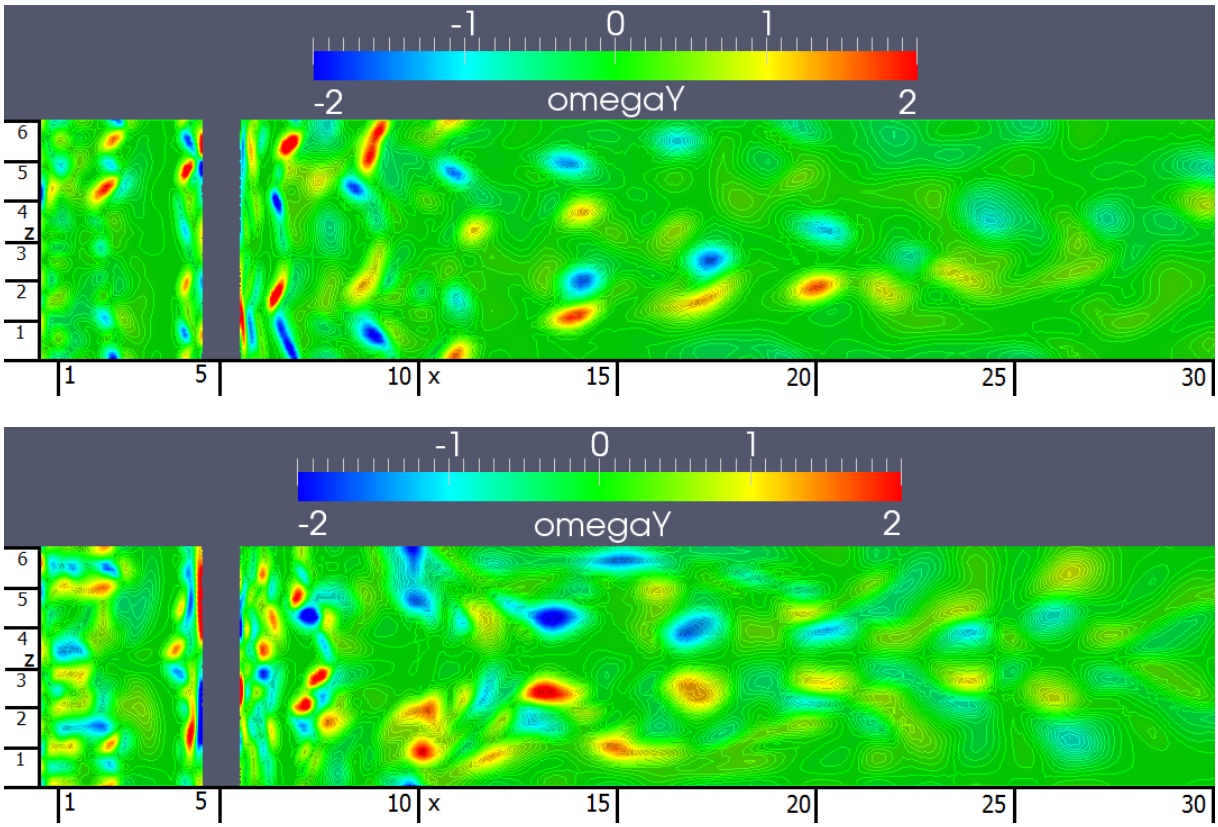

Figure 4.12: Cross stream vorticity (ω_y) in y = 0 in HF (top) and LF (bottom) region

Figure 4.12 shows cross stream vorticity (ω_y) in y = 0. The figure only shows the domain downstream of cylinder1 as the vorticity is negligible upstream of that cylinder. It is clear to see from this figure that the difference between the HF (top) and LF (bottom) regions is smaller for TCE_4D than for OneCyl (see e.g. figure 4.5 and 4.6). The higher concentration of mode B instabilities in the near wake, as seen around cylinder2 in figure 4.10, can also be seen here. This figure shows that they are also present in the wake of cylinder1. Further downstream of cylinder2 we see a mix of mode A and mode B wavelengths. There seems to be an additional intermediate wavelength of about three diameters in the far wake (around x = 25). This intermediate wavelength has also been reported by Robichaux et al. (1999) [20].

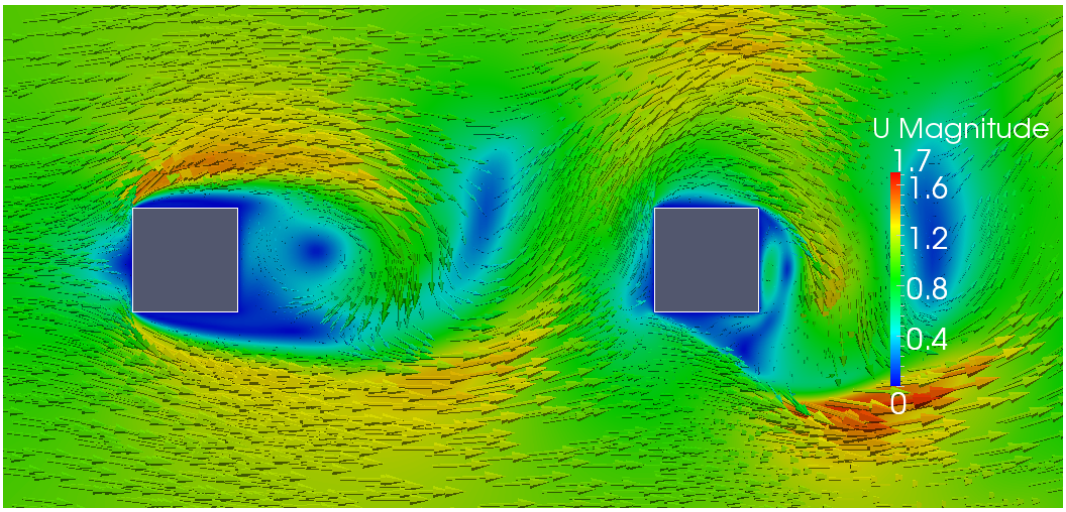

Figure 4.13: Velocity vectors and velocity plot colored by velocity magnitude for HF

From table 4.5 we also see the large average and rms drag, and rms lift, on cylinder2. As can be seen in figure 4.13, for the HF region, the vortex shedding flow from cylinder1 creates large cross stream velocity in its wake (comparable to the streamwise velocity), and an arc of high velocity flow over one side of cylinder2 and low velocity on the opposite side. This creates large pressure differentials which give large forces. Another way of seeing this is that the combined streamwise and cross stream velocity create a flow with large angle of attack on cylinder2. As this swings from one extremity to the other, we get large fluctuating forces and large average drag.

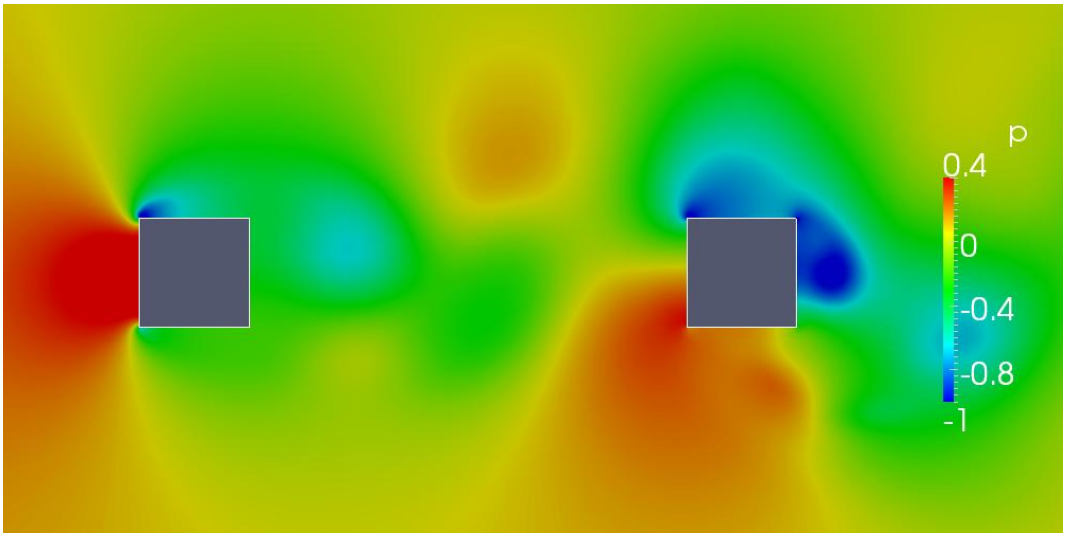

Figure 4.14: Pressure plot in HF region

Figure 4.14 shows the corresponding pressure plot. The color grading range has slightly clipped ends for better emphasis on the pressure around cylinder2. The high and low pressure

zones are evident in this figure. Also evident from the figure is the fact that the pressure variations are, as expected, significantly larger on cylinder2 than cylinder1.

4.4 TCE_3D

First of all, notice the two different meanings of 3D: “Three-dimensional” and “S/D = 3”. The flow for S/D = 3 exhibits the double vortex shedding seen in the previous section. Unlike TCE_4D this case does not exhibit any 3D effects, but pulsations are still present; see figure 4.4 and 4.5. As discussed previously, the pulsations are part of the transition from 2D to 3D flow and can be observed both in the 2D and 3D part of a transitional flow (like in figure 4.3). It seems at lower separation distances the pulsations cannot trigger 3D effects for some reason.

One possible reason is that when S/D decreases the necessary aspect ratio to trigger mode A instabilities increases. As stated in Barkley & Henderson (1996) [19] for CC flow the necessary aspect ratio is about 4 diameters at onset and increases to 6.7 diameters at Re > 300. The decreasing separation distance could have a similar effect. More about this later.

The flow still exhibits the double vortex shedding seen for S/D = 4. At some point one would expect a transition to single vortex shedding, i.e. vortex shedding only from cylinder2.

In the force coefficients plot in figures 4.15 and 4.16 we can clearly see that several frequencies are involved in both the lift and the drag signal for both cylinders.

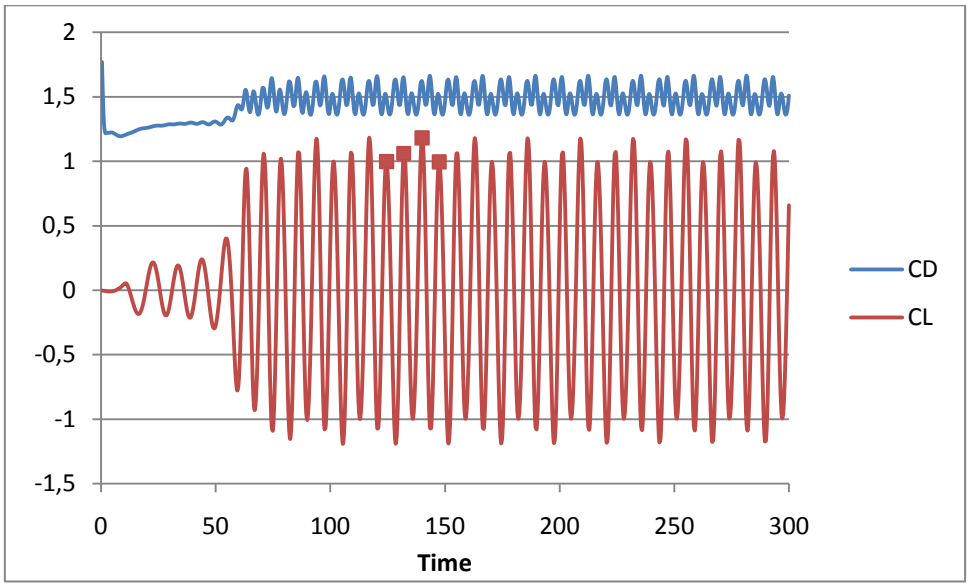

Figure 4.15: C_D and C_L signal for cylinder1 for S/D = 3

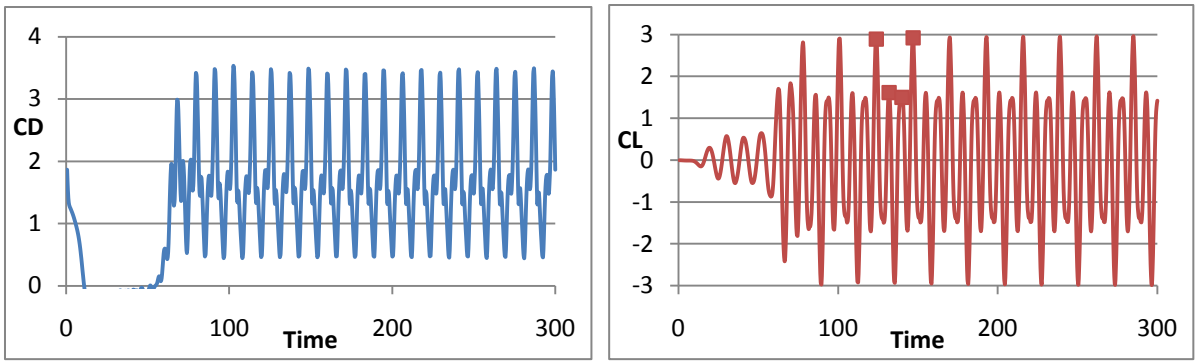

Figure 4.16: C_D (left) and C_L (right) signal for cylinder2 for S/D = 3

Comparing the lift signals for the two cylinders we see a phase shift between them. The highest peak during a pulsation period for cylinder2 trails the highest peak for cylinder1 by one vortex shedding period; about 7.5 time units (third and fourth squares in figures 4.15 and 4.16 (left), respectively). Note that data were written to file only every second, so the times do not correspond to the exact peaks, but they are pretty close, and close enough.

All signals exhibit sawtooth shapes, just like we see for OneCyl (figure 4.3). Since a sawtooth wave comprised of a sine wave and its harmonics, we would expect there to be several harmonics in action, or at least several frequencies even if they are not harmonics. Figure 4.17 shows the spectral densities for all four force signals from an FFT analysis in Excel.

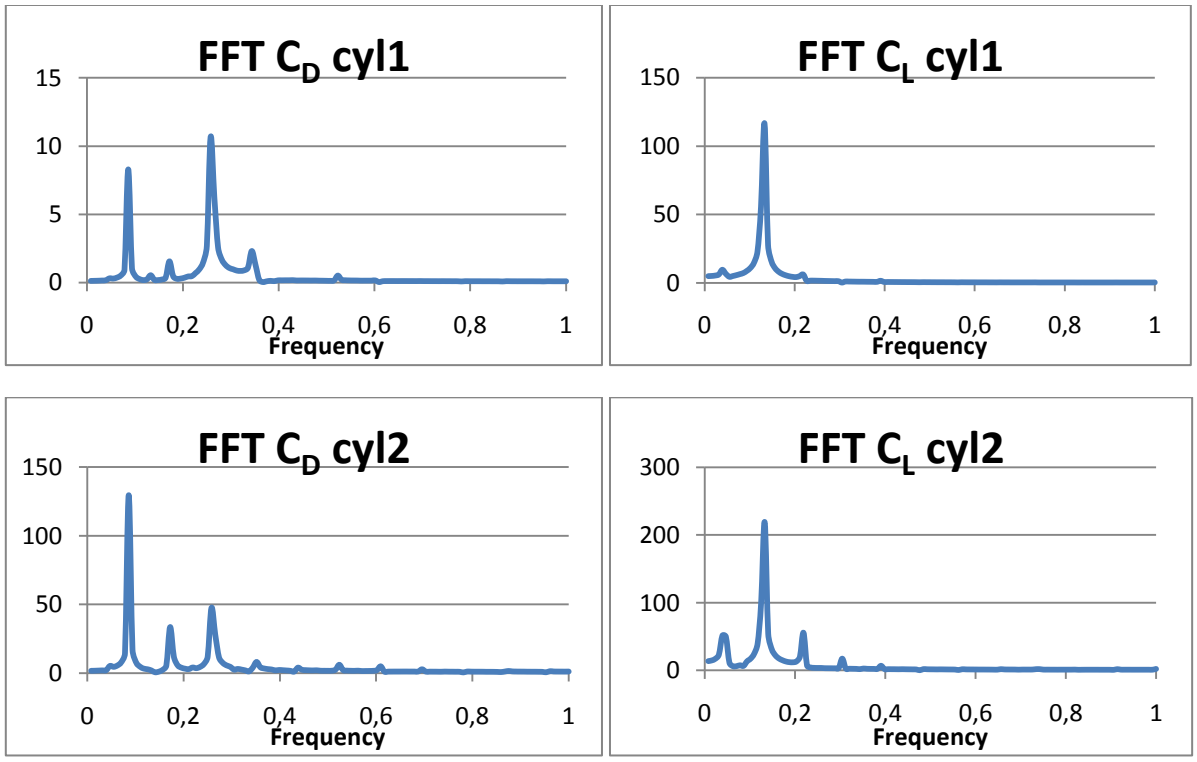

Figure 4.17: Spectral densities for the drag and lift signal for S/D = 3

The spectral density for C_L on cylinder1 has the most notable peak, and determines the value of the Strouhal number as St = 0.133 ($T_v \approx 7.5$ time units). The same frequency is found from the highest peak in the spectral density for C_L on cylinder2. Both lift signals are dominated by energy around the shedding frequency with only tiny peaks on either side. Strangely, these peaks correspond to 0.294·St and 1.647·St, respectively. However, very little energy is associated with these.

Both drag signals exhibit four peaks in the spectral density (albeit some of them rather small). The second, third and fourth peaks are the first three harmonics of the first peak. The first peak has frequency 2/3·St, the second 4/3·St, the third 2·St and the fourth 8/3·St. In other words, the second, third and fourth frequencies are the first three harmonics of the first frequency. The majority of the drag fluctuating energy is concentrated around 2/3·St and 2·St (first and third peaks). When inspecting the force signal plots, and especially figure 4.16 (right) for C_L on cylinder 2, we can clearly see a pulsation in lift with a frequency 1/3·St. Since fluctuating drag has twice the frequency of lift, the 2/3·St peak for drag corresponds to the most apparent pulsation frequency and the 2·St peak corresponds to the vortex shedding frequency. With St = 0.133, the pulsation period $T_p \approx 22.5$ time units. This is quite a bit lower than the 64 second pulsation period found for both OneCyl and TCE_4D.

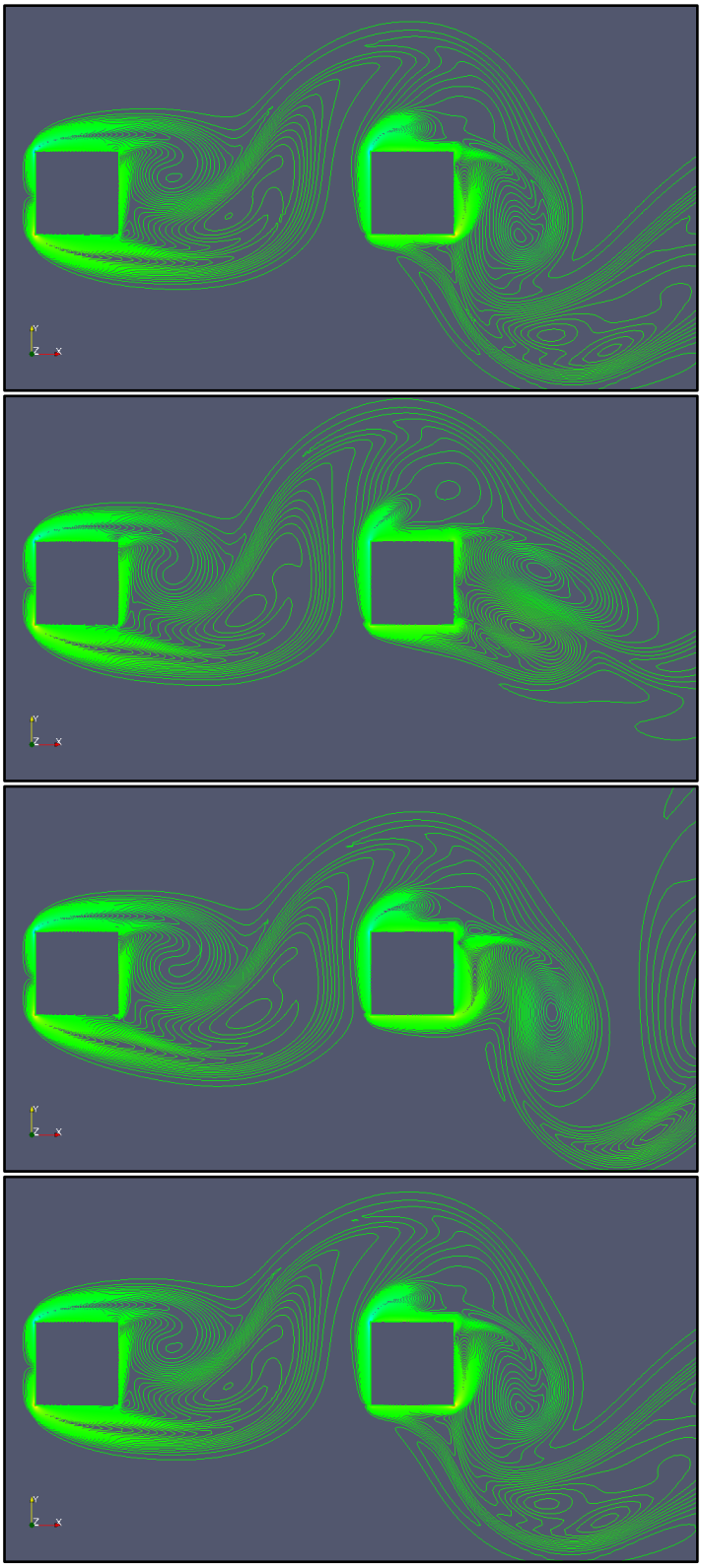

Figure 4.18: Contours of streamwise vorticity (ω_x) at z = 3 (midspan)

Figure 4.18 shows contours of streamwise vorticity, ω_x, at the midspan for the four peaks inducated by squares in figures 4.15 and 4.16 (right) – instants of maximum lift. Top: t = 124; second: t = 132; third: t = 140; bottom: t = 147. $\Delta\omega_x$ = 0.28. The figure covers four vortex

shedding periods and one pulsation period. Thus, the first and fourth plot (first and fourth peaks in figures 4.15 and 4.16 (right)) correspond to the same stage in both vortex shedding and pulsation, and they look very similar. Comparing these two to the middle ones, there are some obvious differences.

Firstly we look at cylinder1. In the first and fourth plots we can see that the lower vortex is shorter than in the seond and third plots. This causes a higher opposing force to the upper vortex and reduces the lift. In the second plot the lower vortex is stretched, giving a lower opposing force and increasing the lift. In the third plot the lower vortex is even more stretched, increasing this effect. Thus, we see that the development *low, medium, high, low* of lift on cylinder1 can be understood from the vorticity plots.

For cylinder2 the situation is a bit trickier as the flow is more chaotic around this cylinder. The lift force development for cylinder2 is *high, low, low, high*. The first and fourth plots are very similar, as they correspond to the same stage in both vortex shedding and pulsation. But comparing the second and third plots with each other and with the first and fourth is not straight forward. There are several effects which work in conjuction to give the final results and it is difficult to directly see this result from the plots.

From figure 4.16 we can also see that the mean drag force and force fluctuations on cylinder2 are very large, like for TCE_4D. Just like in that case, cylinder2 will be affected by both its own vortices and, most importantly, the highly angled flow from cylinder1. The nature of the double vortex shedding regime seems to be very violent. This will also be brought up in chapter 4.6.

4.5 TCE_2D

Whereas all other TCE cases needed less than 100 time units to reach fully saturated state, i.e. a state where memory effects from the startup are negligible, the TCE_2D case needed almost 700 time units. This case exhibits none of the pulsation effects seen in the previous chapters. The levels of forces are very small for S/D = 2. That is evident from figure 4.19 below.

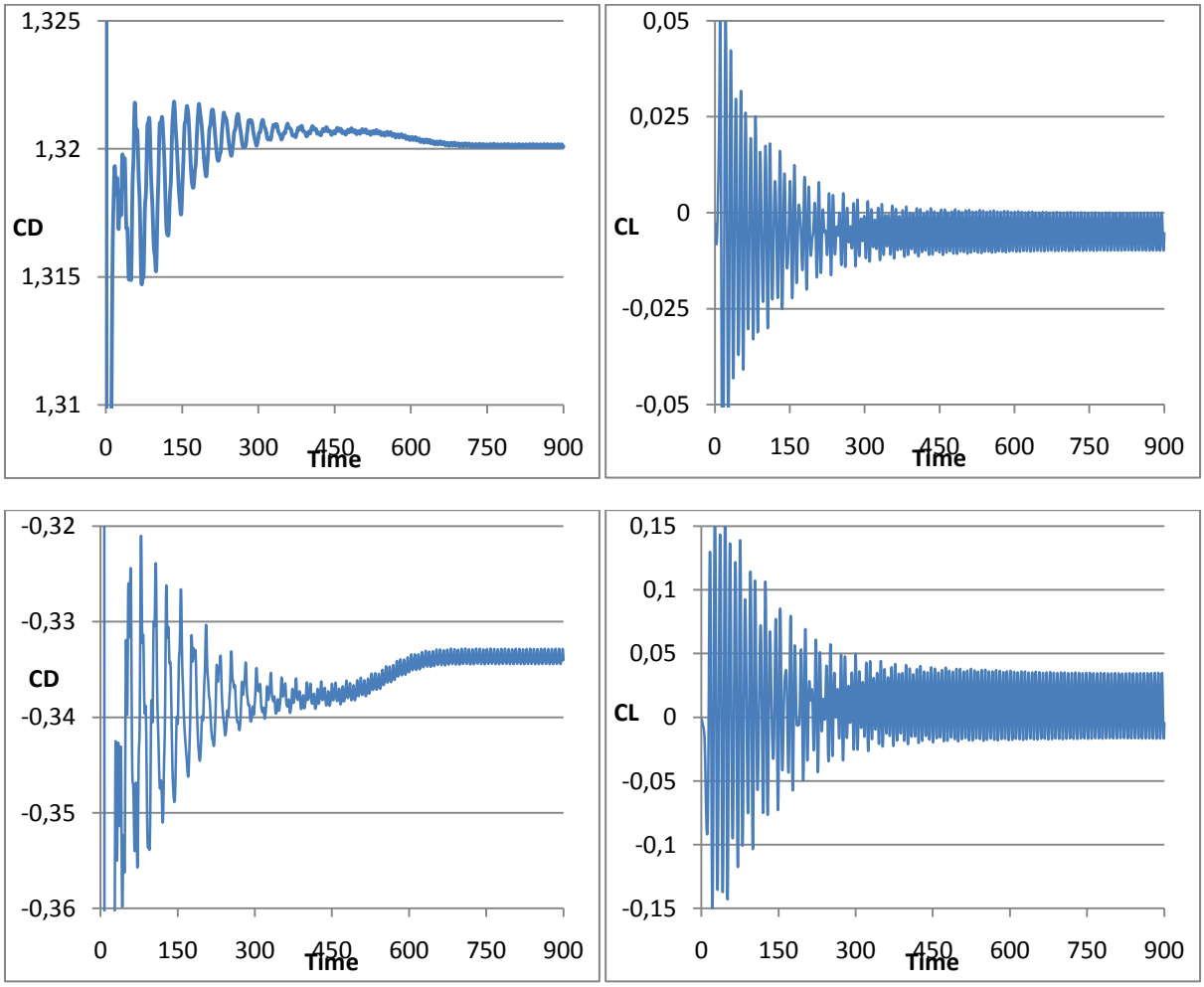

Figure 4.19: C_D and C_D signals for cylinder1 (top) and cylinder2 (bottom) for TCE_2D

The startup looks very different from the other cases. The fluctuations seem to build up to some level pretty quickly and then decrease in an exponential-like fasion. The forces settle down at around t = 500, but then, over a time period of about 150 time units, cylinder1 experiences a decrease in C_D and cylinder2 an increase in C_D. The drag values are affected to a much greater degree than the lift values.

One of the advantages of CFD compared to experiments is that one has information of the whole flow field at all times; even the startup. Figure 4.20 shows the first 128 time units (256 values, since the data are written to file twice per second in this case) of the development of C_D and C_L for cylinder2. The signals for cylinder1 exhibit similar behavior.

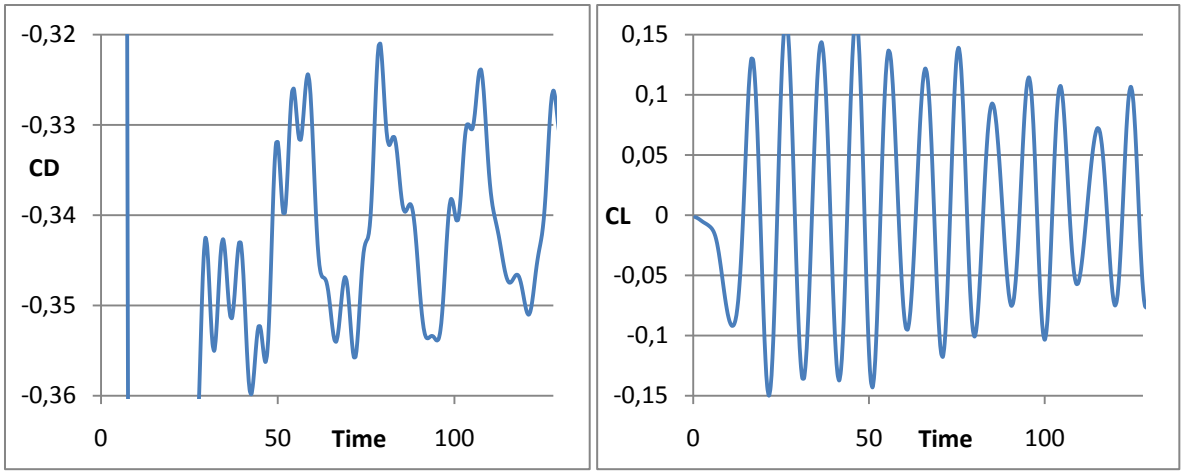

Figure 4.20: C_D (left) and C_L (right) for cylinder2 during startup

From figure 4.20 we see that the lift signal has one main frequency and at least one additional weaker frequency. The drag signal, however, seems have many frequencies. To investigate this I did an FFT analysis in Excel. I have chosen 256 values because the FFT tool requires the number of values to be a multiple of 2. The results are shown in figure 4.21.

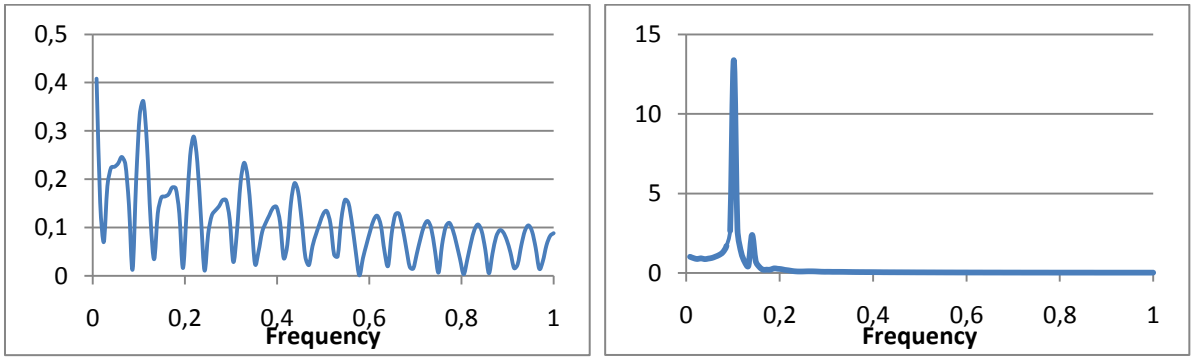

Figure 4.21: Spectral densitites for C_D (left) and C_L (right) for cylinder2 during startup

The drag signal has a lot of frequencies, their distribution following a seemingly exponential wave itself. This has not been investigated in detail. The lift signal has one very marked frequency of $f_v = 0.102$ and a little peak at $f_v = 0.141$.

A Fourier analysis of 256 values in the fully saturated state (t = 772.5 to t = 900) shows that the startup problems eventually die out and the spectral densities show very well defined frequencies here; see figure 4.22.

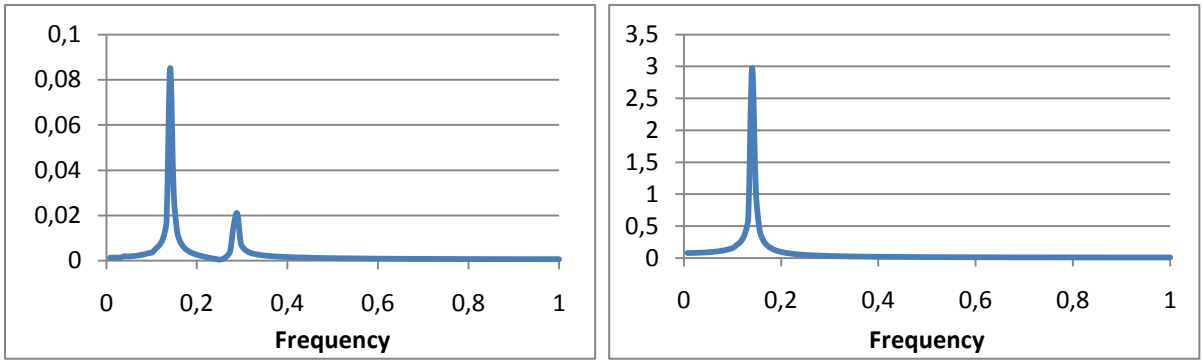

Figure 4.22: Spectral densities for C_D (left) and C_L (right) for cylinder2 in saturated state

The little peak in the lift spectral density in figure 4.21 has now grown to become the only frequency for the lift signal. That is, the dominating frequency of the lift signal has increased from $f_v = 0.102$ during startup to $f_v = 0.141$ in saturated state. The latter value is used to define the vortex shedding frequency. That gives St = 0.141.

As for drag, the multitude of frequencies in figure 4.21 have now collapsed into one main frequency. This frequency actually corresponds to the vortex shedding frequency itself and not twice the vortex shedding frequency, as one would expect. There is a little peak at twice the vortex shedding frequency, but it has only ¼ of the value of the highest peak. This phenomenon is what Sohankar et al. (feb 1999) [12] refer to as period doubling. In their calculations for a single square cylinder it shows up for Re = 500, in 2D calculations only. Such a flow is inherently three-dimensional, and they suggest that the period doubling is one of the ways this three-dimensionality can appear in a 2D calculation. Period doubling could also be the reason behind the four (albeit two small) peak in the drag spectral density for TCE_3D.

If that is the case, it could, as suggested in chapter 4.4, point to an onset wavelength for mode A instabilities higher than the actual computational spanwise dimension which here is six diameters. As suggested by Sohankar et al. (jul 1999) [13] the period doubling phenomenon could also be related spatial/temporal resolution, in addition the the domain size. This has not been investigated.

Table 4.6 shows C_D ave, C_D rms, C_L ave and C_L rms for both cylinders in a considerably stable period in time before the increase/decrease in drag ($380 \leq t \leq 420$) and in fully saturated state ($700 \leq t \leq 900$). These periods will be known as *period 1* and *period 2*, respectively.

Time period	**C_D ave cyl1**	**C_D rms cyl1**	**C_L ave cyl1**	**C_L rms cyl1**	**C_D ave cyl2**	**C_D rms cyl2**	**C_L ave cyl2**	**C_L rms cyl2**
Period 1 $380 \leq t \leq 420$	1.321	0.0001	-0.0049	0.0040	-0.338	0.0008	0.010	0.0195
Period 2 $700 \leq t \leq 900$	1.320	0.00004	-0.0050	0.0035	-0.334	0.0006	0.0088	0.0185

Table 4.6: C_D and C_L values for the cylinders in period 1 and period 2 for TCE_2D

Again the low values of fluctuating forces are evident. Comparing period 1 and 2 we see that all changes are very small. The exception is C_D rms on cylinder1 which is actually halved. This is most likely because of the fact that the averaging for period 1 is started a little too early - before the seemingly exponential decay of the envelope curve has flattened out sufficiently.

We can see that the average lift is different from zero for both cylinders in both cases. It also hardly changes between the periods. The same goes for rms lift. For cylinder1 average lift is negative, and actually the maximum lift cylinder1 will ever experience in steady conditions is hardly positive. But for cylinder2 the mean lift is actually positive. That would point to a flow which is not completely symmetric with respect to the oncoming flow, in both time periods. To check this, an inspection of averaged flow fields for both time periods was done. The averaging has been done over two vortex shedding periods; t = 401 - 414 for period 1 and t = 901 - 914 for period 2.

Figure 4.23 shows averaged streamlines in the gap and in the wake. The way one finds streamlines in paraView is to either show all streamlines which pass through a circle with some radius from a given point, or all which pass through a given line. I used the latter method. The streamlines which pass through some line crossing the gap, only recirculate in the gap. Therefore, to show the streamlines in the wake as well I needed to make another figure with the line crossing the wake. This is actually a good way to illustrate that the gap and the wake are separate recirculation zones.

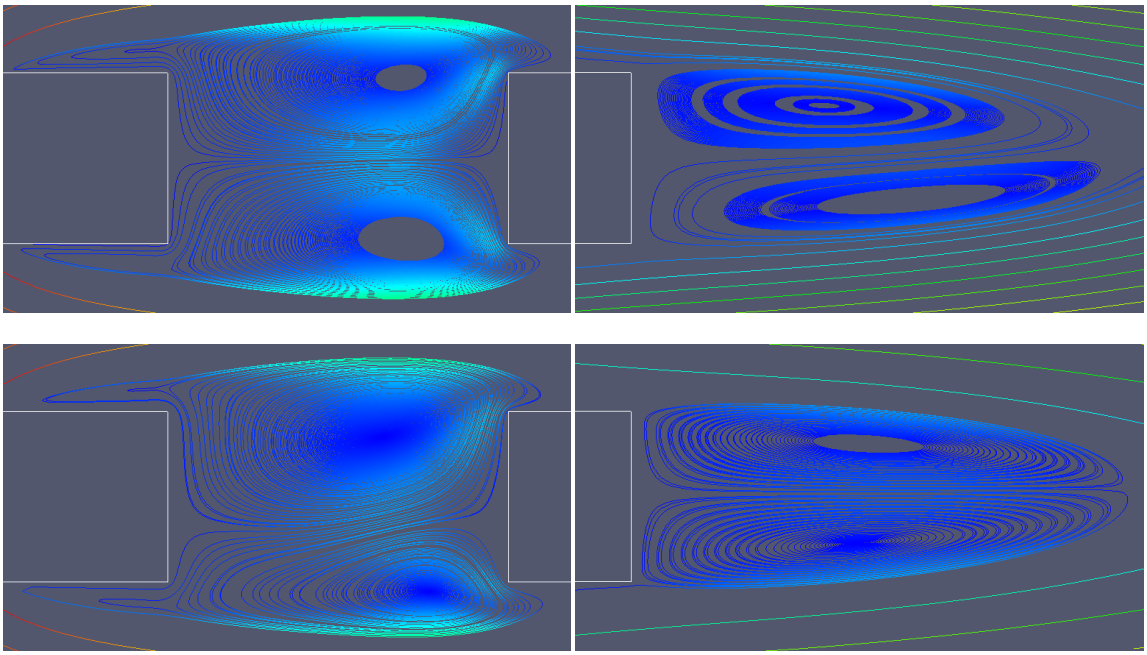

Figure 4.23: Averaged streamlines in the gap and wake in period 1 (top) and 2 (bottom)

We can see that the averaged streamlines in both periods are actually non-symmetric. In period 1 this mostly affects the wake while in period 2 it is more significant in the gap. This is the reason for the non-zero averaged lift in both periods.

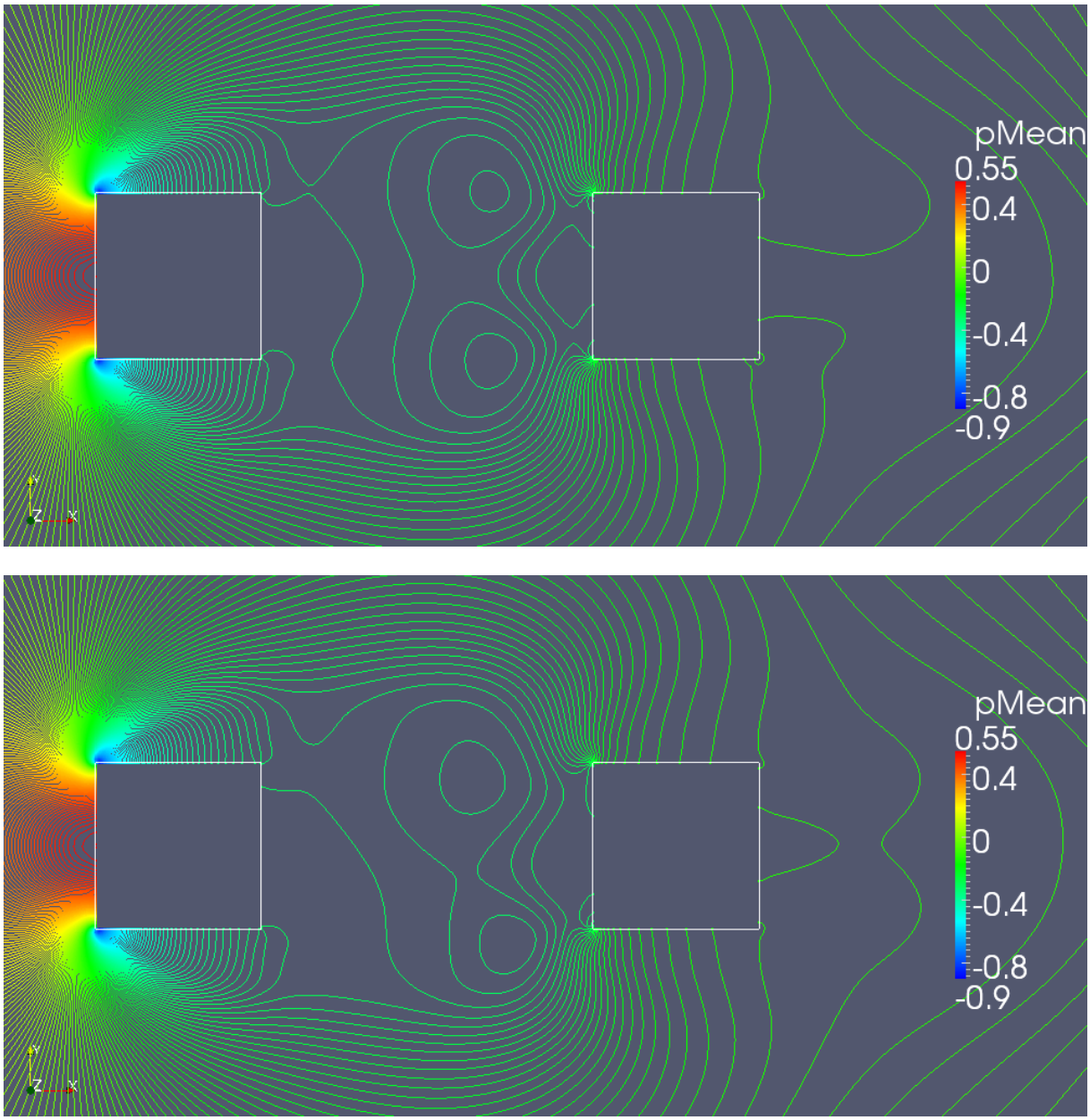

Figure 4.24: Averaged pressure contours in period 1 (top) and period 2 (bottom)

Figure 4.24 shows averaged pressure contours for period 1 and 2. I chose not to add the pressure color plot as backing as it only made the figure harder to read. It is still not easy to read from the figure that the average lift is negative on cylinder1 and positive on cylinder2 - in both periods, as the values do not change between periods. One has to remember that the values are very small. This figure paints the same picture as the streamlines in figure 4.32,

namely that in period 1 the flow is most unsymmetric in the wake and only a little unsymmetric in the gap whereas the opposite is true for period 2. The most notable change between the two periods is the change in drag, as seen in figure 4.19.

Mainly the drag is affected by the change of flow pattern. It is likely due to the fact that drag is less affected by the vortex shedding than the lift is. That is, the largest part of the contribution to the lift (if not all) comes from the vortices, whereas the largest part of the contribution to the drag comes from the pressure differential between the upstream and downstream faces of the cylinders. In Faltinsen [26] it is stated that the amplitude of the oscillatory drag is about 20 % of the amplitude of the oscillatory lift. The fluctuating parts are brought about by the vortex shedding. It seems, then, that the change in flow pattern is what lowers drag on cylinder1 and increases it on cylinder2 as we go from period 1 to period 2.

From figures 4.23 and 4.24 we can see that - even though the changes are small - the tendency is:

a) A cylinder gets more drag with symmetric upstream and downstream flow (cyl 1, period 1) than with symmetric upstream and unsymmetric downstream flow (cyl 1, period 2)

b) A cylinder gets more drag with unsymmetric upstream and symmetric downstream flow (cyl 2, period 2) than with symmetric upstream face and unsymmetric downstream flow (cyl2, period 1).

Spanwise vorticity contours are shown in figures 4.25 and 4.26 to reveal the small differences between the two extremes ends of a vortex shedding period, i.e. minimum and maximum lift on cylinder1. Cylinder1 leads cylinder2 by only about 0.5 time units, i.e. about 7 % of a vortex shedding period (about 14 time units), which means they are more or less in sync.

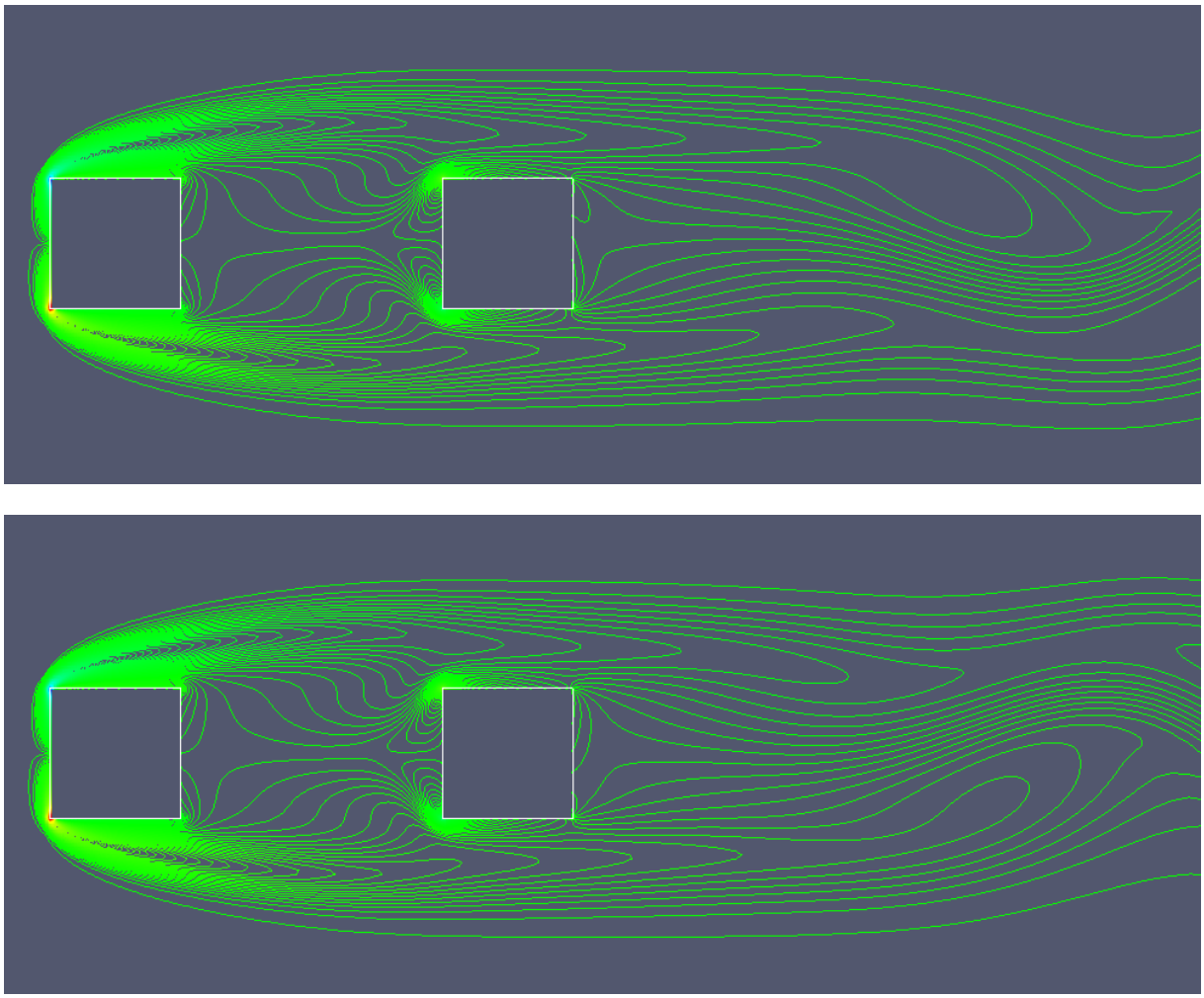

Figure 4.25: Contours of spanwise vorticity (ω_z) in period 1

Figure 4.25 show contours of spanwise vorticity in period 1. Top: t = 408, minimum lift; bottom: t = 419, maximum lift. In period 1, one would be hard pushed to notice any difference at all in the gap for the two extremes in the vortex shedding period. The flow near the back face of cylinder2 is only slightly different as well. The only difference to be read from figure 4.25 is seen in the wake, and it looks like one would expect in the two ends of the shedding period.

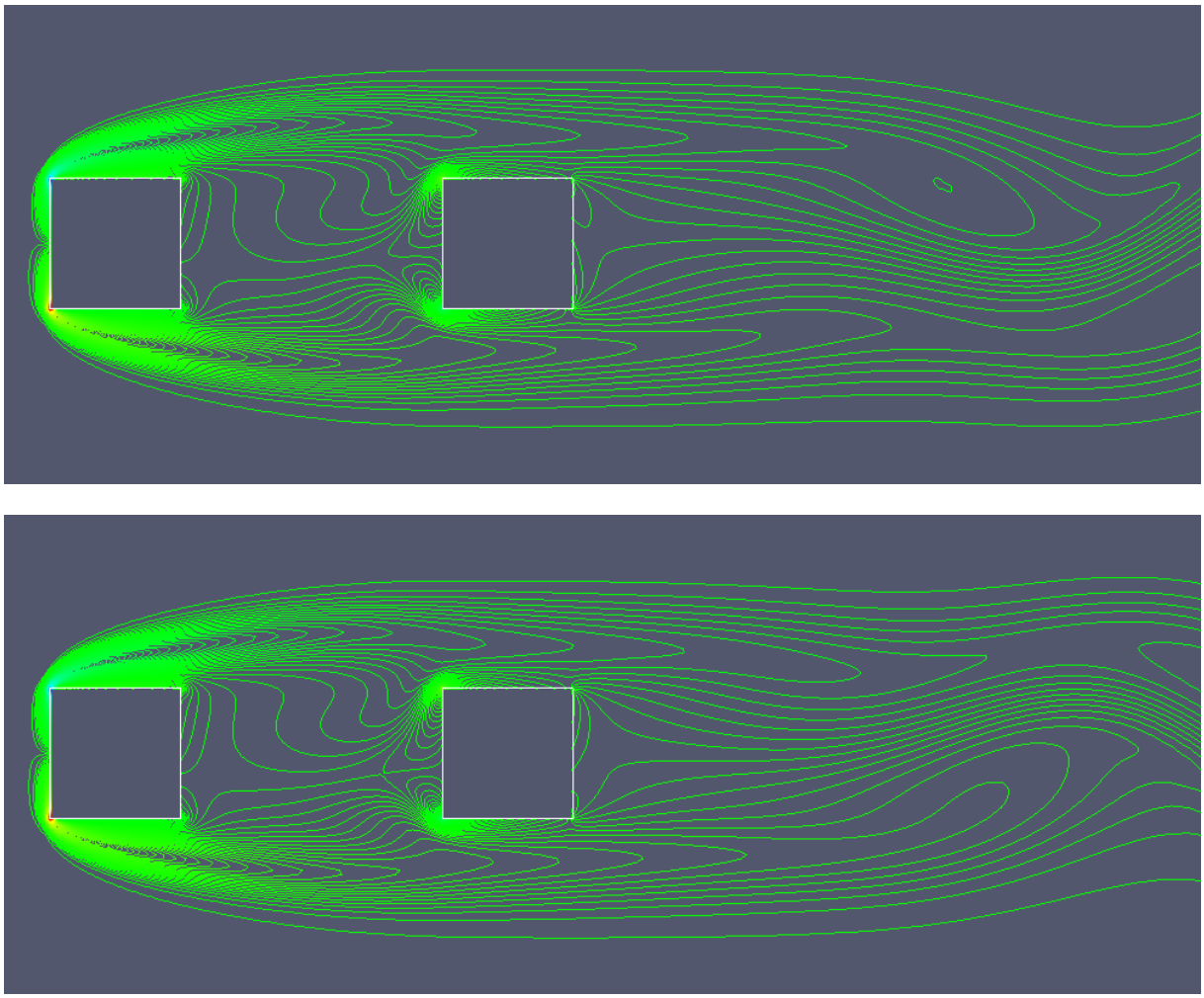

Figure 4.26: Contours of spanwise vorticity (ω_z) in period 2

Figure 4.26 shows contours of spanwise vorticity in period 2, the fully saturated state. Top: t = 793, minimum lift; bottom: t = 797, maximum lift. It is pretty much the same story when comparing the vorticity contours in this case. Here the flow in the gap is unsymmetric, and a small difference between the figures can be spotted there. But once again the large difference is in the wake.

Figure 4.25 and 4.26 quite effectively show how the fluctuating forces can be so small for this case. The change from the double vortex shedding flow in TCE_3D is massive. It should be noted, though, that TCE_2D is kind of a special case, as the fluctuating forces are 4-5 times larger for TCE_1D. The average drag is similar in both cases. TCE_1D exhibits none of the unsymmetric behavior seen in this chapter. TCE_1D will be discussed in chapter 4.7

4.6 Critical separation distance

Observing that for large S/D we have double vortex shedding and a repulsive force between the cylinders and for smaller S/D we have single vortex shedding and an attractive force between the cylinders, the question becomes: what is the critical separation distance, S_c, where single vortex shedding changes to double vortex shedding? And is there a separation distance where the force between the cylinders is zero?

To investigate this I did several runs to narrow down the area where the transition from single to double vortex shedding happens. Since the flow was two-dimensional even for S/D = 3, I did all these runs in 2D. The transition would be somewhere between S/D = 2 and S/D = 3. I assumed it would be closer to 3 than 2, so I chose S/D = 2.8 as the lowest value, and observed single vortex shedding there. After six runs I had narrowed it down to $2.91 < S_c < 2.92$.

The case of S/D = 2.92 had to be run to a time $t \approx 275$ before proper vortex shedding started compared to only $t \approx 60$ for S/D = 3.

S/D	C_D ave cyl1	C_L rms cyl1	C_D ave cyl2	C_L rms cyl2	C_D diff	Shedding
2.95	1.492	0.780	1.724	1.533	-0.232	Double
2.93	1.494	0.783	1.732	1.551	-0.237	Double
2.92	1.492	0.783	1.737	1.542	-0.245	Double
2.91	1.295	0.020	-0.302	0.167	1.598	Single
2.90	1.296	0.019	-0.304	0.166	1.599	Single
2.80	1.298	0.019	-0.312	0.155	1.610	Single

Table 4.7: Force coefficients for the two flow regimes; double and single vortex shedding

Table 4.7 shows the force coefficients on the two cylinders in the area around the critical length. C_D diff is the difference in force (coefficient) between the cylinders. C_D diff > 0 means attractive force as the drag on cylinder2 is lower than on cylinder1, whereas C_D diff < 0 means repulsive force. As we can see, we can never hit a distance where the force between the cylinders is zero because we suddenly switch from one distinct flow scheme to another.

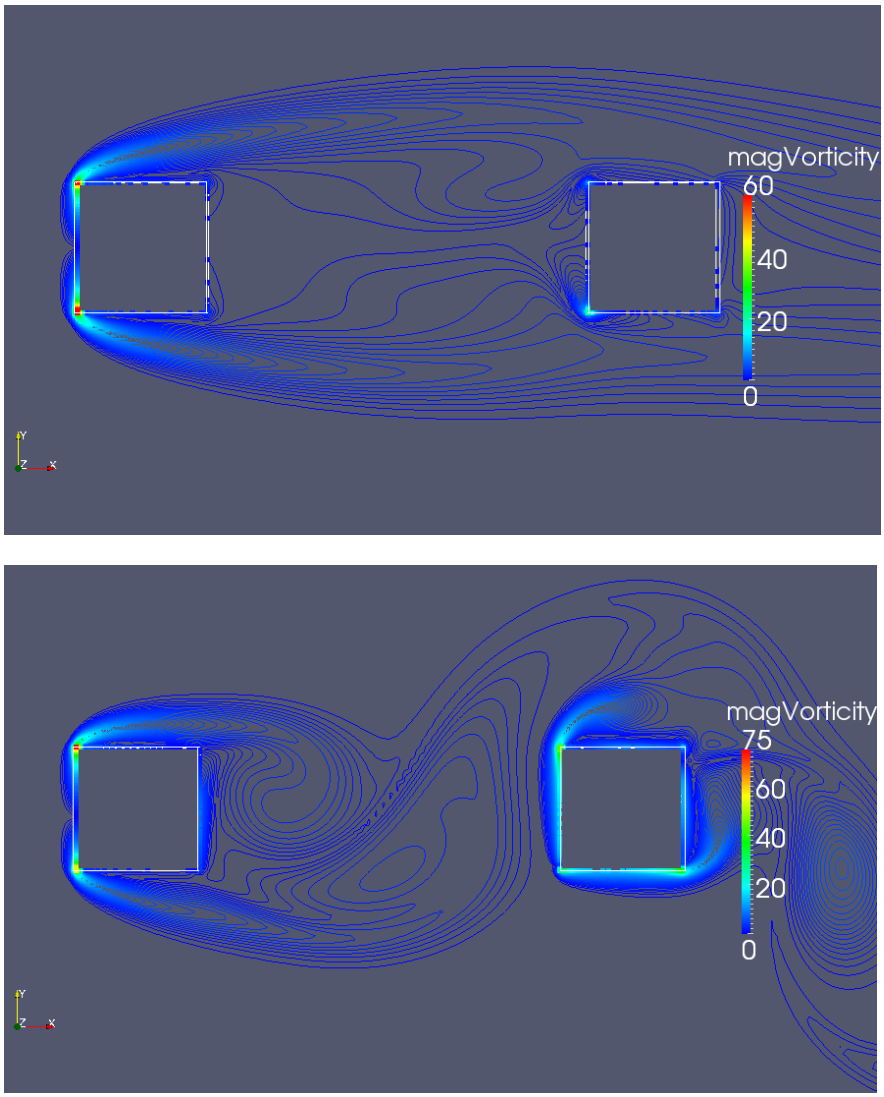

Figure 4.27: Contours of vorticity magnitude for single and double vortex shedding flow

Figure 4.27 shows the big difference between single (top) and double (bottom) vortex shedding flow. The single vortex shedding flow is very well behaved, with high concetration of vorticity only around the front and sides of cylinder1. The double vortex shedding regime is much more violent. The concentration of vorticity around cylinder2 has greatly increased. There is much more energy involved when we have double vortex shedding. This is also evident from the higher level of forces. As expected the vorticity contours for S/D = 3 (figure 4.18) look very similar to those for S/D = 2.92 (figure 4.27 bottom).

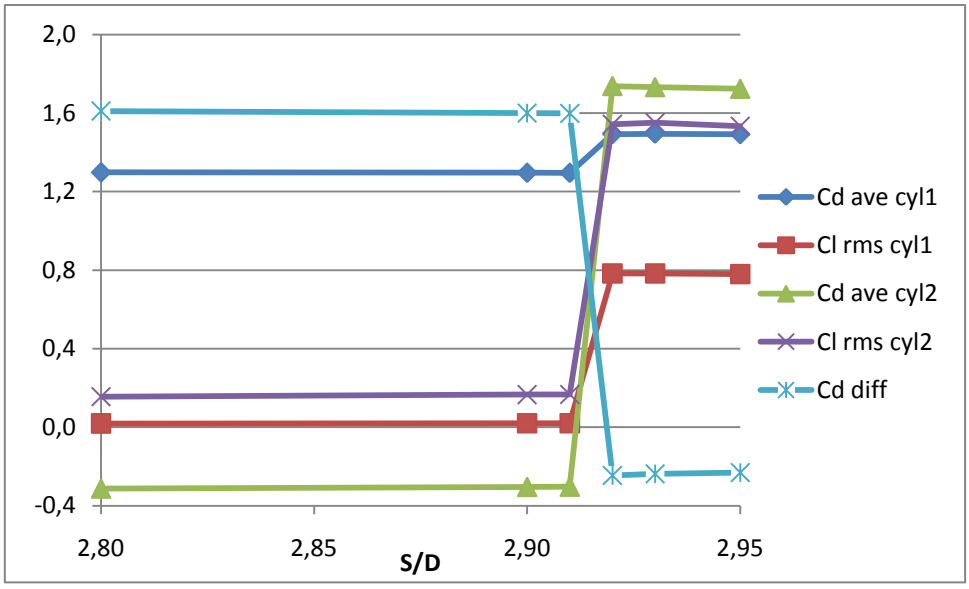

Figure 4.28: Development of forces from single to double vortex shedding flow

Figure 4.28 shows the development of C_D ave, C_L rms and C_D diff as we cross the critical distance, S_c. For single vortex shedding the lift on cylinder1 is very close to zero, as expected. As the separation is increased above the critical length, we see a jump (from approximately zero) in lift on cylinder1 due to the addition of vortex shedding from this cylinder. The jump in drag force is much more subtle. The addition of vortex shedding only increases the drag by about 15 %. The artithmetic increase in lift is close to four times higher than the corresponding increase in drag. This is in accordance with Faltinsen [26] who states that the amplitude of the oscillatory drag is about 20 % of the amplitude of the oscillatory lift.

The effect on cylinder2 is much bigger, both in terms of drag and lift. It goes from feeling a small attractive force from cylinder1, and small lift forces, to feeling a large repulsive force which is actually higher than the drag on cylinder1, and significantly higher lift forces. The vortices seem much more powerful for the double vortex shedding flow. Not only does cylinder2 get lift from its own shed vortices, but also the angled flow from cylinder1 as discussed previously.

The difference in the kinematic pressure field between S/D = 2.91 and S/D = 2.92 is shown in figure 4.29. Notice the different scaling. The pressure fields are not only completely different in the gap itself, but also in the wake of cylinder2. For the single vortex shedding case we can see that the kinematic pressure is less than zero everywhere in the gap and positive in the wake of cylinder2, whereas the opposite is the case for double vortex shedding flow. This is responsible for the large difference in force on cylinder2.

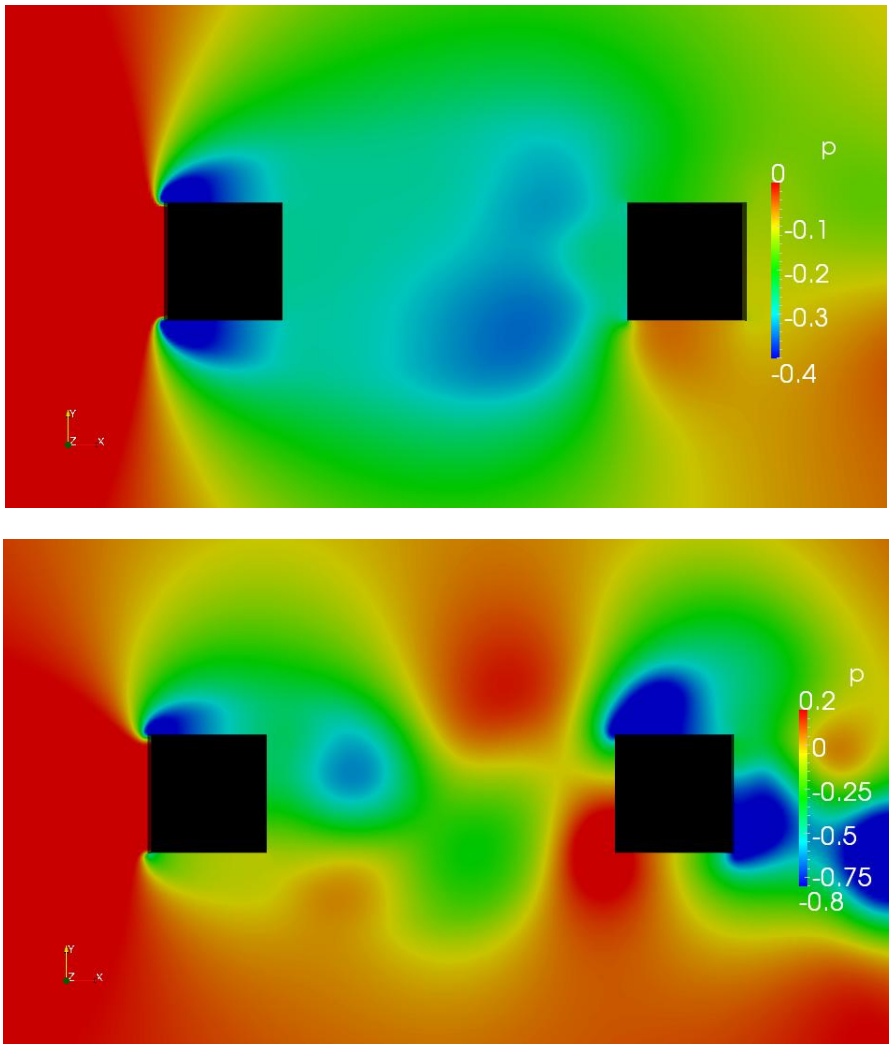

Figure 4.29: Pressure field for single (top) and double (bottom) vortex shedding flow

The critical length is found to be $2.91 < S_c < 2.92$ at Re = 200 in the present study. In my project work [3] at Re = 100 the flow exhibited single vortex shedding for S/D = 3. The exact value for the critical length S_c was not found, but from this one can conclude that the critical length decreases with increasing Reynolds number.

4.7 For separation distance S/D ≤ 1

For separation distances less than or equal to one diameter one would expect the two cylinders to start to feel like one long body. The flow in the gap will be increasingly restricted as the cylinders move closer to each other. How close must they get to act like one single body?

Table 4.8 shows a comparison of flow parameters for S/D = 1, 0.5, 0.1 and 0. For the fourth case, TCE_0D, a single body with length 2.1D and height D has been used. With this setup we can directly investigate the effect of the gap for S/D = 0.1, as the body in TCE_0D is equal to the two bodies in TCE_01D with the gap closed off. The drag and lift coefficients are in all cases based on $A_f = A \cdot D$. C_D sum is the total force in the x-direction for both bodies. For TCE_0D *cyl1* corresponds to the rectangular body and of course *cyl2* has no value. C_D rms values are omitted as they were all very low and varied relatively little. C_L rms values are relatively low too, but they show a much more marked increase as S/D decreases.

Case	C_D ave cyl1	C_L rms cyl1	C_D ave cyl2	C_L rms cyl2	C_D sum	St
TCE_1D	1.374	0.025	-0.294	0.08	1.081	0.156
TCE_05D	1.404	0.052	-0.260	0.117	1.144	0.164
TCE_01D	1.454	0.095	-0.253	0.149	1.202	0.172
TCE_0D	1.199	0.230	-	-	1.199	0.168

Table 4.8: Flow parameters for S/D = 1, 0.5, 0.1 and 0

When comparing the three former cases with TCE_0D we need to consider the total drag, C_D sum. Even for S/D = 1 the difference in C_D sum is only about 10 %. For S/D = 0.5 it is down to 5 % and for TCE_01D there is almost no difference at all. At least in terms of total drag it seems the bodies feel as one already from S/D = 1.

Flow patterns and the gap

The most interesting thing to look at for these cases is the flow pattern around the cylinders. Depending on Reynolds number and length/height ratio (L/H), one will see different flow regimes around the cylinder [4]. At very low Reynolds number the flow will separate at the trailing edge (TE) rather than the leading edge (LE) due to immediate reattachment. This is called reattached flow. At higher Reynolds numbers (but still laminar), separation from LE will occur and steady reattachment becomes impossible. This is known as detached flow. In an intermediate Reynolds number range the flow will experience both reattachment and detachment during a vortex shedding cycle. In this case steady reattachment cannot be obtained. The flow will either fully separate from LE or reattach somewhere on the cylinder surface and finally separate at TE, depending on where in the vortex shedding period the flow is. For a square or rectangular cylinder the separation points are fixed to the sharp corners, unlike a circular cylinder where the separation points can move. Okajima (1982) [4] investigated reattachment/detachment experimentally for rectangular cylinders of different L/H ratios. He observed that for a given Reynolds number, the flow is detached for low L/H

and reattached for higher L/H. And for a given L/H ratio, the flow is reattached for low Reynolds numbers and detached for higher Reynolds numbers.

Numerical studies by Sohankar et al. [9] and [10] on square cylinders have shown that at $Re \leq 100$ separation at all times occurres from TE, predominantly from TE and occasionally from LE at Re = 125, predominantly from LE at Re = 150 and from LE at all times for $Re \geq 175$. As Okajima [4] showed, these limits will increase as L/H increases. For L/H = 2, the flow will be reattached for Re less than about 500. At some separation distance between the cylinders in this study one could expect the detached vortices from the upstream cylinder to reattach on the downstream cylinder, almost as if the cylinders were one body with L/D > 2. At a slighty longer separation distance the detached vortices from cylinder1 will roll up in the gap (double vortex shedding scheme).

The wake in a detached flow will be wider than in a reattached flow. This means the vortices will be further apart in a detached flow, and will interact at a slower rate, thereby decreasing the Strouhal number. The wider wake for detached flow also increases the pressure drag.

From table 4.8 we can see that the Strouhal number increases as S/D decreases. This would point to a flow with a wake which is getting narrower. However, the drag increases, for both cylinders. This could point to exactly the opposite: a wake which is getting wider. But it could also be connected to the near-body flow. In detached flow the the recirculating bubble creates a near-body flow which is directed upstream. This implies that the frictional part of the drag will actually be negative. If we get reattaching flow somewhere on cylinder2, this cylinder would get a positive frictional drag which of course would increase C_D sum.

At the Reynolds number used in this study the frictional part of the drag is small, but it could have an effect. Sohankar et al. (1995) [9] observed that for $Re \leq 125$ the fricitional contribution to the drag was positive and beyond that it was negative. This Reynolds number value is valid for L/H = 1. For L/H > 1 this crossover Reynolds number will be higher according to Okajima [4], which means the frictional drag might be positive when the cylinders get close to each other, at least on cylinder2. However, the main contributor to variation in drag will be the pressure drag. In the current study only the total drag coefficient was considered.

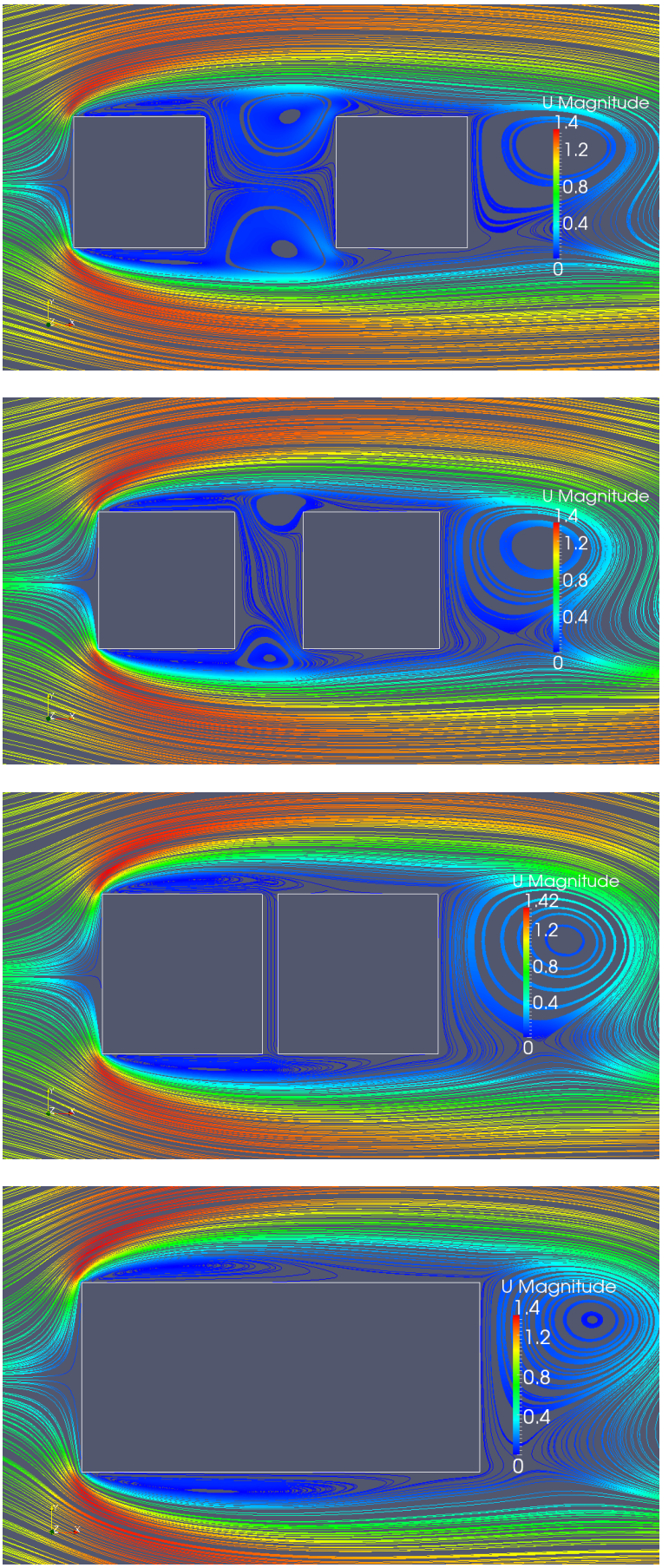

Figure 4.30: Streamlines for S/D = 1 (top), 0.5 (second), 0.1 (third) and 0 (bottom)

Figure 4.30 shows streamlines for decreasing S/D, all at instants of maximum lift on cylinder1. For S/D = 1 and 0.5 the cylinders are in sync. For S/D = 0.1 cylinder2 leads cylinder1 by about 15 % of a vortex shedding period. Cylinder1 has detaching flow in all cases, whereas cylinder2 experiences a reattaching flow hitting its surface at around 1/3 to 2/3 downstream of LE. Here we can see how the point of reattachment on cylinder2 varies through a vortex shedding period as this is taken from one of the extremes. From figure 4.30 it is not straight forward to determine whether the contribution from viscous drag varies. The flow in the gap goes from bottom to top at the stage of vortex shedding shown in the figure.

For S/D = 1 (top) we see that two separation bubbles form in the gap, and there is little transfer of fluid between the top and bottom of the gap as the flow goes through a vortex shedding period. The motion of the stagnation point, L_s, on cylinder1 is 24 % of the diameter. L_s is defined as the double amplitude of the motion, i.e. the motion from top to bottom. In paraView it was traced by viewing vorticity magnitude with highly reduced range (from zero to a small fraction of the maximum value) and seeing where it approached zero for instants of maximum and minimum lift. L_r is a measure of how much the two recirculation zones deform during a vortex shedding period.

For S/D = 0.5 (second) the recirculation zones we see for S/D = 0.5 are much smaller, but the transfer of fluid between the top and bottom is larger. The motion of the stagnation point on cylinder2 is here 60 % of the diameter. A piston mode flow is developing in the gap, but it gets stopped in both ends by the recirculating flows and cannot be completed. From the figure we can see that on the side with the longest length before reattachment on cylinder2 (in this case the bottom side) the flow actually turns around and flows against the flow direction and up into the gap. On the other side (here: top side) the flow joins into the upstream directed flow in the recirculating zone on cylinder1. This is also shown by vector plots in figure 4.32.

With S/D down to 0.1 we see that the piston mode flow is unrestricted by recirculating zones and allowed to develop completely. This means we have stagnation along the entire upstream face of cylinder1 and L_s has no value. The flow through the gap will follow the same route as explained for S/D = 0.5. The velocity of the flow in the gap (y-velocity only) is very small. This can be seen from figure 4.32 (bottom). The change from S/D = 0.1 to S/D = 0 seems pretty unremarkable. It can be concluded that both in terms of total drag and flow pattern TCE_01D and TCE_0D are very similar.

Excluding the flow in the gap, the only other significant difference to be spotted from figure 4.30 is between S/D = 1, 0.5 and S/D = 0.1, 0. The flow reattaches slighty further upstream on cylinder2 in the latter cases (or strictly, the second part of the rectangle in the TCE_0D case). That implies that the frictional contribution to the drag should increase. But, as previously mentioned, this is only a small contributor to drag. The main contributor is pressure drag, which we shall be looking at next.

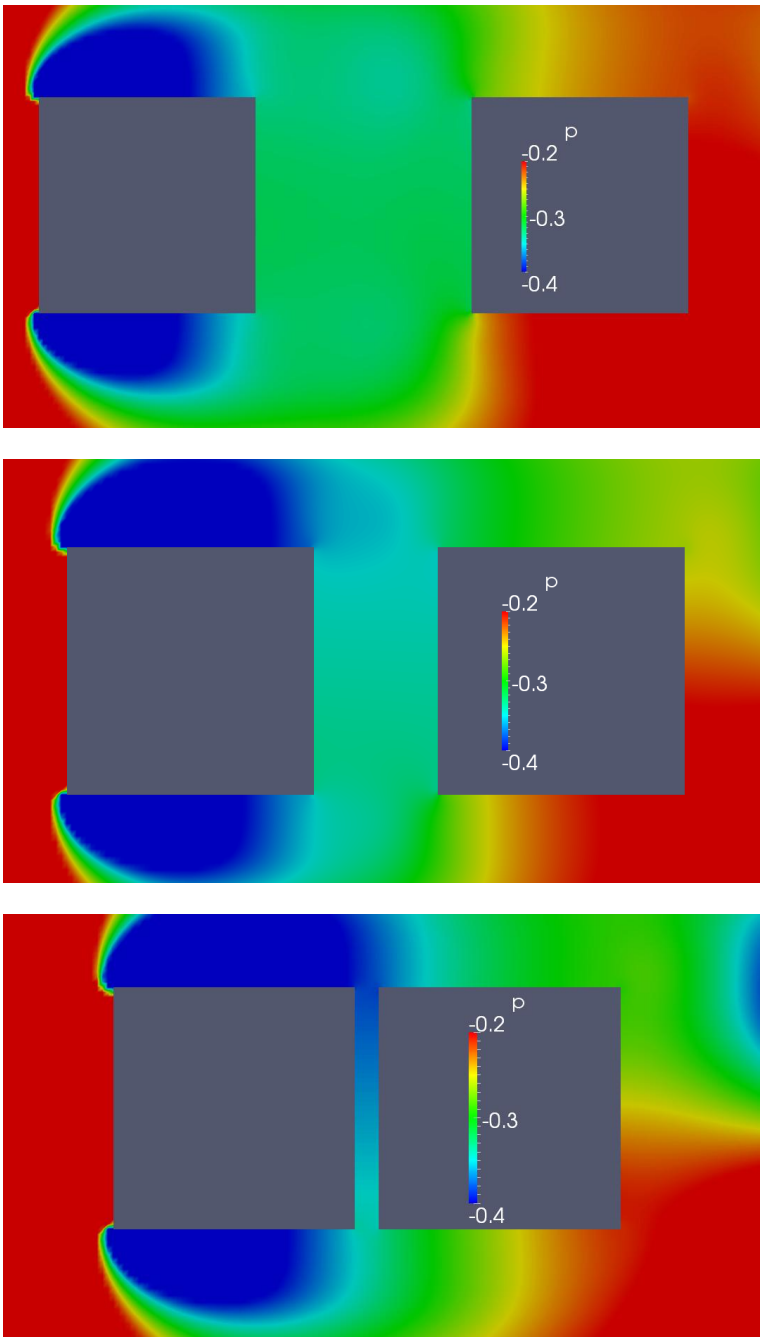

Figure 4.31: Pressure in the gap for S/D = 1 (top), 0.5 (middle) and 0.1 (bottom)

Figure 4.31 shows the kinematic pressure in the gap. The range has been reduced to make it easier to point out variation in the gap. The pressure on the upstream face on cylinder1, the stagnation pressure, is constant throughout a vortex shedding period and constant between the cases. The pressure drag on cylinder1 is determined by the suction on the downstream face, as discussed in chapter 4.2. From figure 4.31 we can clearly see that the mean pressure on the downstream face of cylinder1 decreases, increasing the pressure drag. This agrees with the development of C_D ave cyl1 from table 4.8. The increase from S/D = 1 to S/D = 0.1 is about 6 %.

For cylinder2 it is not straightforward to see the development of the pressure drag, as it is a function of the variation on both the upstream and downstream face. Also, the reduced range,

which makes it easier to see what happens in the gap, makes in harder to see the pressure variation on the downstream face of cylinder2. The increase in drag on cylinder1 (reduction of propulsion as the drag is negative) is about 15 %. This cannot be contributed only to variation in frictional resistance as it is a small contribution.

We see a clear pressure gradient in the gap for S/D = 0.1. The gap flow is pressure driven – a Poiseuille channel flow. In figure 4.32 it can also be seen that it has a velocity profile.

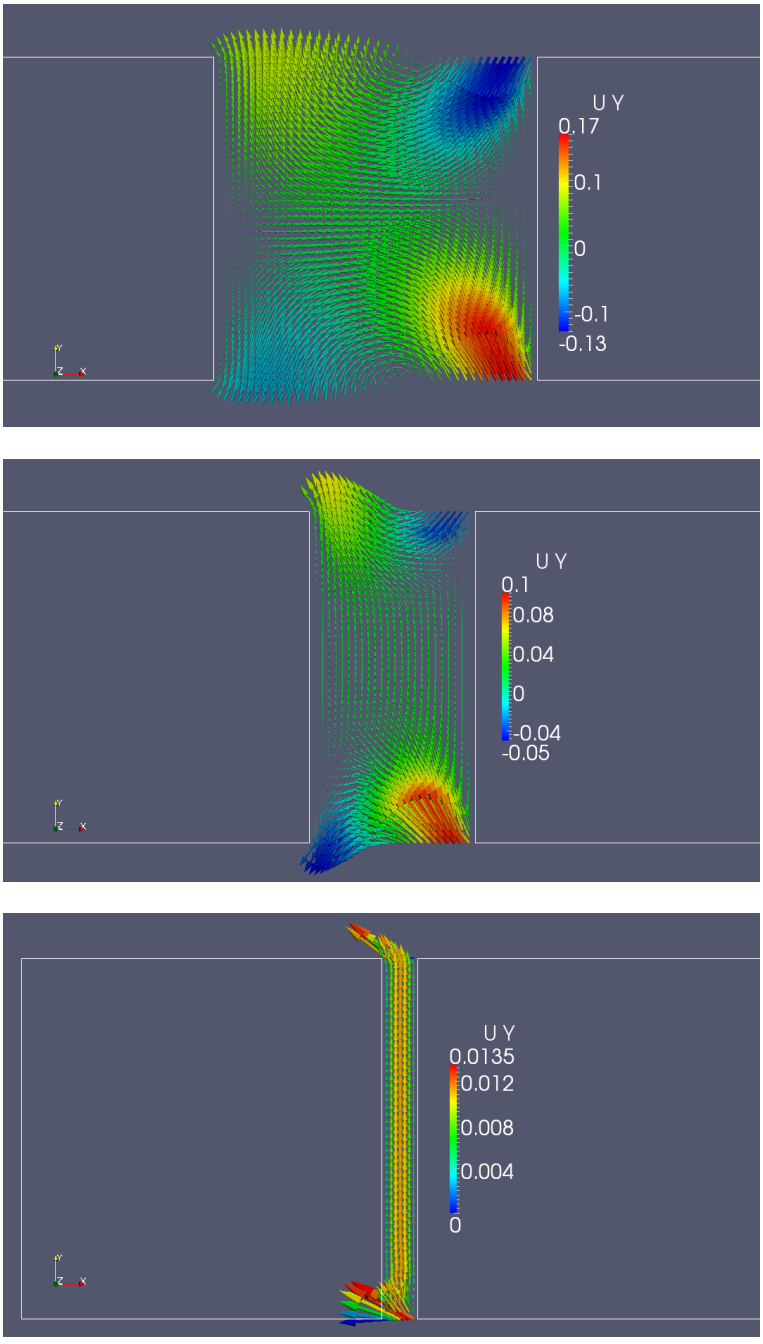

Figure 4.32: Velocity vectors in the gap for S/D = 1 (top), 0.5 (middle), 0.1 (bottom)

Figure 4.32 shows velocity vectors in the gap for S/D = 1, 0.5 and 0.1. The vectors are colored by the y-velocity, which is in the vertical direction in this figure. In the bottom figure the clearly see the Poiseuille flow in the gap. As can be seen from the legend, also the y-velocity is really small in this case. The two other velocity components are practically zero in this case.

In all three figures we can see the gap flow described under the discussion on streamlines, i.e. that the flow reattaches on cylinder2, turns around, flows into the gap and joins the recirculating zone on cylinder1 on the other side.

When looking at table 4.8 we see that the variation in C_L rms on the cylinders is much larger than the variation in drag. C_L rms is 3.8 times and 1.9 times higher for cylinder1 and cylinder2 for S/D = 0.1 than S/D = 1, respectively.

Vortex shedding frequency and pulsations

The spectral density graphs for TCE_1D show very sharp and well-defined peaks. Both drag spectral densities have two large peaks. One corresponds to the vortex shedding frequency and one to twice the vortex shedding frequency. The lower frequency is probably a sign of the period doubling previously seen for S/D = 3 and S/D = 2. One can only just make out an extremely slow and very weak pulsation from the lift signals. It does not show up in the FFT analysis. Since it is so weak, and difficult to trace in the force signal graphs, it has been disregarded.

The TCE_05D case also exhibits very well-defined peaks in the spectral densities, and it also has a doublepeakedness in drag, but the double period peak is significantly lower than in TCE_1D. In contrast to TCE_2D and TCE_1D, this case exhibits the pulsation phenomenon seen in TCE_4D and TCE_3D. The pulsation frequency did not show up in the Fourier analysis (reason unknown), but the period was found by inspection of the lift signal to be T_p = 31 time units; 5 times the vortex shedding period. This is notably lower than the 64 time units found for TCE_4D, but higher than the 11.6 time units found for TCE_3D. Pulsation periods will be discussed more in chapter 4.8.

Once again the spectral density peaks are well-defined for TCE_01D, but contrary to TCE_1D and TCE_05D all four spectral density graphs have a strange wavy behavior outside of the peak areas. This can be seen in figure 4.33, for drag on cylinder1. This also shows that we have period doubling here as well.

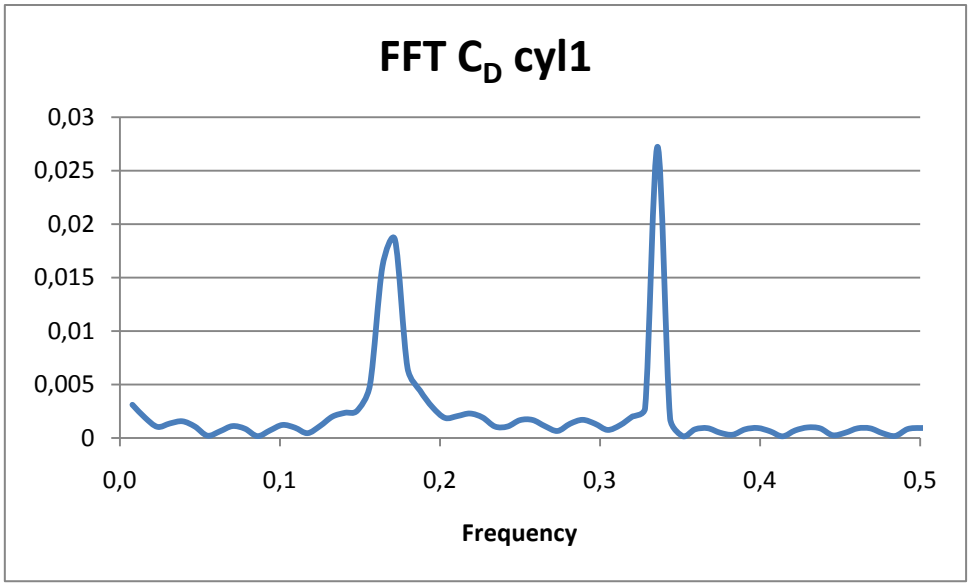

Figure 4.33: Spectral density for C_D on cylinder1 for S/D = 0.1

In figure 4.21 and 4.22 (in chapter 4.5 on TCE_2D) the horizontal axis extends to 1 as opposed to 0.5 in figure 4.33 here. The reason is that for TCE_2D the data was written to file twice per time unit whereas it was written to file only once per time unit for TCE_01D (to reduce the amounts of data). Due to the effect of downfolding [21], the highest frequency one can use without the danger of getting false information is half the sampling frequency. As the second peak in figure 4.33 coppresonds to the highest frequency in the flow, this is no problem here; nor is it in any of the other Fourier analyses carried out in this study. The pulsation did not show up in the Fourier analysis for S/D = 0.1 either, but once again it was found by inspection of the lift signal. The pulsation period T_p = 107. That is an almost four-fold increase from TCE_05D.

Comparison of TCE_01D and TCE_0D

When comparing TCE_01D and TCE_0D, there is very good agreement in average drag (less than 1 % difference) and Strouhal number (2-3 % difference); see table 4.8. To be able to compare rms lift one has to add the C_L rms values for cylinder1 and cylinder2 in TCE_01D and compare them to C_L rms for the rectangle in TCE_0D. Adding rms values is valid as the rms function is linear. This will be proved next.

For a set of *n* x-values the RMS value is given as:

$$x_{RMS} = \sqrt{\frac{\sum_{i=1}^{n} x_i^2}{n}} \qquad (4.3)$$

$$(2x)_{RMS} = \sqrt{\frac{\sum_{i=1}^{n}(2x_i)^2}{n}} = \sqrt{\frac{\sum_{i=1}^{n}4x_i^2}{n}} = 2\sqrt{\frac{\sum_{i=1}^{n}x_i^2}{n}} = 2x_{RMS} \quad (4.4)$$

When adding rms lift values the phase shift between the cylinders is not accounted for. As previously noted, there is a phase shift of about 15 % of a vortex shedding period between the cylinders for TCE_01D. Since lift force is allowed to work on the lid in the gap for the TCE_0D case, the comparison of lift is a little more complicated than the comparison of drag. The 6 % difference between C_L rms for TCE_0D and the sum of C_L rms values for TCE_01D can be accounted for by the effect of the lid over the gap and by the phase shift between cylinder1 and cylinder2 in the latter case.

The largest difference between the two cases, though, is a surprising ~50 % longer pulsation period for TCE_0D. This will be discussed more later.

Comparison of TCE_0D and OneCyl

Another interesting comparison is TCE_0D vs. OneCyl. What effect does a roughly doubled body length have? Table 4.9 shows a comparison of integral values for OneCyl and TCE_0D. All values for OneCyl are for the 2D part of the flow development. The pulsation period has been omitted as the pulsations are part of the 3D flow for OneCyl. All coefficients are based on the frontal area, A_f.

Parameter	OneCyl	TCE_0D
C_D ave	1.494	1.199
C_D rms	0.030	0.009
C_L rms	0.429	0.219
St	0.148	0.168

Table 4.9: Integral values for OneCyl and TCE_0D

Both C_D average and St point towards a difference in flow pattern between the two – detached flow for OneCyl and reattached flow for TCE_0D. A reattached flow with narrower wake will have lower pressure drag, which is the main contribution to the total drag at this Reynolds number, and frequently interacting vortices which give a high Strouhal number. This is confirmed by streamline plots for both in figure 4.34.

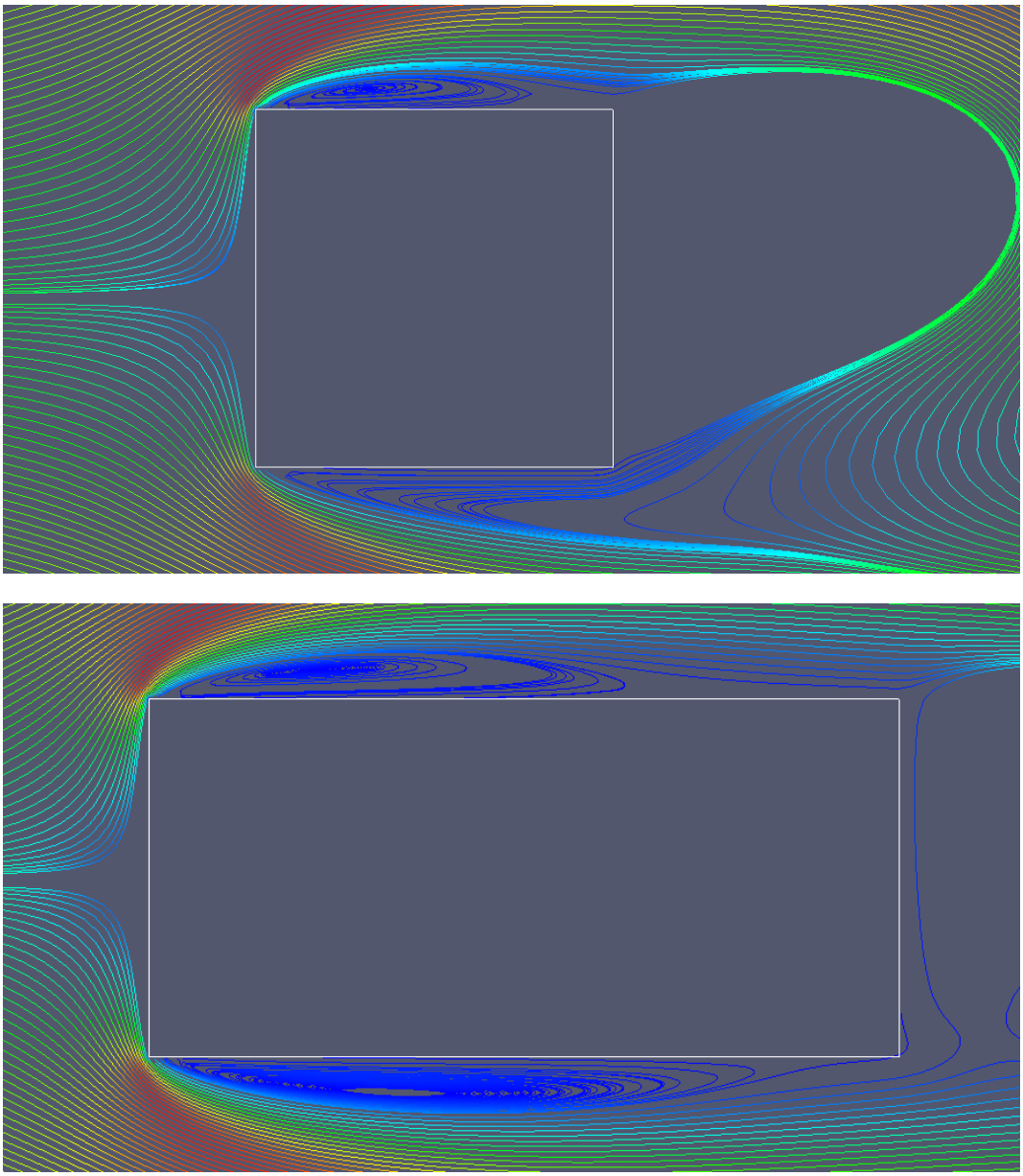

Figure 4.34: Streamlines for OneCyl in 2D region (top) and TCE_0D (bottom)

Both cases in figure 4.34 correspond to instances of maximum lift, as usual. In connection with figure 4.23 in chapter 4.5 it was noted that the gap and wake are separate recirculation zones. It is the same deal here for the recirculation zones on the top/bottom and the wake. That is why the wake is deficient in figure 4.34. The point of the figure is to show the differences of the recirculating zones on the top/bottom faces.

In figure 4.34 (top) for OneCyl we can see that the flow actually reattaches just upstream of TE. One must remember, though, that this in the case of maximum lift. The flow will be detached for all time steps except very close to maximum and minimum lift.

The extra length of the TCE_0D body allows the flow to be reattached at all times, like demonstrated by Okajima [4]. The flow reattaches a fair distance upstream of TE, even in the

case of maximum lift. The reattachment point moves a distance of about 1/3 diameter between maximum and minimum lift.

The rms values are much larger for OneCyl than for TCE_0D (double for lift, triple for drag). This could be connected to the flow pattern around the body. TCE_0D has final separation from TE, whereas OneCyl has separation from LE. The vortices form closer to the body in the detached flow. In chapter 4.2 on force pulsation we saw the large influence of the distance between the body and its vortices. The difference in flow pattern is likely the main contributor to the large difference in forces between TCE_0D and OneCyl.

Additionally, twice as long a body is likely to have a lower streamwise coupling of forces. That is, the pressure on the top and bottom surfaces will vary more along the body's length for TCE_0D than for OneCyl. Inspection of pressure plots seems to confirm this, but the contribution is likely much smaller than the contribution from variation in flow pattern.

4.8 Pulsations, 3D effects and integral parameters for varying S/D

Based on the knowledge obtained in chapter 4.2 through 4.7 we can divide the TCE flow into five flow schemes by S/D:

S/D range	Vortex shedding	Pulsation	Dimension of flow
$0 \leq S/D \leq 0.5$	Single	Yes	2D
$1 \leq S/D \leq 2.91$	Single	No	2D
$2.92 \leq S/D < 3$	Double	No	2D
$3 \leq S/D < 4$	Double	Yes	2D
$4 \leq S/D$	Double	Yes	3D

Table 4.10: The five flow schemes for TCE

The exact S/D value where 3D effects are suppressed has not been investigated, but based on the current results the table can be presented this way. The period doubling phenomenon, which is present in all of the flows which do not develop to 3D, i.e. for S/D = 3, 2, 1, 0.5, 0.1, is one way suppressed inherent 3D effect can reveal themselves. It is believed that the S/D limit for suppression of 3D effects is dependent on the computational aspect ratio. As S/D decreases, the onset wavelength for mode A instabilities might become higher than the aspect ratio and thus 3D effects cannot appear. With a higher aspect ratio one might see 3D flow for lower S/D values. This has not been investigated, but is suggested as future work.

For S/D = 2, 1 the pulsations phenomenon is absent. It is present both for longer and shorther separation distances. Inspecting table 4.11, which shows the pulsation period and the ratio between the pulsation period, T_p, and the vortex shedding period, T_v, one can see that this ratio approaches unity from either side of S/D =2, 1.

Case	Pulsation period, T_p	T_p/T_v
TCE_4D	64	8.5
TCE_3D	11.6	1.54
TCE_2D	-	-
TCE_1D	-	-
TCE_05D	31	5
TCE_01D	107	18.4
TCE_0D	149	25

Table 4.11: Pulsation periods

I can think of two reasons for this behavior:

a) The pulsation frequency coincides with the vortex shedding period and becomes indiscernible as a separate frequency for S/D = 2, 1.
b) As discussed in chapter 4.3 (TCE_4D) it seems the upstream cylinder governs the pulsation through the subsequent stretching and compression its vortices. For S/D = 2, 1 this might not be allowed to happen due to the interaction between the cylinders. For S/D < 1 the cylinders feel so much like one body that cylinder2 now takes over control over the pulsation through deformations of its vortices.

The large difference in T_p/T_v ratio between TCE_01D and TCE_0D is surprising (about 36 %). In most other respects these two cases are very similar. There are only two differences between the two cases. The gap is closed off in TCE_0D. And since the maximum number of cells along a line in Mega is 100, the cells are a tad strechted for TCE_0D compared to TCE_01D. TCE_01D has 50 cells on each cylinder and eight in the gap, whereas TCE_0D has 100 cells distributed on the same length. The distribution is not quite similar either. But it seems unlikely that these small differences should create a discrepancy as high as 36 %.

In figures 4.35 through 4.38 the development of various parameters as function of separation distance, S/D, are presented. All values used for TCE_2D are from period2 as this is assumed to be fully saturated state. For TCE_4D the 2D values are used.

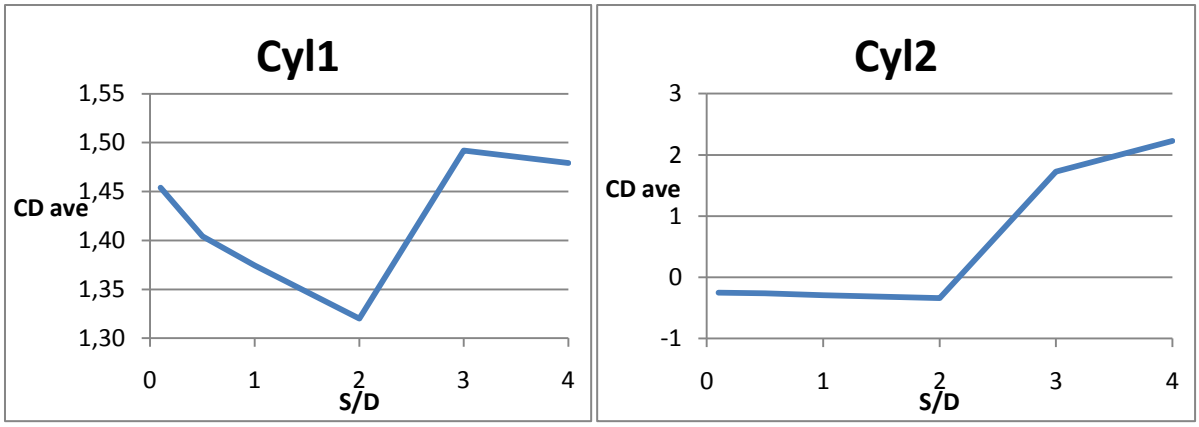

Figure 4.35: C_D ave for cylinder1 (left) and cylinder2 (right) for varying S/D

It is important to note that the scales in the two figures are very different. The average drag on cylinder2 will be much more affected by the varying S/D than cylinder2. The development of the two curves is a little different between S/D = 3 and S/D = 4. C_D average on cylinder1 will reach its maximum for TCE_3D whereas C_D average on cylinder2 reaches its maximum at the highest separation distance studied, S/D = 4.

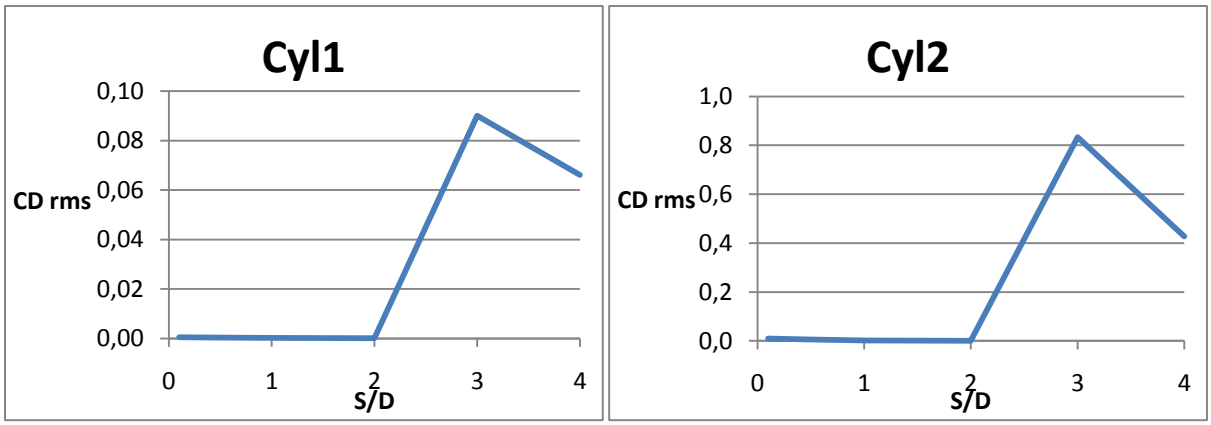

Figure 4.36: C_D rms for cylinder1 (left) and cylinder2 (right) for varying S/D

In this figure of C_D rms for the two cylinders the scale is 10 times finer on the left, and the curves look very similar. Unlike C_D average in the previous figure, these curves develop equally from S/D = 3 to S/D = 4. Percentage-wise both cylinders are affected equally, at least for high S/D, but the actual force is much higher for cylinder2. At high S/D this cylinder of course experiences the violent double vortex shedding scheme. For low S/D the values are close to zero and hard to compare in a graph, but in general they are larger for cylinder2.

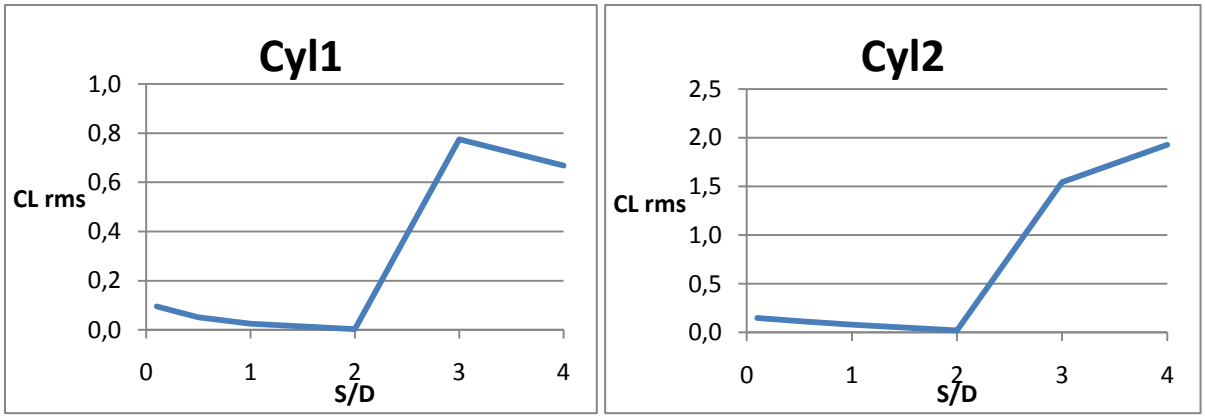

Figure 4.37: C_L rms for cylinder1 (left) and cylinder2 (right) for varying S/D

Here the scale is 2.5 times finer of cylinder1. The differences between C_L rms on the two cylinders are not as large as for C_D rms, but still considerable. Just like for C_D average we see a similar behavior until S/D = 3, after which we see a drop for cylinder1 and a further increase for cylinder2. Both reach their minimum for the rather strange S/D = 2 case where the forces are really small. Only there do they take very small values, unlike the C_D rms values which are close to zero for $S/D \leq 2$.

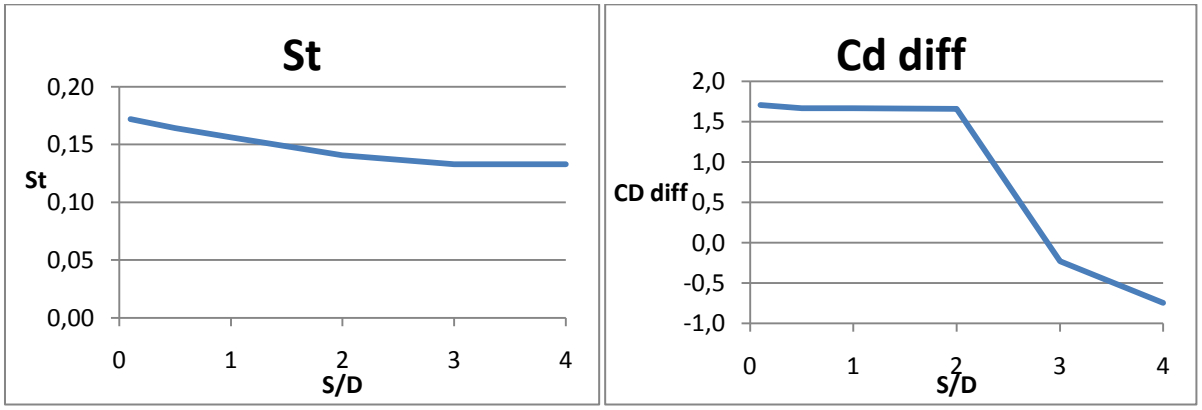

Figure 4.38: Strouhal number (left) and C_D diff (right) for varying S/D

The Strouhal number is the only parameter which does not experience a steep increase as S/D crosses the critical separation distance S_c; it decreases steadily until S/D = 3, where it levels off. C_D diff changes from positive for low S/D values to negative for high S/D (as it crosses S_c). For low separation distance the vortex shedding scheme is single and the cylinder want to move towards each other. For high separation distance the vortex shedding scheme is double and the cylinders feel a repulsive force between one another.

In figures 4.35 through 4.38 all parameters except the Strouhal number seem to experience a pretty steep, but continuous, increase between S/D = 2 and S/D = 3, that is, as the flow

changes between single and double vortex shedding. But as noted in chapter 4.6, the flow will not vary along a continuous line between S/D = 2 and S/D = 3, but rather experience a sudden jump between S/D = 2.91 and S/D = 2.92. Having the corresponding value for these two separation distances would have accentuated this discontinuity in the plots, but not all parameters were calculated for S/D = 2.92 and 2.91. I chose to make all graphs consistent and thus omit the values around S_c. The sudden jump in forces between single and double vortex shedding flow can be seen in figure 4.28.

The stagnation point motion, L_s, also discussed in chapter 4.7, is defined as the double amplitude of the motion of the stagnation point as a ratio of the diameter. Its dependence on S/D is shown numerically and graphically in table 4.12 and figure 4.39, respectively.

Case	Cylinder1	Cylinder2
TCE_0D	< 0.02	-
TCE_01D	< 0.02	-
TCE_05D	< 0.02	0.6
TCE_1D	< 0.02	0.24
TCE_2D	< 0.02	< 0.02
TCE_3D	0.12	0.92
TCE_4D	0.10	0.92
OneCyl	0.04	-
TCE_4D w/splitter plate	0	-

Table 4.12: Motion of the stagnation points

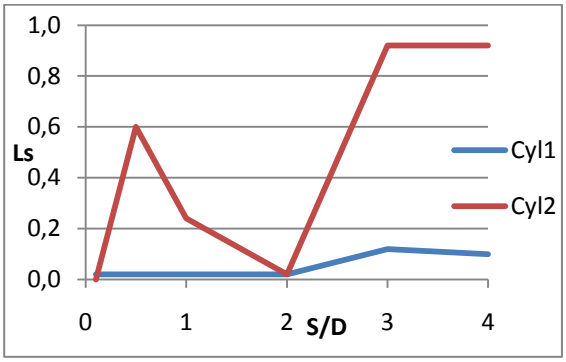

Figure 4.39: Motion of the stagnation points

OneCyl and the splitter plate case are not represented in the graph on the right. We see that for S/D ≤ 2 the stagnation point on cylinder1 moves only slightly, traversing less than 1/50 of the central part of the face (less than one cell). For the double vortex shedding flows the motion is notably larger. The difference between TCE_4D and OneCyl is a little surprising. It seems the existence of cylinder2 has a large influence on the motion of the stagnation point on cylinder1.

On cylinder2 we see that in the double vortex shedding flow (S/D = 4, 3), the stagnation point traverses almost the entire front face of the cylinder. TCE_2D is a rather special case as the flow is unsymmetric with respect to thee incoming flow, and the flow pattern changes at a very high time step. The mean position of the stagnation point is located in the middle of the upstream face in neither period 1 nor period 2. In period 1 mainly the wake is non-symmetric, and the offset of the stagnation point of cylinder2 is only about 5 % of the diameter in the positive y-direction. In period 2 the offset is 20 % of the diameter, also in the positive y-direction. In this period it is mainly the gap which is non-symmetric. In both periods the actual motion of the stagnation point is very small; less than 2 % of the diameter. The large motions for S/D = 1, and S/D = 0.5 especially, is due to the flow in the gap discussed in

chapter 4.7 (the developing piston mode flow). For S/D = 0.1 we have stagnation on the entire upstream face on cylinder1.

In the splitter plate case one would not expect the stagnation point to move as the flow is stationary (no time dependence), and this is confirmed here.

5 Results and discussion for free surface model (TCE_FS)

The free surface is difficult to deal with. It is an interface between air and water, and it is free to move. It is governed by certain free surface conditions [23]: Continutity requirement (Laplace equation), requirement of zero pressure difference on the surface (dynamic free surface condition) and the requirement that a fluid particle on the surface will stay there (kinematic free surface condition). Additionally, for finite water depth we require no normal velocity at the bottom. For infinite water depth there will be no normal velocity anyway because of the attenuation of the fluid particle motion with increasing submersion. Lastly, gravity is of course of fundamental importance for the free surface. The waves on the surface are gravity waves where the restoring forces are gravity and buoyancy.

In this study the free surface will be modeled by assuming mirror condition about y = 0. This models a rigid surface, which doesn't allow normal velocity. By using different boundary condition on the mirror plane tangential velocity can either be allowed or prohibited.

Since the mirror assumption eliminates the vortex shedding, the flow at the outlet will be quite a lot smoother than for TCE. Therefore the downstream extent of the domain has been reduced from L_u = 29.5 to L_{uFS} = 19.5 for these TCE_FS runs. Otherwise the domain is exactly the same, but of course chopped in half. The height of the domain, H_{FS}, is half of the original domain; H_{FS} = H/2. The height of the cylinders is defined as h = D/2. The Reynolds number is still based on D and it has the value Re = 200 here also.

The wake has 100 elements in the x-direction for all S/D. For smaller S/D they will get stretched a little, but in all cases their clustering increment is adjusted to give square cells along the cylinder surface, as described in chapter 4. The total number of elements will be dependent on S/D, but lies between 125 x 400 (S/D = 4) and 125 x 300 (S/D = 0).

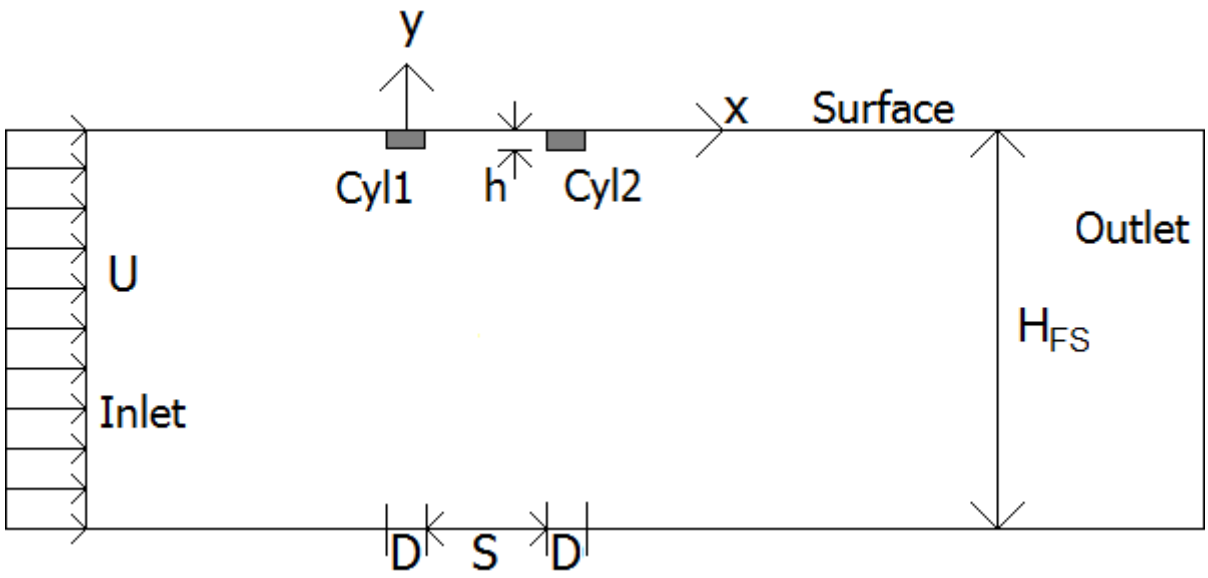

Figure 5.1: Flow configuration for runs with symmetry assumption

We can see that when the separation distance S/D is low, this configuration is comparable to the flow over a forward facing step.

As an intermediate step between the TCE and TCE_FS runs I introduced a splitter plate in the gap and wake for one of the TCE runs (TCE_4D); see figure 1.3. Otherwise the domain was left untouched. This is the first approximation to the free surface problem. This will eliminate the vortex shedding and normal velocity at y = 0. The splitter plate has boundary condition symmetryPlane to allow tangential velocity.

This case was run in 3D with A = 6, N_z = 40 and boundary condition symmetryPlane on the frontAndBack planes. This run was used to assess the assumption that this low Reynolds number flow without vortex shedding will be completely two-dimensional. A comparison between this case and the corresponding case for proper half domain, i.e. TCE_FS_sym with S/D = 4, is presented in chapter 5.2.

As discussed in chapter 1, the ideology for the half domain calculations is to start with a strict mirror plane boundary condition which we loosen up as we go along. For the proper runs with mirror condition I started with the strictest boundary condition: wall on the entire mirror plane, hence the name *TCE_FS_wall*. Then I did a hybrid version with symmetryPlane on the upstream part of the surface and wall in the gap and wake – *TCE_FS_symwall*. Lastly, the most realistic model of a free surface without introducing two-phase flow is *TCE_FS_sym* where the whole surface has boundary condition symmetryPlane. The assumption of two-dimensionality is valid. Therefore all TCE_FS runs have been done in 2D.

5.1 TCE_FS_wall and TCE_FS_symwall

Having boundary condition wall upstream cylinder1 means we allow a boundary layer to build up. The thickness will be dependent on the upstream extent of the domain, and thus the flow will be as well. For the low Reynolds number used in this study the boundary layer will quickly get relatively thick. The thickness, $\delta_{99\%}$, of the boundary layer on a plate plate aligned with the flow is given by the exact formula by Blasius [22]:

$$\frac{\delta_{99\%}}{x} = \frac{5}{\sqrt{\mathrm{Re}_x}} \rightarrow \delta_{99\%} = 5\sqrt{\frac{\nu x}{U}} \tag{5.1}$$

where Re_x is the Reynolds number based on the distance, x, from the plate's leading edge (here: distance from the inlet). In this particular case with $\nu = 0.005$ m_2/s, U = 1 m/s and x = L_u = 9.5 we get $\delta_{99\%} \approx 1.1$ diameters at the front of cylinder1 *if it were not there*. This formula will of course not be valid close to the body, but it still gives a good picture of how thick the boundary layer gets, and how much this affects the upstream flow. The height of the cylinders in this configuration is 0.5 diameters, which means the whole of cylinder1 will be inside the boundary layer, pretty much regardless of the validity of formula at the front of cylinder1. The

implication of this is that the wall will carry much of the resistance cylinder1 should have carried, thus lowering the drag on the cylinder considerably.

Figure 5.2 shows a comparison of the upstream part of the surface with boundary condition wall and symmetryPlane, respectively, for S/D = 4 in steady state conditions. With boundary condition wall (TCE_FS_wall) the drag coefficient on cylinder1 is C_D = 0.551 whereas it is more than double that, at C_D 1.266, for boundary condition symmetryPlane (TCE_FS_symwall).

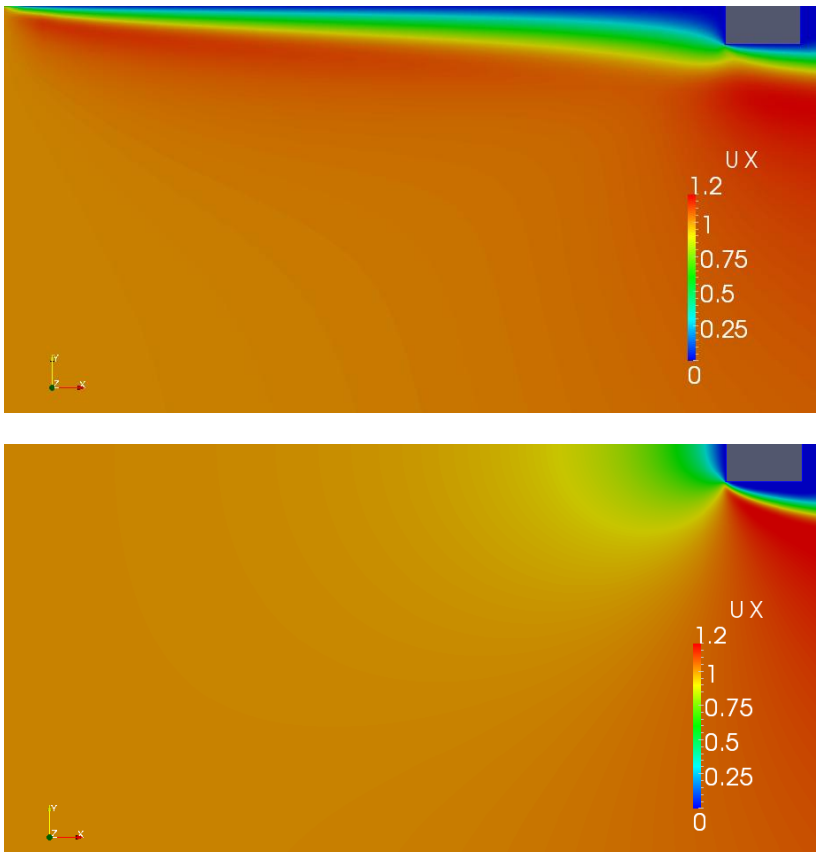

Figure 5.2: Upstream part of the surface with BC wall (top) and symmetryPlane (bottom)

In figure 5.2 the big difference between wall and symmetryPlane is evident. This comparison shows that boundary condition wall is clearly unphysical in this context. This result was expected and thus only one run was done in this configuration, namely for S/D = 4.

The two different boundary conditions on the surface for TCE_FS_symwall necessitated the division of the surface into two parts, which were given the names frontPlane and rigidSurface. In terms of the boundary condition on the upstream part of the surface (frontPlane) the solution becomes independent of the upstream extent. In terms of the distance to the inlet the upstream extent was found sufficient for the vortex shedding TCE flows and should therefore be sufficient here as well.

For this configuration calculations with S/D = 4, 3, 2, 1, 0.5 and 0.1 have been done. Just like for TCE an additional calculation with S/D = 0 and total length 2.1D to see the influence of the gap for S/D = 0.1 has been done. These runs will be compared closely to TCE_FS_sym in the next sections to reveal the influence of prohibiting tangential velocity on the surface in the gap and the wake.

5.2 TCE_FS_sym

With boundary condition symmetryPlane on the whole surface, this will be the closest model of a real free surface in this study. It is interesting to compare this to the first approximation to the free surface problem – the full domain with splitter plate. If we disregard the fact that the stagnation point on cylinder1 is free to more in the splitter plate case, TCE_FS_sym is really just one half of that domain. I have found that the stagnation point does not move at all. That should make these two cases very similar. In the comparsion I have also added the TCE_FS_symwall to see how boundary condition wall in the gap and wake affects the integral quantities.

Table 5.1 shows a comparison of drag and lift coefficients for both cylinders, and the length of resirculation zone behind cylinder2, L_r. All cases have S/D = 4. In terms of lift, the flow in the half domain of course will be very different from the splitter plate case. Comparing lift between full domain and half domain cases makes no sense. C_L values for the splitter plate case have been omitted. Also notice that the values are not averages like in chapter 4, as the solution will be time independent. Values for the latest time step are used.

Case	C_D cyl1	C_D cyl2	C_L cyl1	C_L cyl2	Recirc. length
TCE_4D w/splitter plate	1.248	-0.331	-	-	3.5
TCE_FS_4D_sym	1.256	-0.339	-0.845	-0.183	3.5
TCE_FS_4D_symwall	1.266	-0.266	-0.803	-0.144	3.6

Table 5.1: Comparison of integral parameters for free surface models with S/D = 4

All coefficients are based on the same area as in TCE – the frontal area, $A_f = A \cdot D$. This way direct comparisons can be made. Comparing the splitter case to TCE_FS_sym we see very good agreement. The splitter plate case is a very good approximation. The difference in drag is 2 % at maximum. The recirculation lengths are equal. This is of course expected, at least for the smooth laminar flow in the current study. In a study by Tran et al. [16] (unpublished, hard copy given to me by Prof. Pettersen) of turbulent flow past a semi-infinite thick plate a large difference between half and full domain was observed. This, however, was blamed on the two-dimensional URANS solver which according to Tran et al. created a weak vortex shedding from the plate's LE.

The two half domain cases, TCE_FS_sym and TCE_FS_symwall, are pretty similar as well. The drag on cylinder1 is almost equal, and there is only a 5 % difference in lift. Cylinder1 is

not much affected by the differing boundary condition in the gap and wake. For cylinder2 the differences are notably larger. The 27 % higher propulsion (negative drag) on cylinder2 for sym compared to symwall is likely due to the fact that in the latter case the boundary layer will take some of the forces which cylinder2 should have been subjected to.

The lower lift (higher absolute value) for sym would point to higher velocity around cylinder2. This makes sense as the recirculation zone in the gap likely will be more energetic for sym at high S/D. At lower S/D the fluid in the gap is pretty much still in both cases. The change from wall to symmetryPlane in the wake has made the recirculation length shorter, but it only amounts to about 3 %.

5.3 Recirculation zones and dependence on separation distance

This chapter begins with a discussion on the four recirculations zones in the TCE_FS_sym flow: below cylinder1 and cylinder2, in the gap and in the wake. Reattachment/detachment has been traced the same way as in chapter 4, i.e. by seeing whether the velocity changes sign along the surface (for walls: the first node outwards from the surface).

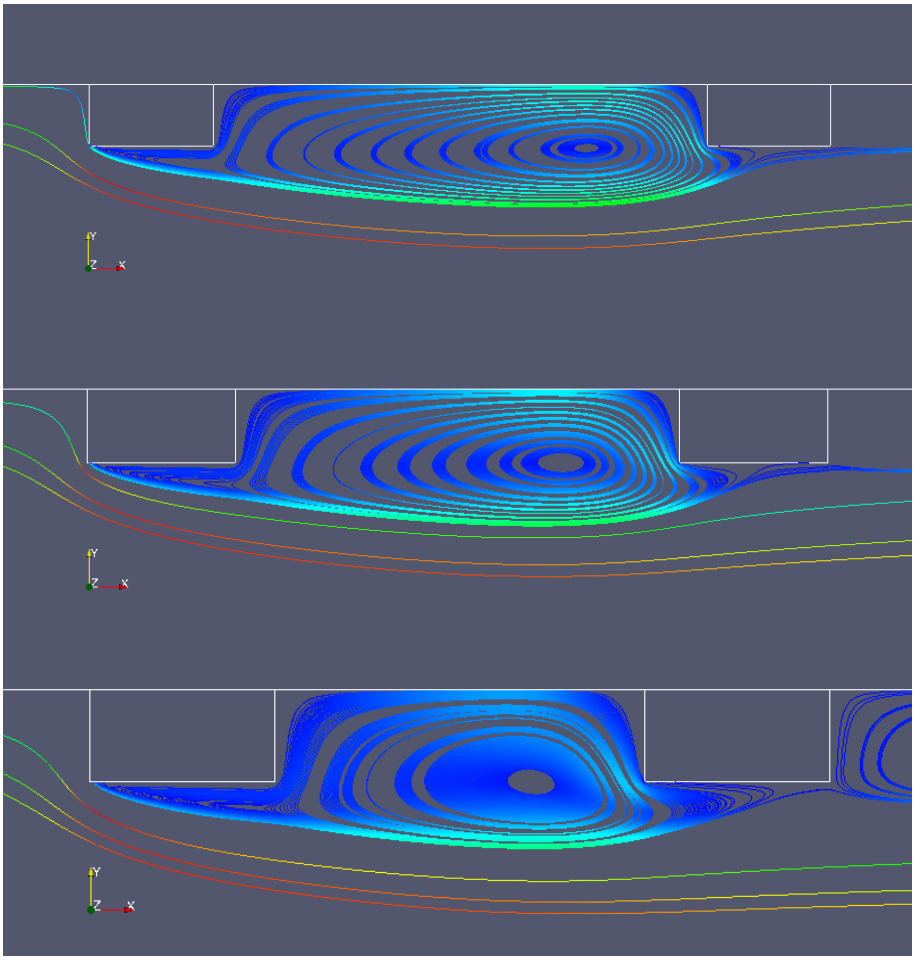

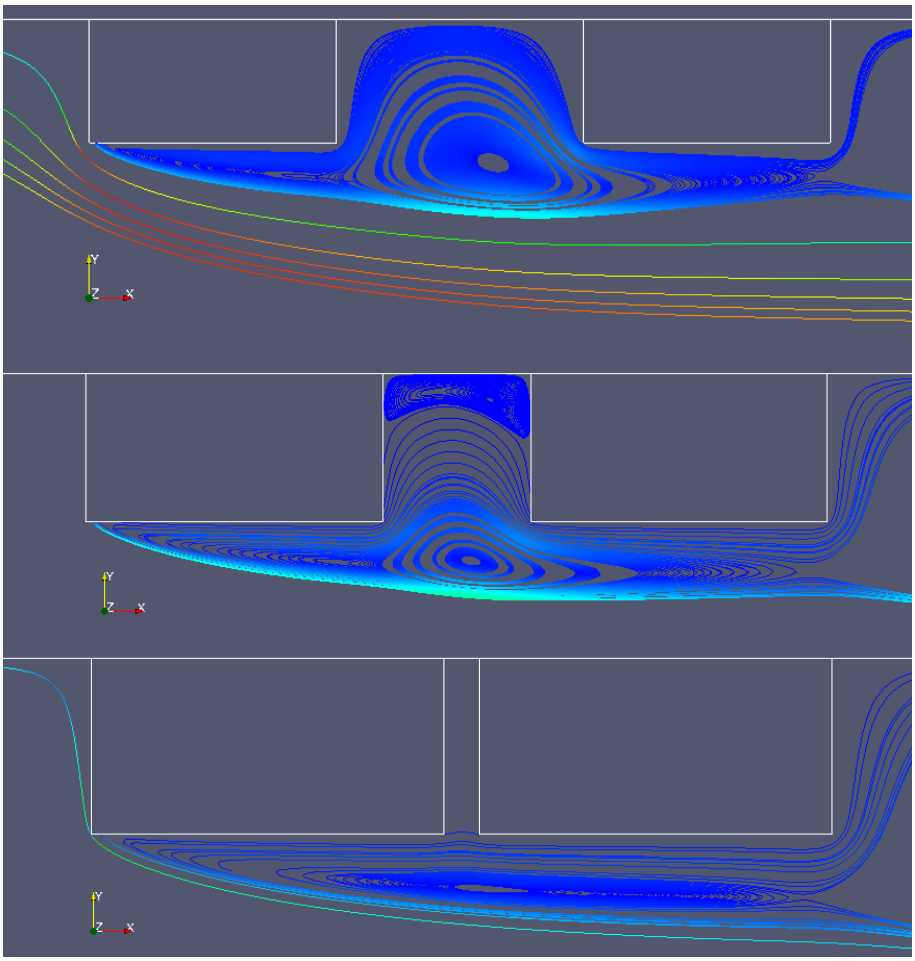

Figure 5.3: Streamlines for TCE_FS_sym for varying S/D

Figure 5.3 shows streamline plots for the six separation distances considered here: S/D = 4, 3, 2, 1, 0.5, 0.1. For S/D = 0.1 (bottom right) the streamlines in the gap have been omitted as they did not aid the figure. The fluid in the gap is almost completely still at this low separation anyway. Compared to the TCE cases the flow in the gap is much more restricted here, as the surface allows no velocity in the y-direction. More about this later.

We see a change in flow pattern under the cylinder as the separation distance decreases – from reattached to detached. This will be discussed next.

Recirculation below the cylinders:

In chapter 4, without the assumption of symmetry about y = 0, we saw that as the bodies moved closer to each other, the detached flow from cylinder1 started to reattach on cylinder2. With the assumption of symmetry the situation is very different. Figures 5.3 and 5.4 show that the flow will never reattach on the downstream cylinder for low S/D in this case.

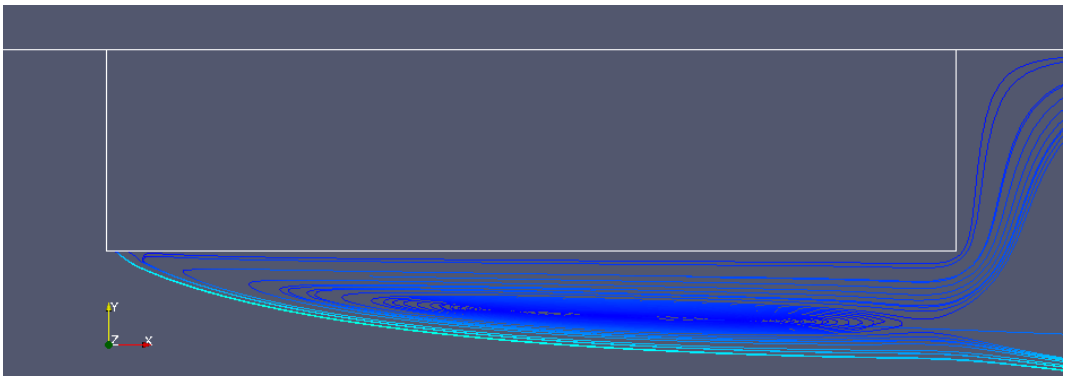

Figure 5.4: Streamlines for TCE_FS_sym with S/D = 0

The implication is that when symmetry conditions are assumed, the critical L/D ratio for the change between reattached and detached flow found by Okajima [4] for vortex shedding flow in infinite fluid is not valid. Presumably this means the critical Reynolds number will be different as well. To recap the finding by Okajima [4]: at a given Re the flow will be reattached for high L/D and detached for low Re, and at a given L/D the flow will be detached for high Re and reattached for low Re.

The findings by Okajima are valid for vortex shedding flow in infinite fluid. When introducing the symmetry condition, the vortex shedding is eliminated (at least in this laminar flow) and also no information is allowed to go through the gap or to cross the wake. These two limitations are highly interconnected. For the TCE_FS runs the Reynolds number is relatively high compared to the onset Reynolds number for vortex shedding (Re ≈ 50 [11]), but the flow is missing one of the properties it should have had: vortex shedding.

In infinite fluid with length L/D = 2.1 the critical Re for reattachment is Re ≈ 500 [4]. In this case we have detachment for Re = 200, and maybe lower (not investigated). One could think that in this case one should instead consider L/h = 4. According to Okajima [4], with length-to-height ratio of 4 the critical Re for reattachment is outside of the Re range he tested in (70-20000), that is, the flow is always detached, just like observed here.

But with the mirror conditions we are really still working with the diameter, D, even if the physical dimension in the y-direction is h = D/2. We should consider L/D = 2. The current cases are all steady. They experience neither vortex shedding nor any other time dependent phenomena in fully saturated condition. That is probably the reason for the large differences reattachment/detachment between TCE and TCE_FS.

In TCE_FS cylinder1 always experiences steady detachment. Cylinder2 experiences steady detachment for for S/D for S/D $\leq$ 2 and steady reattachment for S/D $\geq$ 3. For decreasing S/D the flow changes from reattached to detached. In TCE the flow around cylinder1 is always detached (except near maximum/minimum lift, as discussed in chapter 4.7). The flow around cylinder2 is reattached for S/D $\leq$ 2. S/D = 3, 4 experience both reattachment and detachment during a vortex shedding cycle due to the rather chaotic double vortex shedding flow scheme

in these cases. For low S/D the flow changes from detached to reattached as S/D decreases – the opposite of TCE_FS.

The critical S/D for reattachment/detachment on cylinder2 in TCE_FS is located in the same interval as Sc, the critical S/D for single/double vortex shedding. It would have been rewarding to investigate whether it is the same value; this is suggested as further work.

In TCE reattachment on cylinder2 means that S/D is too low for vortex shedding from cylinder1, as the detached flow from cylinder1 cannot roll up to vortices before it hits cylinder2. However, in TCE_FS it is suggested that reattachment on cylinder2 is a sign that in TCE the flow from cylinder1 would have been able to roll up in the gap and create vortices therein.

Recirculation in the gap

In regards to the gap, the main difference between TCE and TCE_FS (both symwall and sym) is that in the latter the gap is closed off – no information is allowed through.

Comparing the streamlines in figure 5.3 to figure 4.30 (TCE flow with S/D $\leq$ 1) and figure 4.23 (TCE flow with S/D = 2, averaged), they look pretty similar. The main difference is that the TCE_FS solution is time-independent. The stagnation point on cylinder2 does not move, the reciculation zones do not deform and the position of the reattachment points does not change. For TCE_FS_01D there is no pressure gradient in the gap, like we see in figure 4.31 (bottom) for TCE_01D. The streamlines in figure 5.3 do not show the velocity in the gap. Figures 5.5 through 5.8 show plots for u and v in the gap for varying S/D for both symwall (left) and sym (right).

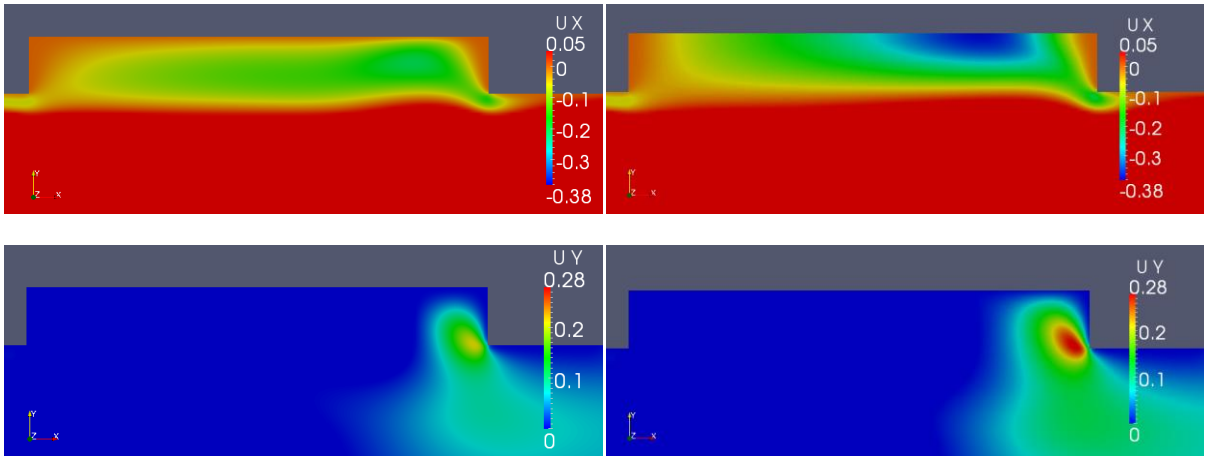

Figure 5.5: u and v in the gap at S/D = 4 for symwall (left) and sym (right)

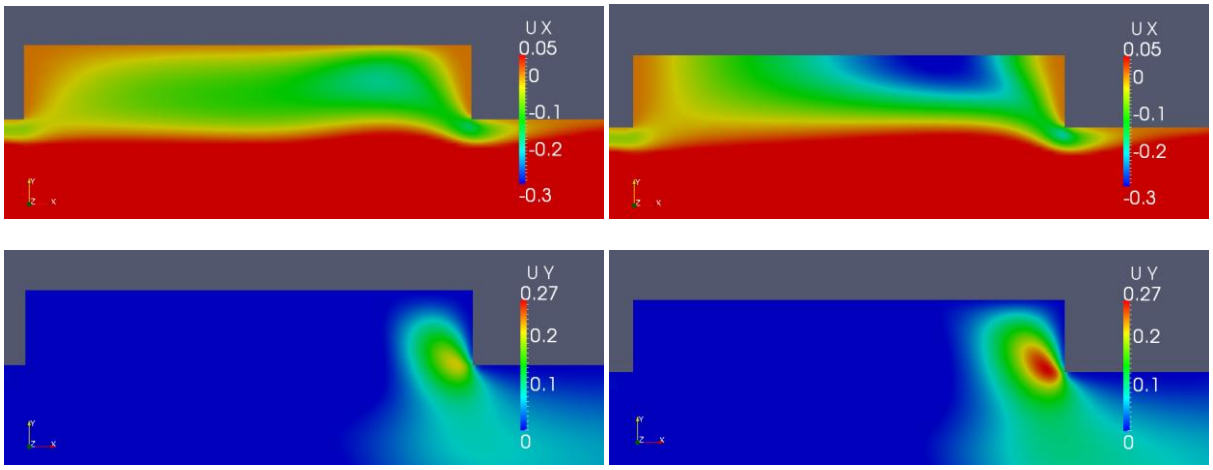

Figure 5.6: u and v in the gap at S/D = 3 for symwall (left) and sym (right)

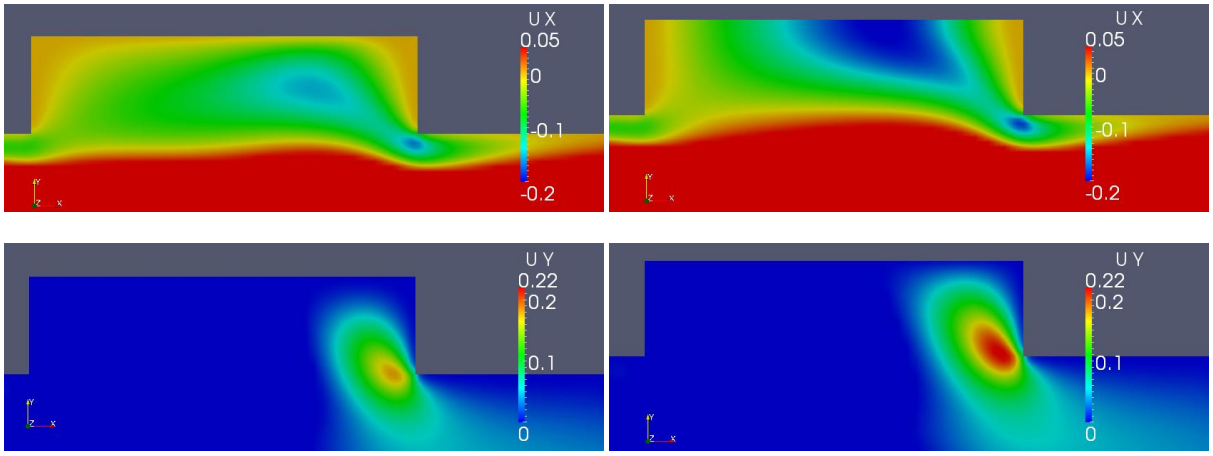

Figure 5.7: u and v in the gap at S/D = 2 for symwall (left) and sym (right)

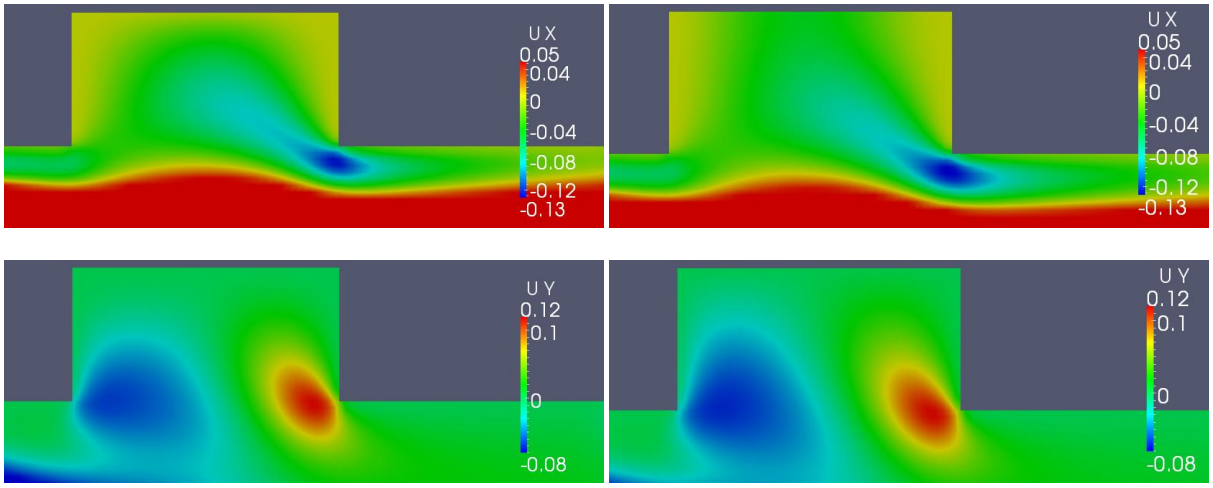

Figure 5.8: u and v in the gap at S/D = 1 for symwall (left) and sym (right)

Figures 5.5 through 5.8 show u and v in the gap with BC symwall and sym for S/D = 4, 3, 2, 1. For each velocity component and separation distance, the color range is the same for both BCs to show the influence of the BC on the surface. The range is changed for varying S/D to shows how the velocities in the gap decrease as S/D decreases.

In the x-velocity figures the difference between the BCs symmetryPlane and wall is evident. One can clearly see how the no-slip condition for symwall inhibits tangential velocity on the surface in the gap. The difference is most notable for S/D = 4, 3, 2. For S/D = 1 the difference is rather small.

In the y-velocity figures we see that because symmetryPlane allows tangential velocity on the surface in thep gap, the recirculation zone has a higher velocity. This creates a higher velocity around LE on cylinder2 and thus creates a larger negative lift (in negative y-direction); also see table 5.4 and figures 5.10 and 5.11 (right).

For S/D = 1 the difference between symwall and sym is very small, and for even lower S/D it is negligible. At these low separation distances the length of boundary with no-slip condition is short and the flow in the gap is restricted in the first place. This combined effect reduces the difference between symwall and sym. Thus, for low S/D the no-slip BC in the gap is allright.

Velocity plots for S/D = 0.5 and 0.1 are not provided because already at S/D = 1 there is little action in the gap. Symwall and sym will also be very close to equal there. For S/D = 0.5 the highest velocity – both x- and y-velocity) is u, v $\approx \pm$ 0.05. For S/D = 0.1 the values are less than 0.001. In practical terms the whole gap is completely motionless at this separation distance.

The recirculation zone in the wake will be discussed next.

Recirculation in the wake

Table 5.2 shows the recirculation length in the wake measured from two different positions; from the back face of cylinder2, which moves, and from the origin, which of course does not move. In the former case the measured length is called L_r and in the latter case it is called x_r.

	Recirc. length, L_r		x-position, x_r	
S/D	**symwall**	**sym**	**symwall**	**sym**
4	3.3	3.5	8.8	9
3	3.9	4.3	8.4	8.8
2	4.9	5.7	8.4	9.2
1	7.4	8.8	9.9	11.3
0.5	7.9	10.9	9.9	12.9
0.1	8.4	12.4	10	14
0	8.4	12.4	10	14

Table 5.2: Recirculation length behind cylinder2

This case will be discussed in more detail later; see figure 5.12. Seeing how equal TCE_FS_01D and TCE_FS_0D seem to be in terms on recirculation length, a more thorough comparsion is done next.

Comparison of S/D = 0.1 and S/D = 0 for symwall and sym

Table 5.3 shows a comparison of C_D sum, C_L sum, L_r and x_r for the two lowest separation distances and the two BCs on the surface in the gap and the wake.

Parameter	**S/D = 0.1 symwall**	**S/D = 0 symwall**	**S/D = 0.1 sym**	**S/D = 0 sym**
C_D sum	1.082	1.080	1.063	1.062
C_L sum	-1.262	-1.301	-1.236	-1.288
L_r	8.4	8.4	12.4	12.4
x_r	10	10	14	14

Table 5.3: Comparison between S/D = 0.1 and S/D = 0 for TCE_FS

For the S/D = 0 case the total length is L/D = 2.1. All coefficients are based on the same area, $A_f = A \cdot D$. For S/D = 0.1 and S/D = 0 the lift force does not not work on the same area since we get a lift force on the lid over the gap for the latter case. The lift coefficients are based on the same area in both cases. Like mentioned in chapter 4.7 the comparison of lift is a little more complicated than the comparison of drag because of the effect of the lid over the gap. The difference in sum lift coefficient is about 3 %. This is relative little, but it is still larger than the difference in drag sum and recirculation length.

Integral parameters

Table 5.4 shows C_D and C_L values for both cylinder and both BCs for varying S/D. These values are also shows as graphs in figures 5.9 and 5.10.

	C_D cyl1		C_L cyl1		C_D cyl2		C_L cyl2	
S/D	**sw**	**sym**	**sw**	**sym**	**sw**	**sym**	**sw**	**sym**
4	1.266	1.256	-0.803	-0.845	-0.266	-0.339	-0.144	-0.183
3	1.280	1.276	-0.829	-0.882	-0.301	-0.360	-0.186	-0.227
2	1.297	1.293	-0.859	-0.911	-0.319	-0.358	-0.243	-0.286
1	1.306	1.286	-0.881	-0.896	-0.296	-0.290	-0.318	-0.354
0.5	1.301	1.274	-0.878	-0.869	-0.256	-0.241	-0.360	-0.379
0.1	1.314	1.279	-0.862	-0.835	-0.232	-0.216	-0.400	-0.401
0	1.080	1.062	-1.301	-1.288	-	-	-	-

Table 5.4: Drag and lift on cylinder1 and cylinder2 for varying S/D

In table 5.4 sw means symwall. For S/D = 0 *cyl1* corresponds to the rectangular body and *cyl2* has no value, just like in chapter 4.7. Table 5.5 shows the drag and lift sums for both boundary condition. These are shown in graphical form in figure 5.11.

	C_D sum		C_L sum	
S/D	**sw**	**sym**	**sw**	**sym**
4	0.999	0.916	-0.947	-1.027
3	0.979	0.916	-1.016	-1.110
2	0.977	0.935	-1.102	-1.197
1	1.010	0.997	-1.198	-1.250
0.5	1.045	1.033	-1.238	-1.248
0.1	1.082	1.063	-1.262	-1.236
0	1.080	1.062	-1.301	-1.288

Table 5.5: Sum drag and lift for varying S/D

In this case there is no phase shift between the cylinders as the solution is time independent. Thus there is no phase shift to take into account when adding lift coefficient values. Sum drag and lift will be discussed more in connection with figure 5.11.

Figures 5.9 through 5.12 show the influence of varying S/D on drag, lift, sum drag and lift, and finally recirculation length in the wake. In these figures the red lines correspond to symwall and blue lines to sym.

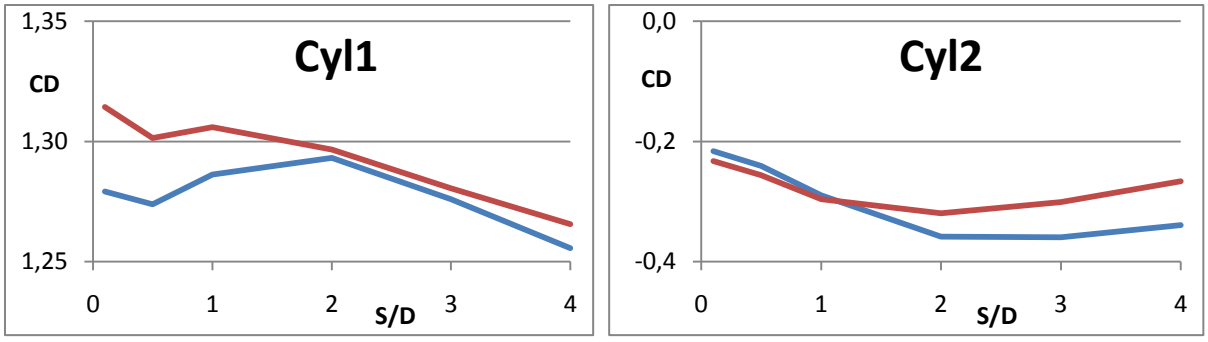

Figure 5.9: Drag on cylinder1 and cylinder2 for varying S/D

For cylinder1 the largest difference between symwall and sym takes place for small S/D, whereas the opposite is the case for cylinder2. As previously mentioned the difference between the BCs wall and symmetryPlane on the surface in the gap is very small for low S/D. Only for high S/D will the wall for symwall take a considerable amount of the force which cylinder2 should have been subjected to. We must note that the drag on cylinder2 is negative, so it is really a propulsion force when drag is defined as positive in the positive x-direction. The difference between sym and symwall at S/D = 4 is about 27 %. The propulsion on cylinder2 will not be very much affected by the difference between sym and symwall for low S/D. In fact, for S/D $\leq$ 1 the propulsion on cylinder2 is slightly higher for symwall. This is explained by the fact that the symwall BC on the surface in the wake will slow the flow down in the area behind cylinder2 thus creating higher pressure on the cylinder's downstream face than is the case for sym.

Cylinder1 shows the larger variation between the two BCs for low rather than high S/D. Due to the scale in the left figure the variation seems to be larger than the 27 % for cylinder2, but due to the different scale of the figures, the discrepancy here is only about 2 %, which is almost negligible. The stagnation pressure on the upstream of cylinder1 is approximately the same for all S/D with a given boundary condition. With a given S/D there is a larger difference for varying boundary condition. Thus, when comparing the same boundary condition for different S/D only the downstream pressure needs to be considered. It is found that the difference between S/D = 4 and S/D = 0.1 with symwall (about 3.5 %) is larger than the difference between S/D = 4 and S/D = 0.1 with sym (about 1.5 %). This creates the 2 % difference between symwall and sym for low S/D.

The strange drop at S/D = 0.5 for C_D on cylinder1 looks more significant than it is, because of the scaling in figure 5.9 (left). The fact that it does not show up in the drag sum (figure 5.11 left) supports this. The deviation from a straight line between the values for S/D = 1 and S/D = 0.1 is less than 1 %.

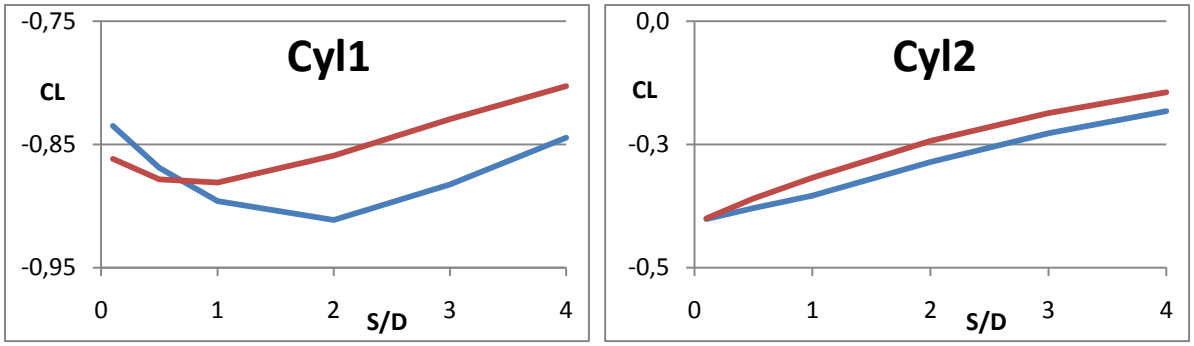

Figure 5.10: Lift on cylinder1 and cylinder2 for varying S/D

For lift the largest difference is found on cylinder1, and for higher S/D. Symwall and sym follow each other nicely for cylinder2. The maximum difference is only about 5 % (see table 5.4). In TCE the lift was created by the circulation from the vortices [23]. In this case the lift is simply created by a sub-pressure under the cylinders due to the velocity (Bernoulli's equation [22]). Thus, the velocity below cylinder1 varies more with S/D than the velocity below cylinder2. This could be due to the fact that the reattaching flow on cylinder2 might reduce the effect on this cylinder, making cylinder1 vary more in total.

The lift is negative as it points along the negative y-axis. For both cylinders the lift is *stronger* (lower value) with sym than symwall because the velocity below the cylinders is higher for sym than for symwall. This can also be seen in figures 5.5 through 5.8 (velocity plots). The crossover at S/D ≈ 0.5 is not well understood.

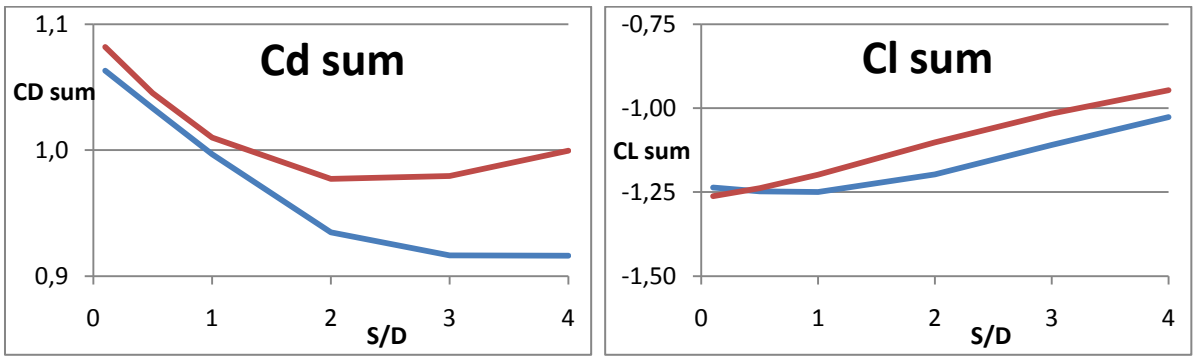

Figure 5.11: Lift and drag sums for varying S/D

Figure 5.11 (left) can be seen as a summary of figure 5.9, and likewise figure 5.11 (right) can be seen as a summary of figure 5.10. It shows how the effects on the two bodies combine. The difference in drag sum between symwall and sym is higher for high S/D for the reasons discussed under figure 5.9 (about 9 % for S/D = 4). The no-slip condition on the wall in the gap will have a pronounced effect only for high S/D. For the lift sum the difference is about the same (8 % at S/D = 4), but unlike the drag sum, the slope of the lift sum stays close to

constant for varying S/D. The drag sum experiences a marked leveling off from S/D = 2 upwards.

If one notices the very different scaling on the left and right figures, figure 5.11 also shows that lift varies notably more than drag as the separation distance is varied.

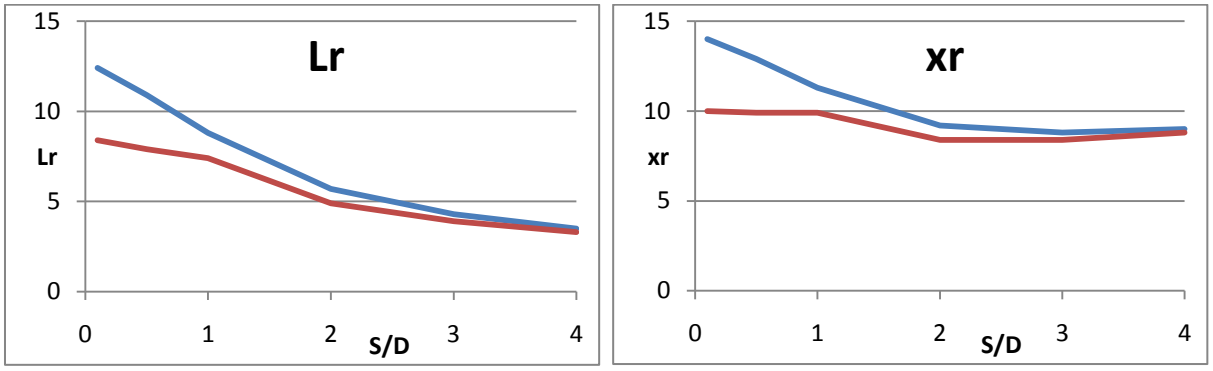

Figure 5.12: Recirculation length behind cylinder2

Since S/D decreases it would be logical to see an increase in L_r. To see the absolute effect we look at the distance from the origin to the end of the recirculation zone. This distance also increases with decreasing S/D. In figure 5.12 the scale are identical so direct comparison is possible. This could mean that the recirculation length is comparatively longer for long bodies, but as a single body with L/D = 1 has not been simulated, this is only a suggestion. On the other hand, it could also mean that two bodies close to each other actually decrease the recirculation length. Again, only a suggestion.

From figure 5.12 (right) we see that when the recirculation length is measured from a fixed point, the origin in this case, the variation is smaller. For symwall the line is pretty flat all the way. Sym exhibits large variation for S/D < 2. Around S/D = 2 it levels off. The increase in recirculation length, both L_r and x_r, for decreasing S/D cannot be connected to an sudden change between reattached and detached flow, but from the streamlines in figures 5.3 and 5.4, one can see that the flow gets more deflected for low S/D. At higher S/D the flow turns more back towards the surface and thus decreases the recirculation length.

L_r and x_r increase more quickly with decreasing S/D for sym than for symwall. At S/D = 4 they are similar, but at S/D = 0, x_r and L_r are 40 % and 48 % longer for sym than for symwall, respectively; see table 5.3.

The recirculation length is equal for S/D = 0.1 and S/D = 0 with both BCs (but different between the two BCs). This is expected as there should be even less difference between these two cases for TCE_FS than for TCE as the gap is closed off here.

There is no big change in the values when the flow changes between detached and reattached (from S/D = 2 to S/D = 3). We see no steep change in values like we see when TCE flow changes between single and double vortex shedding.

The cylinders in TCE_FS will always want to move towards each other. There is much less variation in forces from S/D = 4 to S/D = 0 than for TCE. And the variation is less for sym than for symwall. For symwall the sum drag is 8 % higher for S/D = 0 than S/D = 4. The corresponding value for symwall is 16 %. For lift the values are 25 % and 37 %, respectively (see table 5.5). Lift varies notably more than drag as the separation distance is varied, as discussed in connection with figure 5.11.

When it comes to the length of the recirculation zone in the wake, however, the larger difference is to be seen for sym. The increase in x_r from S/D = 4 to S/D = 0 is 56 % compared to only 14 % for symwall.

For TCE_FS it is not very easy to answer the question “When do the cylinders start to feel like one?” In some respects (drag and lift) they never really feel like two separate bodies, but some parameters will not be similar until they are relatively close (recirculation length). The agreement in terms of recirculation length also depends on the boundary condition on the surface. For symwall x_r levels off completely for $S/D \leq 0.5$, whereas it increases steadily all the way to S/D = 0.1 for sym. In terms of flow pattern, one could say they feel as one for $S/D \leq 1$, as the flow pattern will be similar to the S/D = 0 case for these separation distances.

6 Conclusion

It has been observed that for S = 4 and S ≤ 1 the TCE flow exhibits a phenomenon of distinct low-frequency force pulsations. The pulsation period was highest for the highest and lowest S/D. It seems the pulsations phenomenon is governed by subsequent stretching and compression of the shear layers from the upstream body. For S/D = 2, 1 the pulsations are absent. This could either be because the pulsation frequency coincides with the vortex shedding frequency in these cases, or because the separation distance is too small for this stretching and compression to occur. For even lower S/D the two bodies feel like one long body and the pulsation could be brought about by deformation of the shear layers forming from cylinder2 which now becomes the upstream body.

The flow around a single cylinder at Re = 200 is inherently three-dimensional and the pulsations are part of the transition to 3D flow. But in this case only the S/D = 4 case exhibited 3D effects. All flows with S/D ≤ 3 exhibited period doublings in the drag spectra. Period doublings could appear when an inherently three-dimensional flow is simulated in two dimensions only, or with an aspect ratio too low for the onset of mode A waves. The interaction between the cylinders at S/D ≤ 3 may lead to a higher onset wavelength for mode A istabilities than the aspect ratio necessary for a single cylinder (somewhere between 3 and 6 diameters.)

The changeover points between double and single vortex shedding was found to be in the range 2.91 < S/D < 2.92. Based on the current results and results from my project work [3] it can be concluded that the critical separation distance form double vortex shedding decreases with increasing Reynolds number. The double vortex shedding scheme was characterized by high levels of forces and a repulsive force between the cylinders. In the single vortex shedding scheme the force levels were notably lower, and there was an attractive force between the cylinders. There is a sudden crossover and no point where the force between the bodies is zero. From a comparison with a single long body (S/D = 0) with length L/D = 2.1 it was found that for S/D ≤ 1 the cylinders start to feel like one body. For S/D = 1 the sum drag coefficient is only about 10 % lower than or S/D = 0. A surprising 36 % difference in pulsation period was found between S/D = 0.1 and S/D = 0 cases is not well understood. All other parameters are within a few percents of each other when comparing these two cases.

For the free surface model (TCE_FS) wall as BC on the entire surface is unphysical as a boundary layer will build up in the upstream part of the domain. The hybrid solution symwall with symmetryPlane upstream and wall in the gap and wake showed reasonable agreement with sym, the solution with symmetryPlane on the entire surface. For recirculation length and drag on cylinder1 the agreement was better a high S/D and for force sums, drag on cylinder2 and lift on both cylinders the agreement was better at low S/D. For low S/D the gap flow is very restriced, much more so than for TCE which allows information through. Symwall and sym are indistinguishable in terms of the gap flow at low S/D. In general the variation with S/D is much smaller in TCE_FS than TCE.

TCE changes from detached to reattached flow on cylinder2 for decreasing S/D. For TCE_FS the opposite is true. The changeover between detachment and reattachment for TCE flow is directly connected to the changeover from double to single vortex shedding. For S/D lower than the critical separation distance, shear layers from cylinder1 are not able to roll up to vortices in the gap. It is believed that the detached flow is the TCE_FS equivalent of single vortex shedding in TCE. Detached flow in TCE_FS means that flow would simply sail past the gap without creating vortices. Likewise, the reattached flow in TCE_FS is the equivalent of a vortex rolling up in the gap in TCE flow, creating double vortex shedding.

The recirculation zone in the wake increases with decreasing S/D, both when measured from the downstream face of cylinder2, which moves, and when measured from the origin. The increase for decreasing S/D is likely related to the flow pattern around the cylinders. The flow is more deflected for the detached flow.

6.1 Future work

As my Master Thesis is part of a project on ship-ship interaction, there is more work going on already, on a higher and more realistic level than mine. The interested reader is refered to publications by Ph.D. candidate Tufan Arslan, Prof. Bjørnar Pettersen and Prof. Helge I. Andersson.

Future work to be suggested for studies turned more towards a more realistic ship-ship interaction model than the current study includes turbulence, free surface (two-phase flow), finite water depth, more realistic hull shape including bilges and bilge keels, and a size ratio different from one.

Future work which builds on this Master Thesis

- 3D effects and force pulsations: Investigate the suppression of pulsations for S/D = 2 and 1, and why the pulsation periods vary the way they do. Investigate the suppression of 3D effects for S/D $\leq$ 3, whether a higher aspect ratio will trigger three-dimensionality for lower separation distances than found here and whether period doubling will dissappear in these cases.
- The rather peculiar TCE_2D case with its strange startup (including very strange FFT results for drag), unsymmetric flow behavior, low force level and extremely long time needed to reach saturated condition.
- Different sizes for the two cylinder, like I did in my project work [3], but in 3D.
- Investigate Re and L/D limit for the changeover between detachment and reattachment in mirror conditions, to expand on the excellent article by Okajima (1982) [4]. Critical separation distance for changeover between reattachment and detachment in mirror condition. Simulate the TCE_FS equivalent of OneCyl to study the recirculation zone in the wake to see how its length is affected by introduction of a second body in the wake.
- Investigate the large difference in rms values (most notably drag) between HF and LF regions as discussed in chapter 4.2.

7 References

1. J. M. Hovrud & J. Havn 2010. “CFD used for free surface flow calculations,” Department of Marine Technology, NTNU, 1-4
2. J.M. Hovrud 2010 – “TMR15 Numerical methods in marine hydrodynamics – Exercise 3,” Department of Marine Technology, NTNU, 1-26
3. J. M. Hovrud 2010. ”Project report TMR4520: Interaction between bluff bodies,” Department of Marine Technology, NTNU, 1-35
4. A. Okajima 1982. “Strouhal numbers of rectangular cylinders,” J. Fluid Mech. 123, 379-398
5. R.W. Davis & E.F. Moore 1982. “A numerical study of vortex shedding from rectangles,” J. Fluid Mech. 116, 475-506
6. C. Norberg 1993. “Flow around rectangular cylinders: Pressure forces and wake frequencies,” J. Wind Eng. Ind. Aero. 49, 187-196
7. R.W. Davis, E.F. Moore & L.P. Purtell 1984. “A numerical-experimental study of confined flow around cylinders,” Phys. Fluids. 27, 46-59
8. R. Franke, W. Rodi & B. Schönung 1990. J. Wind Eng. Ind. Aero. 35, 237-257
9. A. Sohankar, C. Norberg & L. Davidson 1995. ”Numerical simulation of unsteady flow around a square two-dimensional cylinder,” 12th Australian Fluid Mech. Conf., Sydney, Australia. 10-15 December 1995, 517-520
10. A. Sohankar, C. Norberg & L. Davidson 1997. ”Numerical simulation of unsteady low-Reynolds number flow around rectangular cylinders and incidence,” J. Wind Eng. Ind. Aero. 69-71, 189-201.
11. A. Sohankar, C. Norberg & L. Davidson 1998. ”Low-Reynolds number flow around a square cylinder and incidence: study of blockage, onset of vortex shedding and outlet boundary condition,” Intl. J. Num. Meth. Fluids. 26, 39-56
12. A. Sohankar, C. Norberg & L. Davidson February 1999. ”Simulation of three-dimensional flow around a square cylinder at moderate Reynolds numbers,” Phys. Fluids. 11, 288-306
13. A. Sohankar, C. Norberg & L. Davidson July 1999. ”Numerical simulation of flow past a square cylinder,” 3rd ASME/JSME Joint Fluids Engineering Conference, San Francisco, USA, July 18-23 1999, pp. 1-6
14. C.H.K. Williamson 1996, “Vortex dynamics on the cylinder wake,” Annu. Rev. Fluid Mech. 28, 477
15. R.D. Henderson 1997, “Non-linear dynamics and pattern formation in turbulent wake transition,” J. Fluid Mech. 352, 65
16. T. T. Tran, R. Perrin, R. Manceau and J. Borée. “Simulation and analysis of the flow over a thick plate at high Reynolds number,” Institute Pprime, Department of Fluid Flow, Heat Transfer and Combustion, CNRS-University of Pioters-ENSMA, SP2MI, Bd Curie, 86892 Futuroscope Chasseneuil Cedex, France, 133-138 (unpublished)
17. S.C. Luo, X.H. Tong, B.C. Khoo 2006, ”Transition phenomena in the wake of a square cylinder,” Journal of Fluids and Structures 23 (2007), 227–248

18. A.K. Saha, G. Biswas, K. Muralidhar 2002, ”Three-dimensional study of flow past a square cylinder at low Reynolds numbers,” International Journal of Heat and Fluid Flow 24 (2003), 54–66
19. D. Barkley and R.D. Henderson (1996), “Three dimensional Floquet stability analysis of the wake of circular cylinder,” J. Fluid Mech. 322, 215-241
20. J. Robichaux, S. Balachandar, S.P. Vanka 1999, “Three-dimensional Foquet instability analysis of the wake of a square cylinder,” Phys. Fluids 11, 560-578
21. P. T. Debevec, “The Excel FFT function v1.1,” École Polytechnique Fédérale de Lausanne, February 12, 2006
22. Frank M. White, “Viscous Fluid Flow, Third Edition,” McGraw-Hill, 2006
23. Bjørnar Pettersen, “Marin teknikk 3 – Hydrodynamikk,” Department of Marine Technology, January 2007.
24. Walpole, Myers, Myers and Ye, “Probability and Statistics for Engineers & Scientists – Seventh Edition,” Prentice Hall, 2002
25. K. Sørli, “Meshing Applied to CFD,” SINTEF ICT Applied Mathematics, Trondheim, October 11, 2010
26. O. M. Faltinsen, “Sea loads on ships and offshore structures,” Cambridge University Press, 1990
27. E. Kreyszig, “Advanced Engineering Mathematics – Eigth Edition,” John Wiley & Sons Inc., 1999
28. www.openfoam.com, Jan-May, 2011
29. www.openfoamwiki.com, Feb-May, 2011
30. www.cfd-online.com, Feb-May, 2011

8 Appendix

On the enclosed CD you will find all spreadsheets and various OpenFOAM files defining numerical schemes, boundary and initial conditions, scripts for linking the frontAndBack planes for cyclic boundary condition, script for decomposing the case for calculation in parallel, and more.